UNIVERSITY
of
THESSALY

Department of
Mechanical and Industrial Engineering
Laboratory of Thermodynamics and Thermal Engines

Postgraduate Specialization Thesis

Thesis Subject:

'Development of a System for the Measurement of Soot Maldistribution and Pressure Drop Characteristics in Diesel Particulate Filters.'

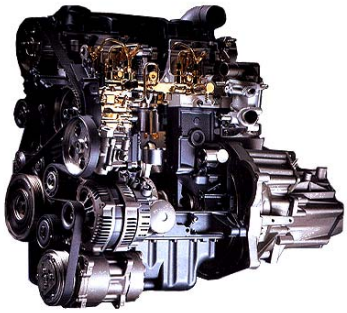

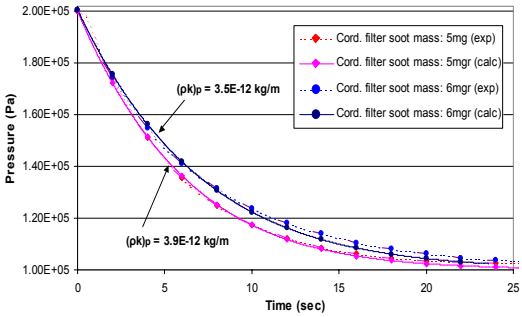

Thesis submitted by
Dimitris L. Psarianos

Thesis Supervisor: A.M. Stamatelos

Volos, April 2002

ΠΕΡΙΛΗΨΗ

Στην παρούσα μεταπτυχιακή εργασία παρουσιάζεται η πειραματική και υπολογιστική διερεύνηση των χαρακτηριστικών φόρτισης φίλτρου των εκπεμπόμενων σωματιδίων από μηχανή Diesel. Επίσης παρουσιάζεται μια εναλλακτική μέθοδος εκτίμησης της μάζας που καίγεται κατά την διάρκεια της αναγέννησης του φίλτρου. Τα πειράματα - μετρήσεις πραγματοποιήθηκαν σε μικρής κλίμακας μοντέλα του φίλτρου αλλά και σε πραγματικό φίλτρο. Τα πειράματα συνοδεύονται από υπολογισμούς και πρόγραμμα γραμμένο σε Fortran 90. Η ορθότητα των υπολογισμών πιστοποιήθηκε με σύγκριση των υπολογιστικών με τα πειραματικά αποτελέσματα. Τα αποτελέσματα αφορούν ένα εκτεταμένο πεδίο λειτουργίας της μηχανής. Έγινε προσπάθεια συσχέτισης των αποτελεσμάτων πειράματος και υπολογισμού μεταξύ των πειραμάτων σε μικρή κλίμακα και στο πραγματικό φίλτρο. Οι τιμές των χαρακτηριστικών παραμέτρων που επηρεάζουν την πτώση πίεσης, οι οποίες προσδιορίστηκαν από την πειραματική διαδικασία, χρησιμοποιήθηκαν ως δεδομένα εισόδου στον κώδικα CATWALL του εργαστηρίου,

και διασταυρώθηκαν οι υπολογισμένες με τις μετρημένες καμπύλες πτώσης πίεσης. Τα αποτελέσματα και τα συμπεράσματα της διερεύνησης παρουσιάζονται αναλυτικά.

ΠΡΟΛΟΓΟΣ

Ο τομέας των μεταφορών αποτελεί έναν από τους κυριότερους μοχλούς ανάπτυξης της παγκόσμιας κοινωνίας και οικονομίας. Στην εποχή της μετάβασης που ζούμε σήμερα, η ελαχιστοποίηση των αποστάσεων φαίνεται πως αναδεικνύεται σε σημαντικό παράγοντα προόδου. Όμως, δεν είναι ο μόνος.

Η οικολογία και η επιθυμία των ανθρώπων για επιστροφή στο φυσικό περιβάλλον ή σε ένα πιο φιλικό περιβάλλον από εκείνο που διαφαίνεται πως διαμορφώνεται απαιτεί από την Βιομηχανία και τις Μεταφορές να συνυπολογίσουν και την Φύση στην πορεία τους.

Έτσι και στην περιοχή της τεχνολογίας του αυτοκινήτου, νέοι νόμοι θεσπίζονται με στόχο την παραγωγή πιο 'οικολογικών' προϊόντων. Η ολοένα και πιο αυστηρή νομοθεσία υποχρεώνει εταιρείες μόνες ή σε συνεργασία με κέντρα έρευνας και ανάπτυξης, καθώς και πανεπιστημιακά εργαστήρια, να μελετήσουν τρόπους μείωσης των εκπεμπόμενων ρύπων και να βελτιστοποιήσουν το σχεδιασμό συστημάτων που τους υλοποιούν.

Σε αυτό το πλαίσιο κινείται η μεταπτυχιακή ετούτη εργασία. Κύριος σκοπός της είναι η διερεύνηση των χαρακτηριστικών φόρτισης κυψελοειδούς μορφής κεραμικών φίλτρων αιθάλης για κινητήρες diesel και η ποσοτική έκφανσή τους μέσω της παραμέτρου $(\rho k)p$. Θα γίνει προσπάθεια για τη συσχέτιση των πειραματικών και υπολογιστικών αποτελεσμάτων των μετρήσεων μεταξύ της μελέτης των φαινομένων σε μικρή κλίμακα και σε κλίμακα πραγματική.

Σε αυτό το σημείο θα ήθελα να ευχαριστήσω τον επιβλέποντα Καθηγητή μου Δρ. Α.Μ. Σταματέλλο τόσο για την επιστημονική καθοδήγηση και την παραχώρηση έντυπου και ηλεκτρονικού υλικού όσο και για τους ωφέλιμους διαλόγους που είχαμε κατά την διάρκεια της εργασίας.

Όπως και τον Καθηγητή Δρ. Ν.Σ. Βλάχο από τον οποίο απέκτησα το όποιο ρευστομηχανικό και υπολογιστικό υπόβαθρο διαθέτω, και τους Καθηγητές Δρ. Β. Μποντόζογλου, Δρ. Ε. Σταπουντζή τους οποίους είχα ως διδάσκοντες κατά την διάρκεια των προπτυχιακών ή μεταπτυχιακών σπουδών, και Καθηγητή Δρ. Ν. Πελεκάση για την επιστημονική γνώση που προσπάθησαν να μου εμφυτεύσουν.

Επίσης θα ήθελα να ευχαριστήσω τον υποψήφιο διδάκτορα του εργαστηρίου κ. Γ. Στρατάκη ο οποίος μου έδειξε τη μεθοδολογία των μετρήσεων που διεξαγάγαμε σε συνεργασία, και είχε ήδη προετοιμάσει την πειραματική διάταξη και τα φίλτρα μικρής κλίμακος, που ήταν απαραίτητα ως σημείο εκκίνησης της εργασίας μου. Επίσης, επιθυμώ να ευχαριστήσω και τον υποψήφιο διδάκτορα του εργαστηρίου κ. Γ. Κωνσταντά, για την υποστήριξη και τις προτάσεις του.

Πίσω από όλα ετούτα τα συμπεράσματα και τους τύπους βρίσκονται τα πρόσωπα των γονέων, των συγγενών και των φίλων, όπως ο Κώστας, ο Χρήστος, η Αργυρώ, η Ειρήνη και η Μαρία. Τους ευχαριστώ.

Η παρούσα εργασία υποστηρίχθηκε από την PSA και το Ε.Θ.Θ.Μ. του Π.Θ. Η υποστήριξή τους εκτιμάται ιδιαιτέρως.

Η δομή της εργασίας έχει ως εξής:

Στο Κεφάλαιο1 παρουσιάζεται μια μικρή εισαγωγή για τους κινητήρες Diesel, τις εκπομπές τους, τα σωματίδια που παράγονται και την τρέχουσα νομοθεσία περιορισμού τους που ισχύει σε Ευρώπη και ΗΠΑ. Επίσης παρουσιάζονται τρόποι ελέγχου των εκπεμπόμενων ρύπων καθώς και τα χαρακτηριστικά των φίλτρων σωματιδίων αιθάλης για κινητήρες Diesel (DPF).

Τα φίλτρα σωματιδίων ανήκουν στην κατηγορία των πορωδών υλικών. Έτσι στο Κεφάλαιο2 γίνεται μια μικρή αναφορά στα πορώδη υλικά και στην ροή και τα φαινόμενα μεταφοράς, γενικότερα, που εμφανίζονται εντός τους.

Στο Κεφάλαιο3 παρουσιάζεται η πειραματική διαδικασία των μετρήσεων σε φίλτρα μικρής και κανονικής κλίμακας. Επίσης επιδεικνύεται η μετρητική διάταξη και το πρωτόκολλο των μετρήσεων.

Στο Κεφάλαιο4 παρατίθεται η υπολογιστική διαδικασία που αναπτύχθηκε για να υποστηρίξει τα πειράματα. Οι εξισώσεις και οι προσεγγίσεις που έγιναν παρουσιάζονται μαζί με τον αλγόριθμο επίλυσης.

Στο Κεφάλαιο5 παρουσιάζονται τα αποτελέσματα της πειραματικής-υπολογιστικής διαδικασίας που επεξηγήθηκε στα προηγούμενα δύο κεφάλαια. Τα αποτελέσματα αφορούν τα φίλτρα μικρής και 1:1 κλίμακας και στόχο έχουν να διερευνήσουν την σχέση μεταξύ των πειραμάτων φόρτισης σε μικρής κλίμακας και κανονικού μεγέθους φίλτρων.

Στο Κεφάλαιο6 παρουσιάζεται η επαλήθευση των προβλέψεων του κώδικα προσομοίωσης αναγέννησης ‘Catwall’, όσον αφορά την πτώση πίεσης, καθώς και μια

παραμετρική μελέτη ως προς την παράμετρο (ρk)p η οποία έχει εξαχθεί από τα πειράματα σε μικρής κλίμακας φίλτρα.

Στο Κεφάλαιο7 αναλύεται μια εναλλακτική μέθοδος υπολογισμού της καμμένης μάζας σωματιδίων εντός της παγίδας στη διάρκεια της αναγέννησης. Θα επεξηγηθεί η σημασία αυτού του υπολογισμού και μετά την θεωρητική παρουσίαση θα γίνει εφαρμογή της μεθόδου σε υπάρχοντα πειράματα.

Στο Κεφάλαιο 8 προσφέρεται η σύνοψη της παρούσης εργασίας και ακολούθως διατυπώνονται ορισμένες προτάσεις για περαιτέρω εργασία επί του θέματος.

Και στο τέλος της εργασίας υπάρχουν τα παραρτήματα στα οποία περιέχονται το πρόγραμμα των υπολογισμών και τα διαγράμματα εναρμόνισης (tuning) της παραμέτρου (ρk)p, το πρόγραμμα των υπολογισμών που συνοδεύουν τα πειράματα, καθώς και ένας οδηγός του κώδικα Catwall.

ABSTRACT

An experimental and computational investigation of pressure drop characteristics of Cellular Ceramic Diesel Particulate Filters (DPF) during the loading and regeneration process is presented in this thesis. Also an alternative method of estimation of the burned mass inside a DPF is demonstrated. The experiments-measurements were performed using mini-scale and full sized filters. A computational algorithm written in Fortran 90 assisted the analysis of experimental results. A validation of the computations has been performed by comparison between the experimental and computational results. The results cover a wide range of engine operation points. The relationship between the experimental – computational results for the mini-scale filter and the full sized filter measurements was investigated. Furthermore, the values of permeability - density parameter values resulting from the mini-scale-filter experiments were used as input data to the CATWALL regeneration code available in the laboratory. The results and the conclusions of the present investigation are presented in detail in the following sections.

PREFACE

Transportation constitutes one of the most significant factors for the worldwide advancement and prosperity. Nowadays, where we live in an ever-changing world, the minimization of traveling time and the advancement of mobility is a desirable means to improve human welfare. However this is not the only one.

Ecological concerns and the human need for a friendlier environment, pose great challenges to Industry and Transportation, which must respect the preservation

of our Natural Environment. Automotive technology could not escape from these demands. New emission standards are promulgated every 3-4 years, and legislation becomes increasingly stringent. Automotive manufacturers must attain emission limits by continuously improving their products. Thus they are forced to intensify research and development activities to improve exhaust emissions of their models, in close collaboration with R&D Institutions and University Laboratories.

The present thesis is related to the last-mentioned subject. Its target is the investigation of the characteristics of Diesel Particulate Filter loading process and the quantitative representation of them using the $(\rho k)p$ parameter. The experimental results will be correlated with computational results in order to find the relationship between the mini-scale and full-scale study of the phenomena that occur during the previously mentioned process.

I would like to express my acknowledgements to my supervisor Professor A.M. Stamatelos for my mentorship and the useful conversations we had during the process of this work.

Also I would like to express my acknowledgements to Professor N.S. Vlachos, which was my supervisor in the first Diploma thesis and had tried to introduce me in the world of CFD and Fluid Dynamics. Furthermore I would like to thank Professor V. Bontozoglou, Professor E. Stapountzis, which were my teachers during the post graduating course and Professor N. Pelekasis.

Special thanks are due to two PhD candidates of the Thermodynamics and Thermal engines laboratory, namely, Mr. G. Stratakis and Mr. G. Konstantas. Mr. Stratakis introduced me in the experimental setup, which he had developed at the beginning of my involvement in the measurements who conducted in cooperation. He gave me useful experience with regard to design, construction and assembly of mechanical systems and measuring devices, such as the mini-scale filters. Also I would like to thank Mr. Konstantas which, which provided me with useful hints.

Furthermore I would like to thank my parents, my sister and my friends. Thanks to Costas, Christos, Argiro, Eirini and Maria.

This work was supported by PSA and L.T.T.E. of U.Th.. Their support is gratefully appreciated.

NOMENCLATURE

A	area, [m^2]
C	Cunningham correction factor [-]
C	average pore size
C_D	Discharge coefficient, [-]
CI	Compression Ignition
Cp	Specific heat [J/kgK]
D	Diffusivity [m2/s]
DI	Direct Injection
$dm_{(i)}$	mass discharged on (i) time step, [kg/sec]
DPF	Diesel Particulate Filter
E	substrate thickness, [m]
e_F	filter collection efficiency
H	enthalpy [J]
h	heat transfer coefficient [J/m2K]
k	permeability, [m^2]
K	permeability [m^2]
k(T)	reaction rate constant
k_b	Boltzmann constant
Kn	Knudsen number
L	single channel filter length, [m]
L	length [m]
$\dot{m}_{real}$	real mass flow rate, [kg/sec]
m	mass, [kg]
M	Mass [kg]
M	Molecular weight
Ma	Mach number, [-]
$\mathbf{m_P}$	mass flux of products [kg/m^2 s]
$\mathbf{m_R}$	mass flux of reactants [kg/m^2 s]
m_v	mass of air present in the vessel, [kg]
P_0	vessel (identical with stagnation) pressure, [Pa]
Pe	Peclet number
p_o	Stagnation pressure, [Pa]
P_T	throat pressure, [Pa]
P_{Tc}	Calculated pressure in throat, [Pa]
P_{TG}	guessed pressure in throat, [Pa]
$\mathbf{q_k}$	conduction [W/m^2]
$\mathbf{q_{ku}}$	interphase surface convection [W/m^2]
$\mathbf{q_r}$	radiation [[W/m^2]

$\mathbf{q_u}$	intraphase convection flux [W/m^2]
R	ideal gas constant, (R_{air} = 287 kJ/(kgK))
SI	Spark Ignition
Stk	Stokes number
t	time, [s]
T	temperature, [K]
T_0	stagnation temperature, [K]
U	mean filtration velocity, [m/sec]
u	velocity, [m/sec]
U	internal energy [J]
V	vessel volume, [m^3]
w	single channel filter width, [m]

Greek letters

γ	specific heat ratio c_p/c_v, [-]
$(\Delta P)_c$	calculated pressure drop across single channel, [Pa]
$(\rho k)_p$	soot layer density times permeability product, [kg/m]
ΔP	pressure drop across single channel filter, [Pa]
ε	porosity [-]
Λ	ratio $(P_{TG} - P_{Tc})/ P_{TG}$
λ	mean free path of gas molecules, [m]
μ	dynamic viscosity, [kg/msec]
ρ	density, [kg/m^3]

Subscripts

a	Ambient
atm	Atmospheric
c	Calculated
ch	Channel
f	Filter
G	Guessed
g	Gas
i	time step
los	Losses
O	Stagnation
o	Initial
P	Particulate
p	Particle
real	not ideal
S	ceramic
s	surface
T	Throat
V	Vessel

Chapter1. INTRODUCTION

The Diesel Particulate Filter is an apparatus for particulate matter collection and incineration, that finds increasing application in diesel vehicles throughout the world. Its usefulness has risen from the social demand for a friendlier environment and the corresponding diesel soot emissions reduction legislation. The emission standards placed by the legislation are increasingly stringent and thus the further development of the various devices used in exhaust gas aftertreatment becomes necessary. Diesel Particulate Filter (or DPF) usually forms a part of an integrated exhaust gas aftertreatment system that may include also a catalytic converter, or an extra NOx trap. The system's operation is electronically controlled by the Engine Management System.

The development of aftertreatment systems and devices involve the collaboration between a wide range of scientists, engineers and industries. This becomes necessary because of the special environmental, engineering and economical importance, and the complexity of this subject. The pollution control engineering is a demanding field and automotive and related industries and other related organizations invest a significant percentage of their budget in research and development.

The current objectives of modern diesel engine technology, where European Industry traditionally takes the lead, are briefly the following: i) reduction of particulate and NOx emissions, ii) reduction of fuel consumption, iii) improvement of driveability and specific power output, iv) reduction of noise and vibration, v) further improvement of reliability and durability, vi) reduction in prime cost, vii) reduction in maintenance cost. The manufacturers' activity in meeting emissions legislation requirements are focused in the optimization of i) diesel engine technology (reduction of in-cylinder pollutants formation), ii) fuels, lubricants and fuel additives, iii) exhaust aftertreatment.

Especially for Diesel Particulate Matter emission reduction, the manufacturers requirements are:

- Use of an effective device and system able to meet the legislations limits.
- The system must be reliable.
- The system must operate in an economical way, in order not to destroy the fuel consumption advantages of the diesel engine.

For the 2004 legislation and beyond, the above requirements are accomplished only by the use of DPF. DPF technology is only necessary for Diesel particulate emissions reduction [1]. Gasoline engines emit very low particulate matter, which easily meets current soot emissions standards.

1.1 Starting point and objectives of the present thesis

The starting point of the present study consisted of:

- An engine assembled in engine bench accompanied with all the needed measurement devices.
- A one – dimensional computer code named 'Catwall' able to simulate the regeneration process.

The code refers to a wall- flow diesel particulate model able to handle thermal and catalytic regeneration by use of fuel additives.

The main objectives of the present thesis are the following:

1. Development of a system for measurement of soot in Diesel Particulate Filters. The system development involves:
   - Development of measurement device for measurement of soot maldistribution and pressure drop against time characteristics in full-scale filters (DPF) and in mini-scale filters.
   - Development of a computational algorithm able to calculate the (ρk)p product a significant parameter of soot in a loaded trap or in mini scale filter, based on the pressure recordings from the above-mentioned device.
2. Further development and application of an alternative method of trap loading estimation.
3. Cross checking of Catwall code against backpressure predictions, using as input data the values of the afore- mentioned significant parameters.

As regards to the first objective, it can be mentioned that a main difficulty encountered in the validation of diesel filter regeneration models lies in the extraction of realistic particulate properties by the experiments. Tests with a real filter loaded and regenerated are more realistic than these with mini- scale filters and synthetic soot accumulation but the operating conditions (particulate loading, flow distribution in the filter, exhaust gas properties) are more difficult to control within prescribed close

tolerances. Better understanding of these effects are sought in this thesis, by means of experimental study of pressure drop and flow distribution inside mini-sized and full sized filter specimens.

A novel technique is developed that allows us to estimate with sufficient accuracy the product of soot layer permeability and soot density in a single filter channel. This is effected through the recording of the discharge process of a vessel containing air, connected to the filter channel, that maybe loaded with real exhaust gas at different engine operation points and up to different particulate loading levels.

The vessel discharges through a specially designed nozzle, modified to be able to connect it directly to the channels of real filters of various cell sizes. Based on the processing of the experimental results, a first approach to the understanding of soot mass and ash residual distribution inside the filter is presented. By comparing loading estimates based on measurements on various channels, we can assess the effect of incompletely regenerated regions and improve understanding and modeling of pressure drop and catalytic regeneration.

1.2 Structure of the thesis

The present thesis is structured as follows:

Chapter1 contains a brief discussion of diesel engine features, emissions, particulates and emission legislation in Europe and in the USA. The next paragraphs are dedicated to the modes of emission control and DPF systems and their operation is presented.

Diesel Particulate Filters are porous media. Thus in Chapter2, porous media and the nonequilibrium processes that occur inside them are discussed, in order to give an idea to the reader about the porous media flow and filtration mechanisms.

The experiments performed for the investigation of pressure drop characteristics are discussed in Chapter3. The experimental procedure, the single-channel and full-scale trap measurement implementation and the measurements' protocols are presented also in the same chapter.

The necessary computational assistance to the experiments performed is demonstrated in Chapter4, where the computational concepts, the filter pressure drop approximations and the computation algorithm are presented.

Chapter5 contains the Results and Discussion of the combined experiments and calculations discussed in the two previous chapters. The results concern the mini- and the full-scale filters- experiments and the final aim of this chapter is to investigate the relationship between the mini-scale and real filter performance in the soot loading process.

In Chapter6 a validation of the predictive capacity of the Catwall code regarding the pressure drop takes place, with the mini- filter experimental results used as input. A significant number of available experiments and tests are employed in this task. There is a list of simulated experiments that poses a parametrical study of (ρk)p parameter for the values obtained by the experiments.

The other critical factor for a successful regeneration simulation is the accurate knowledge of burned soot mass in the filter during regeneration. An alternative estimation method is presented in Chapter7. In this chapter the method and its applications are demonstrated.

Chapter8 offers a synopsis of the work presented in this thesis, in order to give to the reader a thorough view of what has been done in the present thesis, Finally, a presentation of possible directions of future work is given.

At the end of this thesis there are Appendices that contain Fortran code listings, the tuning diagrams for the various cases studied and modeled, as well as a short guide to CATWALL operation and structure.

1.3 Features of Diesel Engines

In Compression Ignition engines (CI) air alone is inducted into the cylinder. The fuel is injected directly into the engine cylinder just before the start of the combustion process. Load control is achieved by varying the amount of fuel injected for each cycle; air flowrate at a given engine speed is essentially unchanged. The compression ratio varies between 12-24 and the efficiency of diesel engine is greater than that of gasoline, as can be seen in Figure 1.

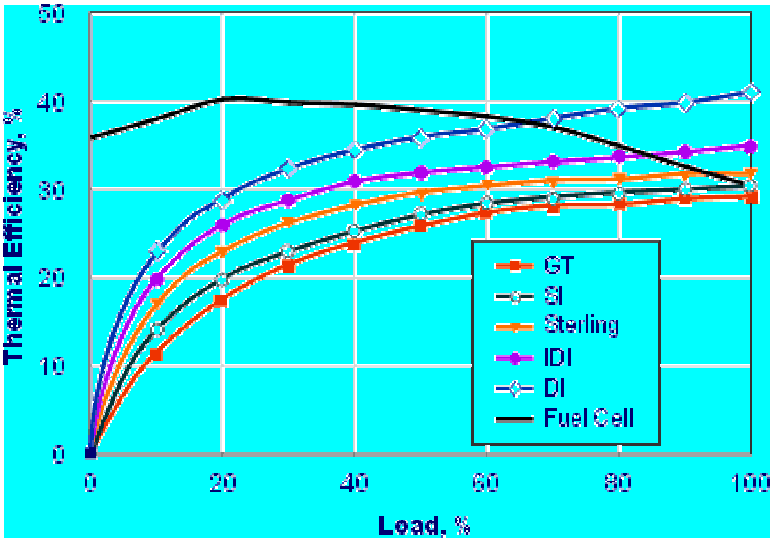

Figure 1 Efficiency of different types of engine. Gas Turbine, Spark Ignition, (In)Direct Injection diesel engine [2].

This type of engine has obviously some advantages and disadvantages presented in Table 1. Modern diesel engine technology diminishes its disadvantages. Today, soot emissions reduction is the last remaining frontier for the diesel engine.

Table 1 Advantages and Disadvantages of Diesel Engine [3]

Advantages	**Disadvantages**
Fuel economy	Noise
Durability	Weight
Low HC emissions	High NOx emissions
Low CO emissions	High particulates emissions
High Torque	Low speed
Reliability	Low air utilization
Low fuel cost	High engine manufacture cost
Low maintenance cost	Low exhaust gas temperature

Figure 2 presents a typical exergy analysis comparison between diesel and gasoline engine.

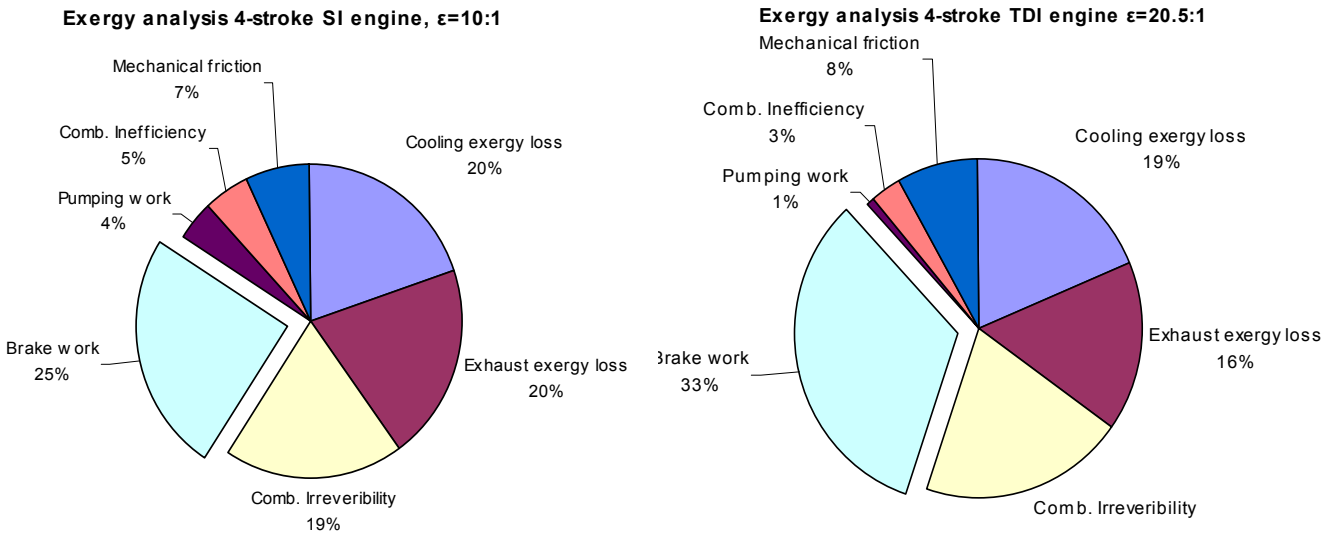

Figure 2 Exergy analysis comparison between a Diesel DI and an Otto (4 stroke) engine. (2000 rpm, mep=3bar) [4]

1.4 Diesel Engine Emissions

Diesel engine emissions are highly complex mixtures. The composition of diesel exhaust varies considerably depending on engine type and operating conditions, fuel, lubricating oil, and whether an emissions control system is present. Various researchers [5,6] have studied the effects of the fuel composition and properties on the particle formation.

Diesel emissions consist of a wide range of organic and inorganic compounds distributed among the gaseous and particulate phases: CO, CO_2 (although it is not a pollutant, it is responsible for the greenhouse effect), NO, NO_2, Nitric oxides, Nitrous oxide (N_2O), NH_3, Volatile organic compounds and evaporation losses, Hydrocarbons (HC), Polynuclear aromatic hydrocarbons, Carboxyl compounds, Organic acids, Halogenated organic compounds, Sulfur dioxide, Dioxins.

The majority of the previous mentioned pollutants when are present in high concentrations are toxic and are suspected for a series of adverse effects on the human life, on the physiology of plants and the integrity of the minerals used in manmade structures. Also air pollution is blamed for the acidification of lakes, for acid rain, for the death of the forests and for reduced visibility in large cities. [7] and [10] offer a more detailed analysis about pollutants and the effects that they have on human health and the environment. Table 2 presents typical values of the exhaust gas components.

Table 2 Typical exhaust gas components [8]

Component	Concentration	Component	Concentration
CO	100-10000 ppm	Aldehydes	0 mg/mile
HC	50-500 ppm C_1	Ammonia	2 mg/mile
NOx	30-1000 ppm	Cyanide	1 mg/mile
SOx	Proportional to fuel S content	Benzene	6 mg/mile
PM	20-200 mg/m^3	Toluene	2 mg/mile
CO_2	2-12 vol%	PAH	0.3 mg/mile

Public health concern has arisen about these emissions for the following reasons:

- The particles in diesel emissions are very small (90% are less than 1μm by mass), making them readily respirable.
- These particles have hundreds of chemicals adsorbed onto their surfaces, including many known or suspected mutagens and carcinogens.
- The gaseous phase contains many irritants and toxic chemicals.
- Oxides of nitrogen, which are ozone precursors, are among the combustion products in the gaseous phase.
- There is likelihood for humans to be exposed to diesel emissions or their atmospheric transformation products in both ambient and occupational settings.

Diesel engines are only one of many sources of ambient particulate matter and gaseous air pollutants [9]. Therefore, it is difficult to measure the exposures from various sources, and to distinguish the potential health risks attributable to exposure to diesel exhaust from those attributable to other air pollutants [10]. Figure 3 shows a comparative graph between CI and SI engine emissions.

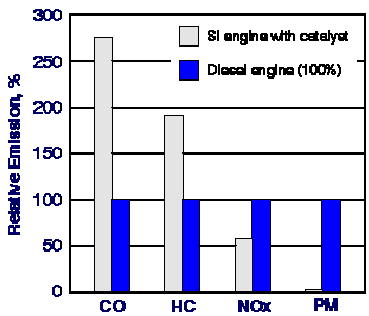

Figure 3 Diesel and gasoline engine emissions during the European driving cycle

1.4.1 Diesel Particulate Matter

The term 'particle' generally applies to aerosols created by the dispersion in air of atomised solids and liquids, powders or droplets, and hence includes the terms "fines, dust, soot, mist, fog and smog". Their diameter is smaller than 10μm.

Inside an engine, the complete combustion of motor fuels composed exclusively of carbon and hydrogen, would only generate CO_2 and H_2O, to the exclusion of any other harmful product. However, the very short time allowed for chemical oxidation processes to take place in combustion chambers, the lack of homogeneity in the carbureted mixtures, and the heterogeneity and rapid variations in temperature never allow the state of ideal thermodynamic equilibrium to be reached.

This means that products of incomplete combustion are present in the exhaust, as well as sulfur compounds from the sulfur-bearing residues remaining in motor fuels. Added to this, combustion products are nitrogen oxides formed by the high-temperature oxidation of the inert nitrogen present as diluents in the air.

In the burning of liquid fuels of the diesel type, the size of the droplets and hence the quality of spraying are extremely important because the formation of soot increases with droplet size. Table 3 summarizes the parameters that favor diesel particulate emissions.

Table 3 Main characteristics influencing particulate formation [11]

Formation of insoluble fraction favored by:	• Elevated temperature • High pressure • Absence of oxygen
Oxidation of the insoluble fraction favored by:	• Elevated temperature • High pressure • Presence of Oxygen
Formation of HC particles favored by:	• Lean mixture zones • Temperatures below the flammability limit • Hydrocarbons layers on the walls of the bowl • Fuel droplets seeping at the nozzle tip
Sources of particles from the lubricant:	• Surface of cylinder liners • Valve stem gaskets • Turbo-compressor gaskets • Recycle of crankcase gases to inlet

Diesel particulates are composed of elemental carbon particles, which may agglomerate and adsorb other species to form structures of complex physical and chemical properties. Diesel particulates have a bimodal size distribution. They are a mixture of *nuclei mode* and *accumulation mode* particles (Figure 4). The nuclei mode

particles are very small - their diameters are usually between 0.007 and 0.04 μm (micron). These particles originate from the primary carbon spherules, which are generated in the combustion chamber. As the exhaust gases cool down after leaving the engine cylinder, nucleation of hydrated sulfuric acid also produces nuclei mode particles, which are known as sulfate particulates. Under certain conditions, nucleation of hydrocarbons may also occur. The accumulation mode particles are formed by agglomeration of carbonaceous, nuclei mode particles.

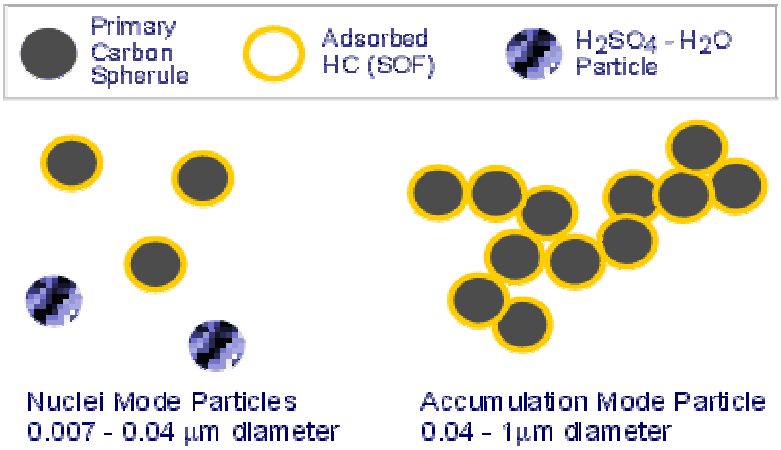

Figure 4 Schematic of Diesel Particulate Matter

Finally, an important fraction of diesel particulates is formed by heavy hydrocarbons, which condense and adsorb on both nuclei and agglomerated carbon particles. DPM is commonly divided into three main fractions, which can be further sub-categorized, as follows [12]:

(A) **Solid fraction (SOL)** (i)elemental carbon, (ii) ash.

(B) **Soluble organic fraction (SOF)** (i) organic material derived from engine lubricating oil, (ii) organic material derived from fuel

(C) **Sulfate particulates (SO4)** (i) sulfuric acid (ii) water

The composition of DPM varies greatly depending on the engine technology, test conditions, and, in the case of sulfate particulates, the sulfur content in the fuel. An example DPM composition from a post-1994 US heavy-duty engine is illustrated in Figure 5.

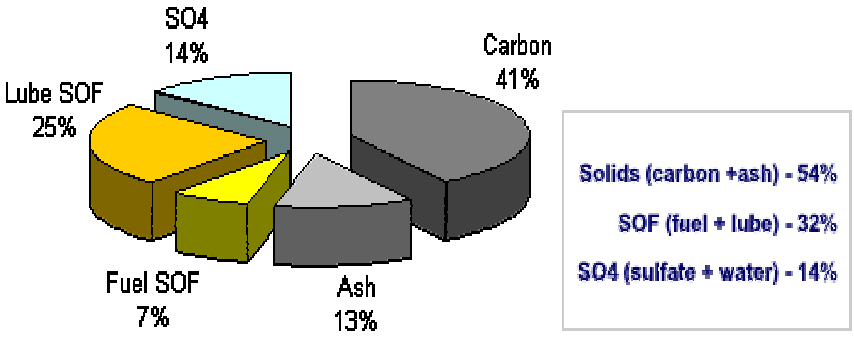

Figure 5 Diesel Particulate Matter Composition

1.4.2 Diesel exhaust particle size

Diesel particulates compose a distribution of various sizes, which can be divided into the following categories as well as ambient particulate matter:

- *PM10* - particulates of an aerodynamic diameter of less than 10μm
- *Fine particles* of diameters below 2.5μm
- *Ultrafine particles* of diameters below 0.1μm or 100nm
- *Nanoparticles*, characterized by diameters of less than 50nm.

A typical size distribution of diesel exhaust particulates is shown in Figure 6. Practically all diesel particulates have sizes of significantly less than 1μm. As such, they represent a mixture of fine, ultrafine, and nanoparticles. The coarse mode diesel particles with aerodynamic diameters above 1μm constitute only a small fraction of the total PM emissions. The coarse particles are not generated in the diesel combustion process. Rather, they are formed through deposition and subsequent blow-off of particulate material from the walls of the exhaust system or the particulate sampling system.

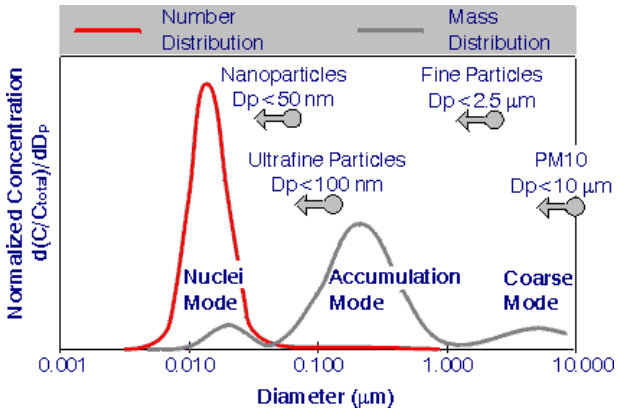

Figure 6 Diesel Particulate Size Distribution [13]

1.5 Emissions Legislation

The automotive industry must produce vehicles in accordance with the latest posed emissions limits [14]. The prescribed limits are different for USA and EU and are described in brief below.

1.5.1 Emissions legislation in the USA

The exhaust emissions are designated from EPA (U.S. Environmental Protection Agency) in 1990. There are two types of regulations: Tier 1 (enacted in 1991 and applied in 1997) and Tier 2 (enacted in 1999 and will be applied in 2004).

Tier 2 Regulation.

Tier 2 regulation is valid for all vehicles of any weight. Thus the larger engines must have higher ecological standards, in order to achieve the permitted emissions limits. Although Tier 1 is implemented for light vehicles down to 8500lb, Tier 2 will be implemented for vehicles about 10000lb. It is valid for any vehicle and for any consumed fuel. All the manufacturers must classify their vehicles into one from eight classes, while the mean value of NOx emission must be less than 0.07gr/mile. Tier 2 will be valid for the time period between 2004 and 2009. Table 4 presents the emissions limits, which are introduced with Tier 2 and are applicable in FTP 75 driving cycle. Emissions are measured in gr/mile.

Table 4 Tier 2 Regulation

Class	50,000 miles					120,000 miles				
	NMOG	CO	NOx	PM	HCHO	NMOG	CO	NOx*	PM	HCHO
Transient classes										
MDPV						0.280	7.3	0.9	0.12	0.032
10	0.125 (0.160)	3.4 (4.4)	0.4	-	0.015 (0.018)	0.156 (0.230)	4.2 (6.4)	0.6	0.08	0.018 (0.027)
9	0.075 (0.140)	3.4	0.2	-	0.015	0.090 (0.180)	4.2	0.3	0.06	0.018
Substantive classes										
8	0.100 (0.125)	3.4	0.14	-	0.015	0.125 (0.156)	4.2	0.20	0.02	0.018
7	0.075	3.4	0.11	-	0.015	0.090	4.2	0.15	0.02	0.018
6	0.075	3.4	0.08	-	0.015	0.090	4.2	0.10	0.01	0.018
5	0.075	3.4	0.05	-	0.015	0.090	4.2	0.07	0.01	0.018
4	-	-	-	-	-	0.070	2.1	0.04	0.01	0.011
3	-	-	-	-	-	0.055	2.1	0.03	0.01	0.011
2	-	-	-	-	-	0.010	2.1	0.02	0.01	0.004
1	-	-	-	-	-	0.000	0.0	0.00	0.00	0.000

* the mean value NOx emissions limit is 0.07gr/mile

Tier 2 regulation will require after-treatment devices such as catalysts or particulate filters, and more ecological fuels. Thus the S contained in gasoline must be less than 300ppm from 2004 and 80ppm from 2006. The limits in diesel fuel have been prescribed since 1999.

1.5.2 European Union's emissions legislation

The 70/220/EEC directive initially designated the emissions limits and it was consisted of Euro 1 και Euro 2 regulations (93/59/EC directive) the more recent regulations Euro 3 and 4 (98/69/EC directive). The regulations, which are valid for the time period between 2000 and 2005 impose improved fuel quality. The least diesel cetane number must be 51 and the maximum sulfur concentration must be down to 350ppm from 2000 and 50ppm in 2005. Gasoline must contain sulfur down to 150ppm in 2000 and 50ppm in 2005. The adopted driving cycle is the NEDC.

European limits for gasoline are distinct from these for diesel engines. Diesel engines must produce lower CO relative to gasoline engines but the NOx limits are slightly sharp. On the other hand gasoline engines have no particulate emission limit. Table 5 presents the EU emission limits.

Table 5 EU Regulations [8]

	Passenger cars						
Standard	Year	Test Cycle	HC+NOx gr/km	NOx gr/km	CO gr/km	PM gr/km	
Euro III	2000	ECE 15/EUDC	0.56	0.5	0.64	0.05	
Euro IV	2005	ECE 15/EUDC	0.3	0.25	0.5	0.025	
Class	Light duty trucks						
I(<1305 kg)	2000	ECE 15/EUDC	0.56	0.5	0.64	0.05	
	2005	ECE 15/EUDC	0.3	0.25	0.5	0.025	
II(1305-1760kg)	2001	ECE 15/EUDC	0.72	0.65	0.8	0.07	
	2006	ECE 15/EUDC	0.39	0.33	0.63	0.04	
III (>1760kg)	2001	ECE 15/EUDC	0.86	0.78	0.95	0.1	
	2006	ECE 15/EUDC	0.46	0.39	0.74	0.06	
	Heavy duty trucks						
Standard	Year	Test Cycle	HC gr/kWh	NOx gr/kWh	CO gr/kWh	PM gr/kWh	Smoke m^{-1}
Euro IV	2005.10	ESC/ELR ETC	0.46	2.0	1.5	0.02	0.5
Euro V	2008.10	ESC/ELR ETC	0.55	2.0	4.0	0.03	0.5

The driving life on any vehicle is 80.000 km in Euro 3 and 100.000 km in Euro 4.

1.6 Modes of emission control

The requested engine emission control can be achieved by modifications applied in the below mentioned critical points [15]. These are in brief:

Diesel engine

- Combustion chamber (optimum design of piston – cylinder head for increased turbulence, leading to decrease in particulate emissions).
- Injection system (optimum injection. The main parameters are timing and duration, amount and scattering of fuel droplets).
- Electronic control of engine (optimum performance in wide spread operation points independently of the aftertreatment limits).
- Recirculation of exhaust gases (E.G.R. NOx emissions regulation)
- Injection of water (NOx emissions regulation)
- Air induction system (optimum design of inlet duct and valve for increased turbulence).

Fuels and lubricants

- Fuels (modification of the fuel composition by reduction of aromatics and S contained in the fuel for sulfur and particulate reduction)
- Lubricants (development of synthetic lubricants with low contain in metal additives for minimization of ash and low volatilisation index for low particulate emissions).
- Alternative fuels (natural oil or animal grease products can be used in diesel engines reducing particulates emissions due to the increased oxygen concentration)

  E*xhaust aftertreatment*
- Oxidizing catalyst
- Lean NOx catalyst (under development, not commercially available)
- Selective Catalytic Reduction (NOx reduction catalyst – commercially available only for stationary engines)
- Particulate trap

It must be mentioned that the NOx and particulates formation mechanisms act conversely. So it is necessary to simultaneously use the respective exhaust aftertreatment technologies.

1.7 DPF Systems and Classification

The combustion of soot, even if facilitated by the addition of catalysts, remain a slow process, and its duration always exceeds the particulate residence time in the exhaust system. For kinetic reasons, it is therefore necessary to eliminate the soot in two steps: filtration and trapping of the particulates in the first phase and then once the critical mass sufficient to maintain combustion is reached, ignition and combustion in a second phase, making sure that the mass to be burned is not so large as to result in temperatures incompatible with the thermal resistance of the trap.

DPF presents an extremely good behavior in soot trapping as its attained efficiency reaches 90% so it's the most efficient after-treatment device as regards particulate emissions [16]. However a list of specific application problems basically related to filter durability, had limited the use of particulate traps mainly on city buses or trucks [17]. Peugeot is one of the first passenger vehicle manufacturers who used DPF in a commercial passenger car.

Diesel filter systems are designed by combining different filter materials with selected regeneration methods. The major system design considerations include

emission performance, pressure drop, durability, maintenance, and cost. Filter system design targets can be listed as follows: (i) High PM collection efficiency: gravimetric particulate collection efficiency, sulfate formation, penetration of small particles (<0.1 μm), particle number emissions, (ii) Reduction of gaseous emissions CO, HC, etc. which is a future trend, (iii) No generation of secondary emissions in the filter: increase of gas emissions (CO, HC, NO_2,…), new gas emissions (dioxins, ...), additive ash emission, fiber loss, (iv) Low pressure drop (average or maximum), (v) High durability, total life span, (vi) Low maintenance requirements, cleaning/service frequency, (vii) Low cost: total investment cost, and low maintenance cost Figure 8 shows a classification of diesel filter systems based on the principle of regeneration.

DPF makes use of the wall – flow filtration concept. The porous walls of the filter do not permit the soot particles to flow through. Thus soot accumulation occurs inside the trap leading to higher backpressures (or the pressure difference) across the trap, which is necessary to force the exhaust through it. The filter type, the form and the amount of soot accumulation, the fuel additive and the engine operation point determine the level of trap backpressure rise. The excessive pressure difference across the trap is undesirable as long as it leads to increased fuel consumption and decrease in available power. Thus the trap must be periodically cleaned by an effective way or, in different words, by burning the accumulated soot particles. Figure 7 presents a schematic diagram of DPF operation.

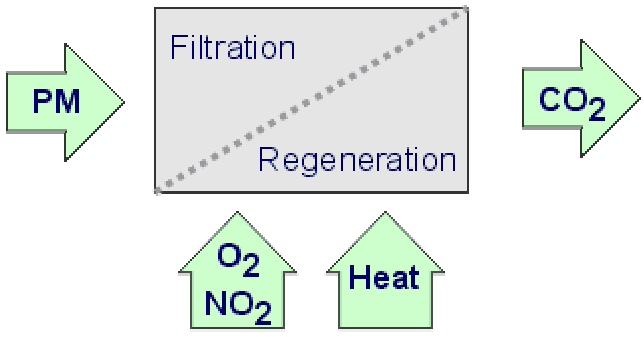

Figure 7 Schematic diagram of the DPF principle of operation

Two of the main parameters involved in loading and regeneration process are the soot mass collected and burned into the trap and the form of the soot accumulated into the trap. The last is indicated by a parameter called (ρk)p product which includes

the effect of density (ρ) and permeability (k) of the particles trapped to the filter. The present thesis is focused mainly to the last two mentioned magnitudes. Some of the research works, which focused on the study of this phenomenon and on the investigation of the full – scale trap loading effects, are presented in [38], [43] and [42].

An acceptable diesel filter system has to provide means of regeneration, preferably a fully automatic regeneration. Most regenerating diesel filter systems of practical importance utilize thermal regeneration, during which the particulates are oxidized to produce gaseous products. The temperature of diesel exhaust gas is, however, too low to sustain auto-regeneration of the trap. That problem may be solved by either (1) decreasing the required soot combustion temperature to a level that is reached during regular engine operation, or (2) increasing the temperature of the trapped soot to a point where it starts oxidizing. The first approach is used in **passive** filter systems, the second in **active** filter systems.

In passive systems the soot oxidation temperature is lowered to a level allowing for auto-regeneration during regular vehicle operation. This can be achieved by introducing an oxidation catalyst to the system.

The second approach is to actively trigger regeneration by raising the temperature in the trap. Most of the active filter systems use either electric heaters or fuel burners. The active trap systems are much more complex than passive filters. They require sophisticated hardware, including an electronic control unit to trigger and control the regeneration process. Their operation may also involve high fuel economy penalties associated with the energy required to achieve temperatures needed for regeneration.

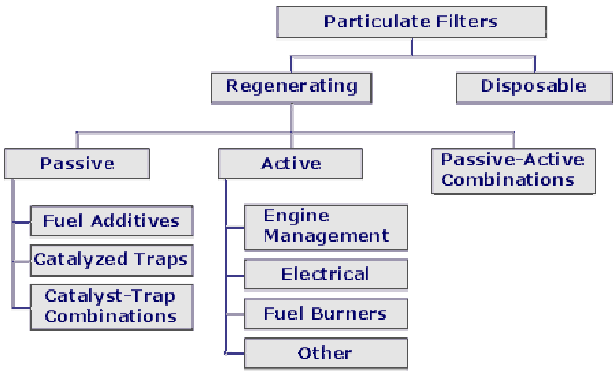

Figure 8 Classification of Filter Systems by Regeneration Method [18]

Design targets for diesel particulate filter materials include high filtration efficiency, high soot holding capacity, high maximum use temperature, low coefficient of thermal expansion, high resistance to thermal stress, high strength, low reactivity with ash compounds, oxidation resistance, coatability with a catalyst, compatibility with regeneration methods (e.g., with fuel additives), low pressure drop (empty, loaded with particulates and ashes), small size, and low weight [19]. Various types of Diesel particulate traps are presented in Table 6.

Table 6 Diesel particulate traps [39]

Type of trap	**Efficiency %**	**Advantages**	**Drawbacks**
Ceramic monolith	60 – 95	• High efficiency • Moderate cost • Can be covered with catalyst	• Moderate ΔP • High ΔP gradient • Subject to thermal shock cracking
Aluminated metallic sponge (precious metal catalyst)	50 – 80	• Low ΔP gradient • Self regenerable • Reduces (HC, CO and odor)	• Moderate ΔP • Low efficiency especially at sigh speed • Produce sulfates
Ceramic foam	30 – 75	• Good thermal shock resistance • Can be covered with catalyst	• Regeneration difficult • Very high ΔP • Low efficiency
Ceramic fiber sponge	>75	• Very high efficiency • Good thermal shock resistance	• Fiber disintegration • High ΔP gradient • Large volume and weight
Woven silica fiber coil filter	>75	• Good thermal shock resistance • Low ΔP • High efficiency	• Large volume demand

1.8 Active DPF control operation

Typical diesel particulate consists mainly of a carbonaceous core (soot formed during combustion), with adsorbed compounds such us unburned and partially oxygenated hydrocarbons (VOF), as well as sulfates and metal oxides [20].

The demand to periodically clean the filter by burning off (oxidizing) the collected particulate (filter regeneration) under unfavourable conditions of low exhaust temperatures met in modern diesel engine exhaust systems, led to the wide application of catalysts [21,22,23,24]. The doping of the diesel fuel with catalytic additives (usually in the form of organometallic compounds) is today a workable catalytic regeneration technique. However, further design optimisation of fuel additive assisted trap systems seems to be necessary, involving the solution of problems related to filter durability and additive ash accumulation.

The support by an active regeneration strategy employing measures by the engine control unit (ECU) is usually employed in practice, to secure the onset of regeneration above a specific soot loading threshold. Filter soot loading can only be indirectly assessed by the ECU, based on the recording of pressure drop, engine speed, exhaust temperature and fuel flow rate [25]. The above parameters that the ECU needs to sense in order to assess the necessity of activating regeneration, are presented in Figure 9.

The estimation of soot mass as function of pressure drop and engine operating parameters has proven to be a complex task. Furthermore, this dependence seems to be affected by filter regeneration history, due to the effects of soot remained from previous, incomplete regeneration events. Such incomplete regeneration may be observed at the filter periphery due to the lower temperatures prevailing there. The effect of residual soot mass from a previous incomplete regeneration becomes prominent if we compare filter loading curves of a virgin filter and a loaded and subsequently incompletely regenerated filter, as presented in Figure 10.

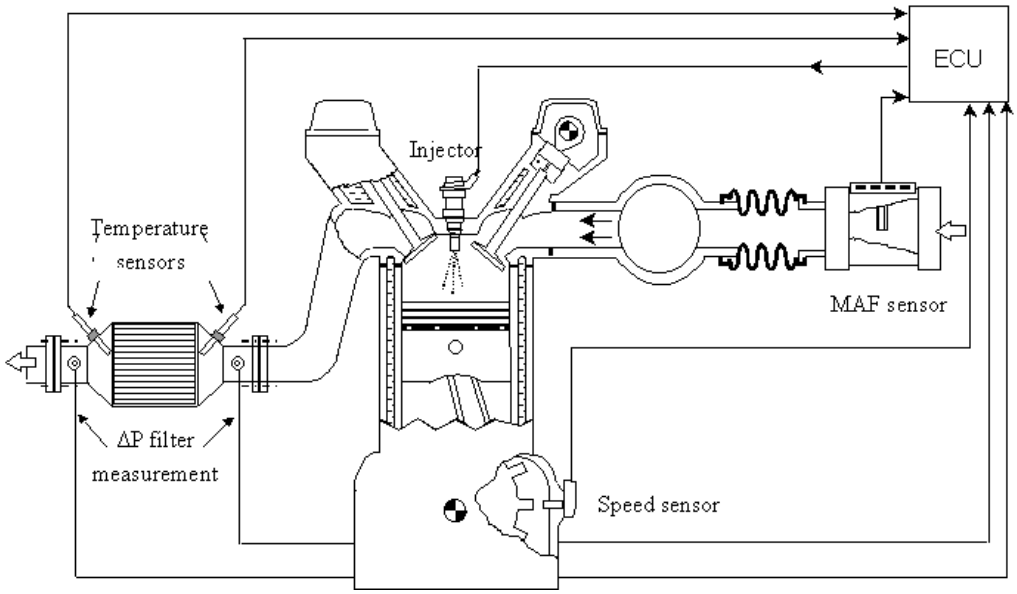

Figure 9. Schematic diagram of an active diesel particulate filter control system

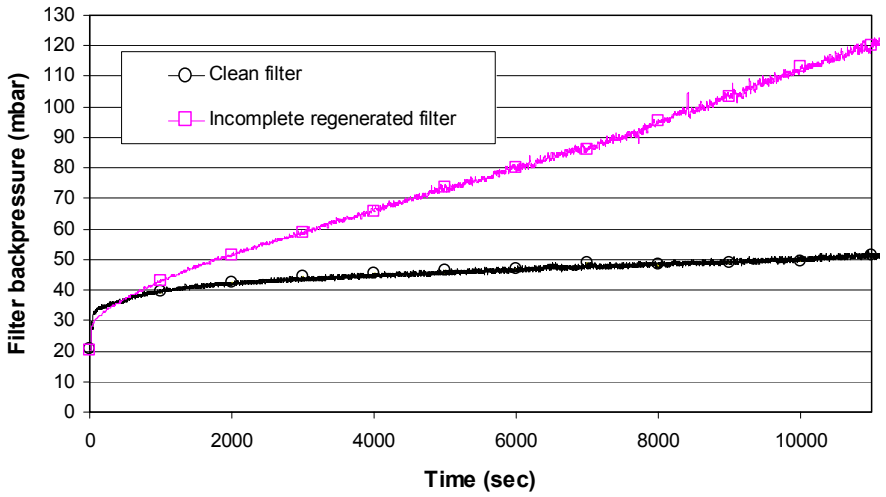

Figure 10.Loading curves for clean and incompletely regenerated filter (Filter type: SiC 14/200 5.66"x6", Engine: DW10ATED speed=1250rpm, torque=30 Nm)

In both cases, initial backpressure is approximately equal. However, the backpressure increase with loading at the same engine operation point (same particulate emissions), is observed to be much steeper with the partially regenerated filter. This can be explained by the fact that total filter pressure drop is governed by the channels of minimal resistance to exhaust gas flow and not to the soot loading of the average filter channel.

On the other hand, design optimization of diesel particulate filter systems is increasingly depended on efficient modeling of the filter regeneration process [26]. A significant number of 1-D and even 3-D models have been presented in the literature

[27,28,29,30], covering thermal and catalytic regeneration. The currently employed models should be able to predict the propagation of regeneration in the trap in real world operation on the vehicle or engine bench by taking into account the dominating processes in the filter, namely [37]:

- filter back-pressure as function of geometrical and operating parameters for different particulate loadings.
- thermal and chemical processes inside the filter, including heat transfer and particulate oxidation by exhaust oxygen (with or without the use of catalytic aids).

Chapter2. POROUS MEDIA FLOW AND FILTRATION MECHANISMS

2.1 Porous Media

Diesel Particulate Filters are porous media. The processes such as the combustion of soot during regeneration and, more generally, the transport phenomena that occur in inert catalytic and combustible porous media are non-equilibrium processes.

The phenomena related with porous media occur under the influence of a large range of geometric length scales, thermophysical and thermochemical properties, and flow, heat and mass transfer conditions as a result a large range of phenomenological length and time scales control the extend of departure from local thermal and chemical process. So it is useful to study intraphase and interphase nonequilibria. In this thesis, a few words will be written in order to give an idea about the flow through porous media and the loading and combustion processes inside them.

2.1.1 Porous media flow

The fluid mechanics of the single – phase flow begins with Darcy law and continues with developing along more rigorous treatments based on the local volume averaging. As with any other technological problem the treatment of this kind of flow has been a combination of direct empirical response on the one hand and a more rigorous first principles approach on the other hand. A porous medium, being an heterogeneous system made of solid matrix with its void filled with fluids, can be treated as a continuum by properly accounting for the role of each phase in transport through this system of phases. Darcy in 1856 was the first to investigate the porous media flow concepts.

As long as DPF are classified in the class of porous media the basic laws for porous media flow can be applied either for filter loading, regeneration and soot permeability measurement.

Single Phase Flow – Darcy Momentum Equation

According to Darcy's law the relationship between the filtration velocity and the pressure drop across the porous media in (Figure 11) is given by equation (2-1)**.** The macroscopic flow is assumed steady and one dimensional.

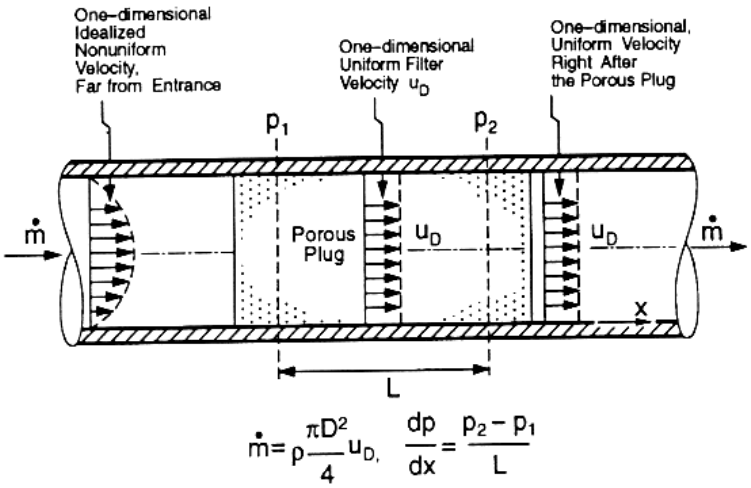

Figure 11 Flow through porous medium

The bulk resistance can be characterized by the viscosity of the Newtonian fluid (fluid parameter) μ and the permeability of the solid matrix (solid matrix parameter) K [33]:

$$-\frac{dp}{dx} = \frac{\mu}{K} u_D \qquad \textbf{(2-1)}$$

The permeability accounts for the interstitial surface area, the fluid particle path as it flows through the matrix, and other related hydrodynamic characteristics of the matrix. The Darcy model has been examined rather extensively and is not closely followed for liquid flows at high velocities and for gas at very low and very high velocity and low pressure. The fluid flow through the matrix can be viewed as flow through tortuous conduits (capillary models) or as flow over objects (drag models).At low gas pressures and for small pore size, the mean free path of the gas molecule may be of the order of the pore size and therefore velocity slip occurs (Knudsen effect).

For isotropic media where the pressure gradient ∇p and the velocity vector $\mathbf{u_D}$ are parallel Eq. (2-1) is generalized to

$$-\nabla p = \frac{\mu}{K} u_D \qquad \textbf{(2-2)}$$

2.1.2 Porosity

The volume occupied by voids, i.e., the total void volume divided by the total volume occupied by the solid matrix and void volumes, is called the porosity. Each void is connected to more than one other pore (interconnected), connected to one other pore (dead end), or not connected to any other pore (isolated). Fluid flows through the interconnected pores only. The volume fraction of the interconnected pores is called the *effective porosity*. In nonconsolidated media, e.g. particles loosely packed, the effective porosity and porosity are equal. In some consolidated media, the difference between the two can be substantial.

In general the voids are nonuniform in their size and in their distribution throughout the matrix. The nonuniformity of the void size and the distribution in their bulk of the matrix are usually presented through distribution of statistically averaged local values (along with deviations). These statistical averages are taken over volumes that are larger than the pore volume but much smaller than the volume of the entire solid matrix.

The nonuniformities near the boundaries (confining solid or free surfaces) can play a significant role in the transfer rates at the boundaries and should be treated with meaningful local distributions (i.e. different than the bulk properties). For example, the packing arrangement of spheres near the boundaries is different than the bulk. When the confining boundary is a solid surface, the larger porosities adjacent to this surface result in reduction of the resistance to the flow and, therefore, to an increase in local velocity in this area. This is called channeling and occurs over a distance of several particle diameters from the surface.

2.1.3 Pore structure

Pores can be very large (often called caverns) or very small (of the order of atomic or molecular size, called micropores or ultramicropores). They are three – dimensional and some of them are connected. Figure 12 gives a classification of the matrix structure. In packed beds of particles, the particles may eventually become consolidated due to physical and chemical reactions. The major divisions are based on ordered, disordered and isotropic. The structures that are most suitable for a deterministic, thorough analysis are simple periodic structures.

2.1.4 Permeability

According to the Darcy law (Eq (2-1)) the permeability K is the measure of the flow conductance of the matrix.

The bulk hydrodynamic behavior can also be obtained from the application of the first principles (mass and momentum conservation) to flow of viscous fluids at the pore level (including pore surface roughness and temperature effects [31]). However, such an application is a very large undertaking for complex geometries and has only been applied in a few simple structures. This is because the geometry of the fluid conduit is three-dimensional and complex. For complex geometries the paths taken are in application of the Navier – Stokes equation to fluid flow through complex channels (capillary models), application of these equations to flow over objects (drag models), and a semiheuristic approach of hydraulic radius. The first two are being pursued more rigorously as part of modern fluid dynamics.

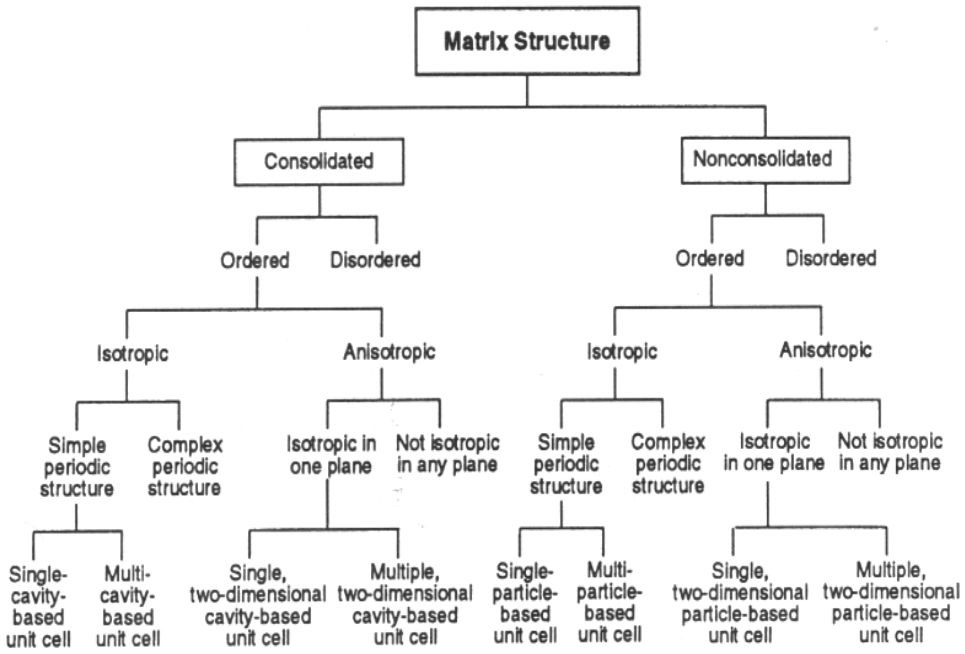

Figure 12 Classification of matrix structure.

2.1.5 Knudsen flow

Deviations from the viscous flow behavior at low pressures (or for very small pore sizes) have been observed because the mean free path of the gas molecule may be of the order of the pore size and therefore velocity slip occurs.

From ideal gas behavior, we have:

$$\rho = \frac{pM}{R_g T} \tag{2-3}$$

where R_g is the universal gas constant (8.3144 kJ/kg.mole.K) and M is the molecular weight. The mean free path of molecules, the average distance the molecules travel between two successive collisions, is given as:

$$\lambda = \frac{k_B T}{2^{2.5} \pi R_m^2 p} \tag{2-4}$$

The Knudsen number is a measure of the probability of the molecule – molecule collision compared to that for the molecule – matrix surface collision and is defined as

$$Kn = \frac{\lambda}{C} \tag{2-5}$$

where C is the average pore size or interparticle clearance and λ is the mean free path of gas molecules. For Kn>>1 flow is referred to as the molecular or Knudsen flow and the fluid velocity at the wall can be considered as zero, while the flow is called viscous in the opposite case (Kn << 1). Then the velocity near the wall is zero. The regime between these two is called the transition – flow regime. For the soot layer, the mean pore diameter is assumed to be close to 0.1 μm. The Kn number is close to unity and slip flow cannot be neglected.

2.1.6 Semiheuristic momentum equations

As much as it is desirable to have one set of governing equations that can describe both the momentum transport through the porous media (K being small) as well as that in the plain media (K being very large), such equations, if they become available [32], will be too complicated to be of practical use. However the Bringman inclusion of a viscous shear stress term (other than bulk viscous shear stress), which can take into account the shear stresses initiated at the surfaces bounding the porous media (macroscopic shear), attempts are being made to arrive at an equivalent of the

Navier – Stokes equation for the description of flow through porous media. Extensions of the Darcy law are being sought to include the following [33].

As regard to flow development in porous media, the macroscopic entrance length as predicted by the macroscopic equations and by the direct simulations is rather small. Using the macroscopic equations the bulk resistance term dampens the velocity in the high flow rate zone and rapidly makes for a uniform velocity field

As regard to boundary generated vorticity (or the boundary effect) it can be written that is similar to the entrance length as long as the damping of the vorticity (shear stress) generated at the confining walls takes place over a very short distance.

High Reynolds number effect: the microscopic flow regime changes as the Reynolds number (pore level) increases and a pore – level flow development term must be added to the Darcy law to account for the extra pressure drop at high Reynolds numbers.

Among the versions of the extended Darcy law for conservation of momentum (differential) is the following relationship [33]:

$$\frac{\rho_0}{\varepsilon^2}\left(\vec{u}\cdot\nabla\vec{u}_D\right)=-\frac{\mu}{K}\vec{u}_D-\nabla p+\rho\vec{g}+\frac{\mu}{\varepsilon}\nabla^2\vec{u}_D \qquad \textbf{(2-6)}$$

the apparent rationale for the appearance of coefficients $1/\varepsilon^2$ and $1/\varepsilon$ in front of the inertial and boundary viscous terms appears to be that since the pore velocities are larger than the average values (averaging symbol '<>' has dropped for simplicity), then these forces should be described at conduit scale by multiplying the velocity by $1/\varepsilon$ (since the inertia term involves product of velocities, $1/\varepsilon^2$ is used). As expected, no rigorous development of Eq (2-6) can be offered.

In an effort to extend the Darcy law (based on the application of local volume averaging) the following semiempirical momentum equation for random porous media have been developed [33]:

$$\frac{\rho_0}{\varepsilon}\left(\frac{\partial\vec{u}_D}{\partial t}+\vec{u}\cdot\nabla\vec{u}_D\right)=-\nabla\langle p\rangle^f+\rho f+\frac{\mu}{\varepsilon}\nabla^2\vec{u}_D-\frac{\mu}{K}\vec{u}_D-\frac{F\varepsilon}{K^{1/2}}\rho|\vec{u}_D|\vec{u}_D \qquad \textbf{(2-7)}$$

(1) (2) (3) (4) (5)

1. Macroscopic inertial force or macroflow development term
2. Pore pressure and body force gradient

3. Macroscopic or bulk viscous shear stress diffusion, also called Brinkman viscous term or bounding surface effect
4. Microscopic viscous shear stress, Darcy term
5. Microscopic inertial force also called Ergun inertial term of microflow – development term

This is a semiheuristic volume – averaged treatment of the flow field. Experimental observations have shown that the microscopic viscous shear stress diffusion and the flow development (convection) are significant only over a length scale of l from the vorticity generating boundary and the entrance boundary, respectively. However equation (2-5) predicts these effects to be confined to distances of the order of $K^{1/2}$ and Ku_D/ν, respectively. We note that $K^{1/2}$ is smaller than d. Then Eq (2-7) predicts a macroscopic boundary layer thickness, which is not only smaller than the representative elementary volume l when l>>d, but even smaller than the particle size. However Eq. (2-7) allows estimation of these macroscopic length scales and shows that for most practical cases, the Darcy law is sufficient.

2.2 Nonequilibrium processes in the transport of heat and reactants in combustion, in porous media

Also the processes involved with the porous DP Filters such as regeneration, are nonequilibrium processes. Nonequilibria can be defined with the help of Figure 13 which presents a rendering of a porous medium characterized by three levels of geometric length scales, the system level L, the pellet level D and the catalytic surface level d i.e. a multiple – length scales porous medium [34].

Local thermal nonequilibrium at a given length scale, by definition occurs when the difference among the local temperature of the phases is comparable in magnitude to the temperature difference across the medium length scale L. This results in local heat transfer among phases which can be sustained through the intraphasic heat transfer or heat generation/consumption.

Local chemical nonequilibrium occurs when the difference among the species chemical potential in the phases is comparable in magnitude to the differences across the length scale immediately larger. This results in mass transfer across the interfaces, which can be sustained through the intraphase mass transport and chemical reaction.

Mechanical nonequilibrium occurs when there are variations in fluid phase pressure, which are comparable in magnitude with pressure differences in larger length scales, or as a result of nonzero force balance at solid surfaces. This results in fluid flow and movement of the solid matrix. The transport and kinetic resistances may delay or prevent the system from reaching equilibrium within the characteristic residence time of the process. These nonequilibria are in contrast to the local thermodynamic equilibrium, which is assumed to exist at phase interfaces.

Nonequilibria occur because of the intrinsic characteristics of the medium e.g. nonuniform distribution of reactants, noncontinuous solid phase, large mismatch between the thermal properties of the fluid and solid phases, or as a consequence of the process to which it is subjected, e.g. fast transients, highly endothermic or exothermic reactions and large variations in the inlet and outlet conditions. The possibility of nonequilibrium allows for redistribution of heat and recirculation, enhanced reaction rates and the formation and freezing of metastable solid phases.

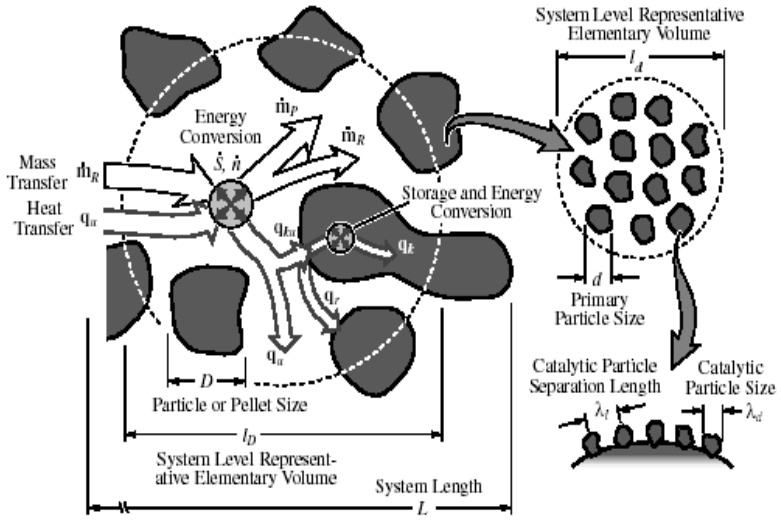

Figure 13 Rendering of a porous medium formed by a continuous gas phase and a dispersed solid phase

The use of porous media in combustion systems results in many advantages, but also poses special challenges for modeling. The volume – averaged models filter out the detailed information at the smaller scales. In most cases, to detect important nonequilibria, one must use detailed local simulations, either using continuum or molecular models, in network or detailed representations of the geometry. Also, in face of the difficulties in obtaining measurements at a pore level, the detailed local

simulations seem to be promising to fill in the gaps in the understanding of the physics at the pore level and its interactions with the macroscopic average variables.

Chemically, the solid phase may be either inert or it may participate directly in the reactions as a catalytic surface or a source of fuel. Figure 13 also represents the different heat (the intraphase convection $\mathbf{q_u}$, conduction $\mathbf{q_k}$, and radiation $\mathbf{q_r}$, and the interphase surface convection $\mathbf{q_{ku}}$) and the mass (generically) shown as reactants $\mathbf{m_R}$ and products $\mathbf{m_P}$) flux vectors, and the energy and mass conversion and storage (energy conversion S and mass conversion n) that are used to describe the transport and reaction during combustion in porous media.

All the physical and chemical processes have phenomenological length and time scales, such as flame thickness, penetration depth, residence time, etc. The phenomenological length scales can be of the same order of magnitude or much different from the geometric length scales. The interaction among the different phenomenological length and time scales and the geometric scales, results in different transport and reaction regimes and leads to thermal and chemical nonequilibria.

Figure 14 presents the case in which the fuel is provided from pyrolysis of the solid as in solid combustion smoldering and particulate trap regeneration or from evaporation of liquid in the form of droplets. In this case the rate of pyrolysis or evaporation may control the reaction. The reaction could also occur inside the solid phase (not depicted) and be controlled by the transport of oxidizer or products.

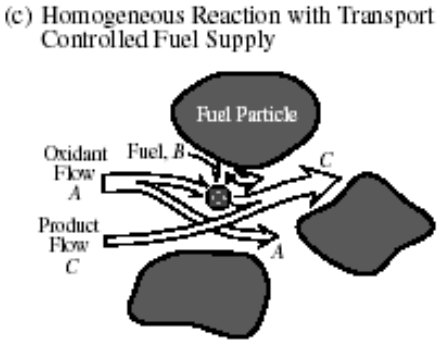

Figure 14 Distribution and transport of reactants
in a chemical nonequilibrium process.

2.3 Filtration mechanisms

The most common design of diesel particulate filter is the *wall-flow monolith*. It is an extruded, usually cylindrical ceramic structure with many small, parallel channels running in the axial direction. It is realized that this description, matches that

of the catalytic converter substrate. Indeed, the design of diesel filter monoliths has been derived from automotive, "flow-through" catalyst substrates. There are, however, two important differences between these structures: (1) the wall-flow monoliths are made of ceramics of higher and more precisely controlled porosity, and (2) adjacent channels in the wall-flow filters are alternatively plugged at each end, thus forcing the gas to flow through the porous walls which act as a filter medium. The flow pattern difference between the flow-through and the wall-flow substrate is illustrated in Figure 15 and in Figure 16 [35].

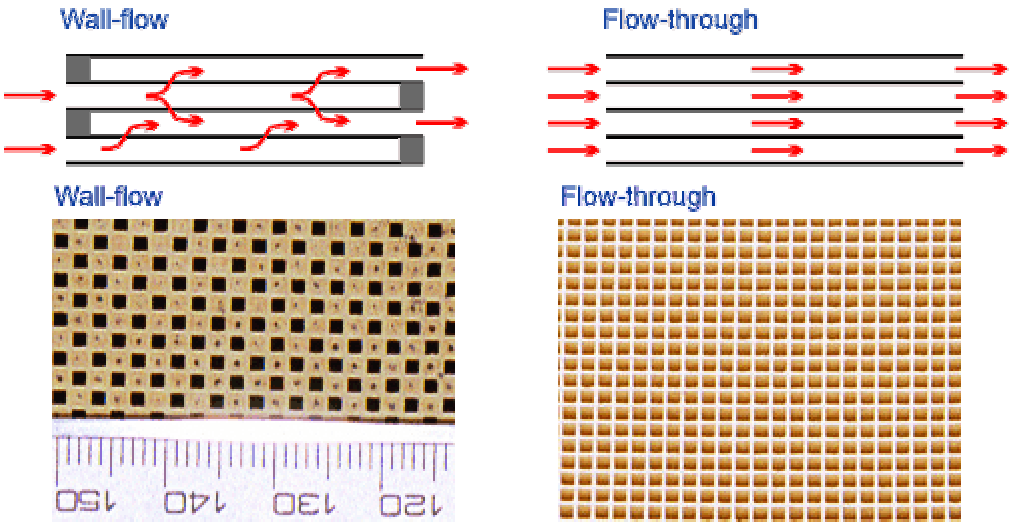

Figure 15. Wall-Flow and Flow-Through Substrates: Flow and inlet cell pattern

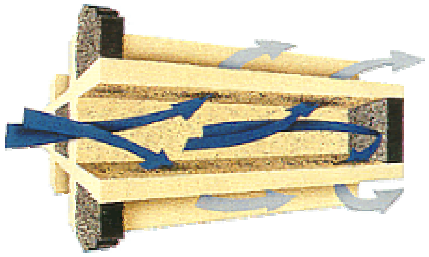

Figure 16 Flow through one channel of a Diesel Particulate Filter

The particulate collection by any type of diesel filter is based on separation of the gas-borne particles from the gas stream by deposition on a collecting surface. This separation involves passage of the gas through a porous barrier, which retains the particulates. Filters, depending on the type of the barrier, may be divided into (1) deep-bed filters and (2) surface-type filters [35]. In the deep-bed filters, the mean pore size of filter media is bigger than the mean diameter of collected particles. The particles are deposited on the media through a combination of depth filtration

mechanisms, which are driven by various force fields. As an example, the force fields may be related to velocity or concentration gradients in the gas. In the surface-type filters the pore diameter is less than the particle diameter. The particles are deposited on the media through sieving. These two types of filtration are shown in Figure 17.

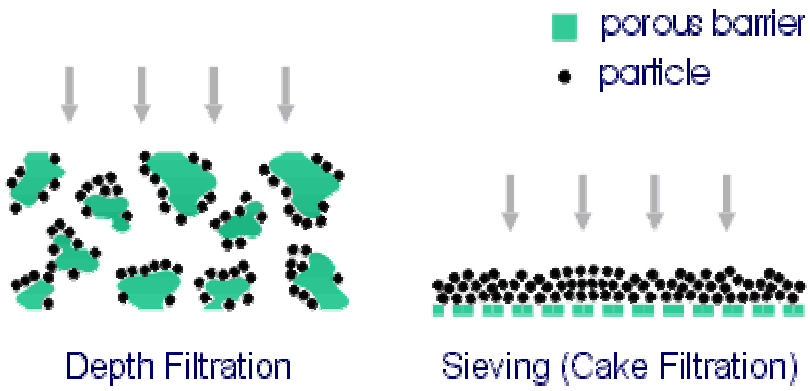

Figure 17 Types of Filtration

Depth filtration is the main filtration mechanism in some dust collection devices, as well as in some types of diesel filters (foam filters, fiber filters). The layer of collected dust, or diesel particulates, is itself the principal filter medium in the surface-type filters. That layer is commonly referred to as "filtration cake" and the process is called "cake filtration". Cake filtration is very common in liquid filtration. Pure cake filtration is not observed in diesel filters or, generally, in dust collecting filters. However, some diesel filters, such as ceramic wall-flow monoliths, may work through a combination of depth and surface filtration. A filtration cake develops at higher soot loads, when the depth filtration capacity is saturated and a particulate layer starts covering the filtration surface.

The depth filtration relies on three mechanisms of aerosol deposition: (i) Diffusional deposition, (ii) Inertial deposition, (iii) Flow-line interception.

These mechanisms are illustrated in Figure 18, Figure 19, and Figure 20. The large circle in the middle represents a collecting body in the filter media; say a fiber in a ceramic fiber filter.

Diesel exhaust gas flows around the filter media, as indicated by the streamlines. The small black-red spheres represent diesel exhaust particles traveling with the gas stream.

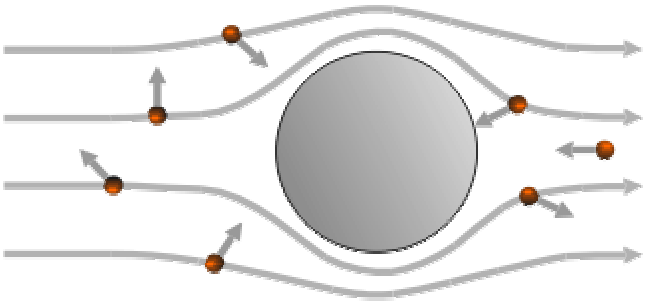

Figure 18 Brownian Diffusion

Diffusional deposition (Figure 18) depends on the Brownian movement exhibited by smaller particulates, particularly those below 0.3 μm in diameter. Those particulates do not move uniformly along the gas streamlines. Rather, they diffuse from the gas to the surface of the collecting body and are collected. The gas molecules collide with the smallest particles and the latter deviate from their streamlines and follow random paths. If they are in the proximity of the cylinder they touch it and are deposited to it. A concentration gradient establishes between the bulk of the flow and the flow near the cylinder, so the particles diffuse to the cylinder. Brownian motion increases and so does, in consequence, the efficiency of deposition. For the quantitative description of the phenomenon, the Peclet number is employed: $Pe = \frac{ud}{D}$, where $D = \frac{Ck_bT}{3\pi\mu d_p}$ is the diffusivity of the particles and k_b the Boltzmann constant [36]. Peclet number may be viewed as the ratio between transport due to convection and transport due to molecular diffusion.

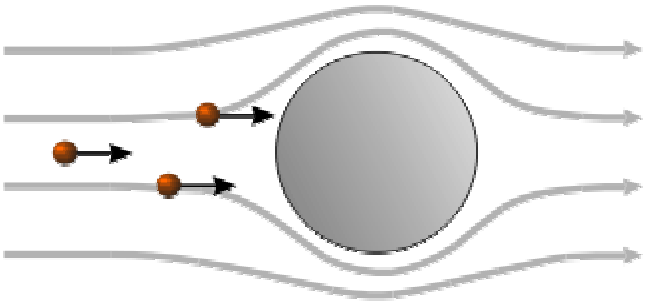

Figure 19 Inertial Impaction

Inertial impaction (Figure 19), also called inertial interception, becomes more important with increasing particle size (mass). On approaching the collecting body,

particles carried along by the gas stream will not exactly follow the streamline, because of its inertia. It will follow a more direct path and end up to the cylinder

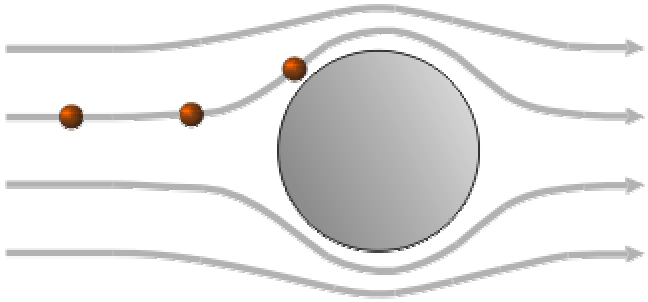

Figure 20 Interception

The deviation will be greater the more the massive the particle and the higher the velocity of particle's approach. This phenomenon is characterized by the Stokes number: $Stk = \frac{C\rho_p d_p^2 u}{9\mu d}$. Where ρ_p and d_p refer to the density and diameter of the particle, d is the diameter of the cylinder, μ and u are the viscosity and velocity of the gas flow respectively. C is the Cunningham correction factor, accounts for slip flow effects and is a function of Knudsen number: $C = 1 + Kn\sqrt{1.257 + .4e^{-1.1/Kn}}$ [29].

Flow-line interception may occur when a fluid streamline passes within one particle radius of the collecting body. Then, a particle traveling along the streamline will touch the body and may be collected without the influence of Brownian diffusion or inertia. Filtration by interception is dominant in aerosols with small particles flowing in greater velocities. A particle with very small mass -hence negligible inertia – in a high velocity flow, practically follows the streamlines of the field quite accurately. If the shorter distance between a streamline and a cylinder is a, then any particle with diameter r > a traveling along this streamline will touch the cylinder and stick to it. Interception is characterized by the interception parameter R, defined as the ratio between particle and cylinder diameter: $R = \frac{d_p}{d}$

Performance of diesel particulate filters may be expressed as the *filtration efficiency* (E) or *penetration* (1-E). The filtration efficiency is the mass ratio of the particulate matter collected on the filter to the particulate matter entering the filter. The penetration is the mass ratio of the particulates escaping to the particulates

entering the filter. Both filtration efficiency and penetration may be expressed as percentages.

The depth filtration is characterized by somewhat lower filtration efficiency and lower pressure drop than the cake filtration. Particulates, which were already deposited on a deep-bed filter, may be also re-entrained by the gas causing a decrease in the observed filtration efficiency. That phenomenon is termed “blow-off” of the collected particulate matter. Blow-offs occur at high exhaust gas flow rates or at rapid flow accelerations.

The cake filtration is characterized by higher filtration efficiency and relatively high - pressure drop. The pressure drop steadily increases with the increase of filtration cake thickness.

Chapter3. EXPERIMENTAL INVESTIGATION OF PRESSURE DROP IN DPF. $(\rho k)_p$ ESTIMATION

3.1 Aims and steps for the estimation of (ρk)p.

The estimation of $(\rho k)_p$ product requires both an experimental and a simple computational process. The experiments are useful because the exact details of the soot loading phenomenon as a function of the engine operation point are not fully understood. Therefore it is useful to have a step-by-step process, which involves experiments, calculations and validation in order to conclude.

The final aim of this research is the accurate prediction of trap backpressure using as input data only the measured values of $(\rho k)_p$ in a full-sized trap and the correlation of trap backpressure with the soot mass loaded at each operational point. This prediction ability helps the post injection system of the vehicle to control and trigger the regeneration process only when necessary, to avoid unnecessary fuel consumption.

The first step of this research consists of simplified experiments, with a mini – scale filter consisting of a single channel. The solution of single channel trap filters is selected because they present some advantages over the full- size trap tests.

The basic advantages of the mini-scale filter are (i) the possibility to accurately weigh the small filter before and after loading and (ii) the exclusion of any 3–D effects in the measurements. Obviously, a measurement in a full-scale trap includes three – dimensional effects such as the diffusion of the expanded air from the measuring device to the other channels of the trap. This complicates the necessary discharge calculations. A subsequent step in this research was the measurement of a real DPF channel, as it will be presented in the following paragraphs.

3.2 Single channel filter specimens

A mini- scale filter is a small filter cut out from a full-sized one, consisting of a central single inlet channel and four exit channels mounted tangentially to the central. The central channel is open in front and tapped backwards. On the contrary the four tangential channels are plugged in the front and open backwards. The pressurized air enters to the mini scale filter (Figure 21) from the open central channel passes through the porous walls (Figure 16) and exits through the four unplugged

channels. Thus it becomes possible to investigate the pressure drop characteristics of a single channel.

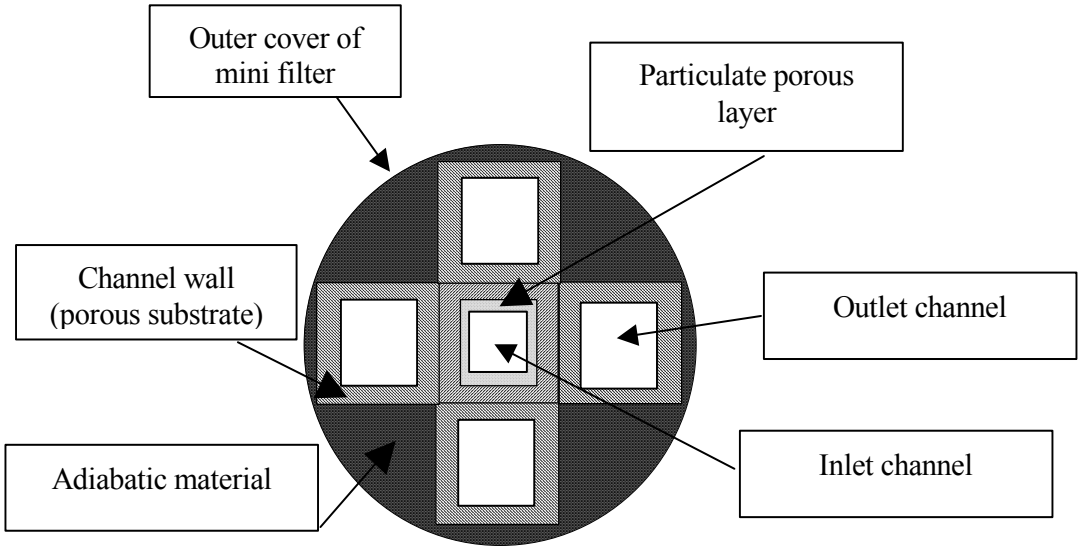

Figure 21 Cross section of mini scale filter

This phase of the experiments did not proceed without problems. A problem that was faced during the experiments was the break off of waterproof cement that was the filling material between the rectangular channels and the circular cover of the mini trap. This matter was damaged sometimes due to the high temperatures and thermal stresses developed in the mini trap and thus there was a loss in the total mass of the filter. The problem was realized when the experimental curves did not agree with the curves obtained by the calculation (the tuning procedure will be discussed in next paragraph) and then the old filling matter replaced by a new one with improved behavior.

The single channel filters were prepared by breaking up two of the most commonly employed filter types:

- a cordierite filter (17x100) and
- a silicon carbide filter (14/200)

The properties of the two types of filter materials are presented in Table 7.

Table 7. Properties of single channel filters used for the experimental study

Property	**Cordierite**	**SiC**
Material Density (kg/m^3)	2510	3080
Porosity (%)	43	42
Cell Size (mm)	1.49x1.49	2.54x2.54
Wall thickness (mm)	0.4138	0.4
Wall density (kg/m^3)	1000	1800
Mean pore size (μm)	33	9
Permeability (m^2)	3.70E-13	1.225E-13

These single-channel filters, are designed to be assembled to the engine exhaust pipe, as presented in Figure 22.

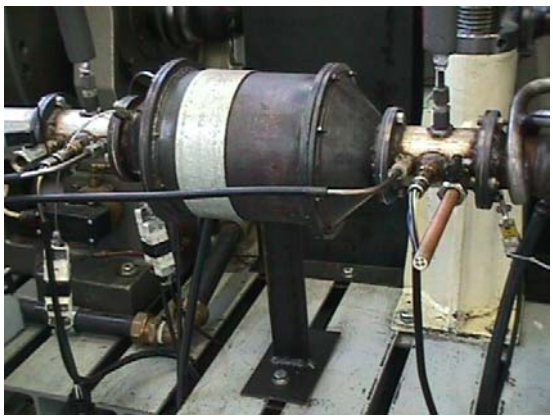

Figure 22. Mini scale filter assembly on engine exhaust system

In the specific experiments presented in this paper, the mini-filters were mounted in parallel to the full-sized diesel filter into the exhaust system of a 2.0 litre displacement HDI turbocharged passenger car engine (Figure 23), running on one of the LTTE engine test benches. The engine specifications are listed in Table 8.

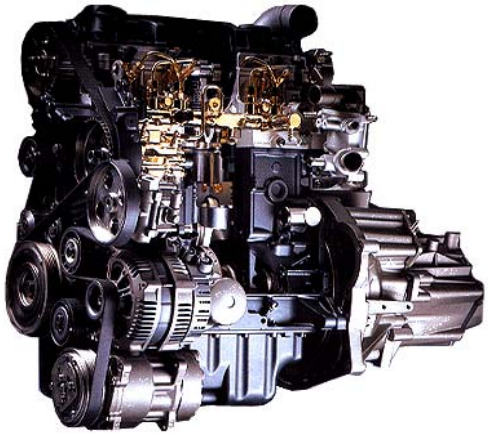

Figure 23 PSA DW10ATED laboratory engine

Table 8. Diesel engine specifications

Manufacturer	PSA
Engine type	HDI turbocharged engine (DW 10 ATED)
Cylinders	4, in-line
Displacement	1997 cm^3
Rated power /rpm	80 kW/4000 rpm
Rated torque/rpm	250 Nm/2000 rpm
Average fuel consumption	5.5 lt/100km

Figure 24 presents the experimental layout of the filter loading experiment. The full-sized filter employed in these experiments is a SiC 14/200.

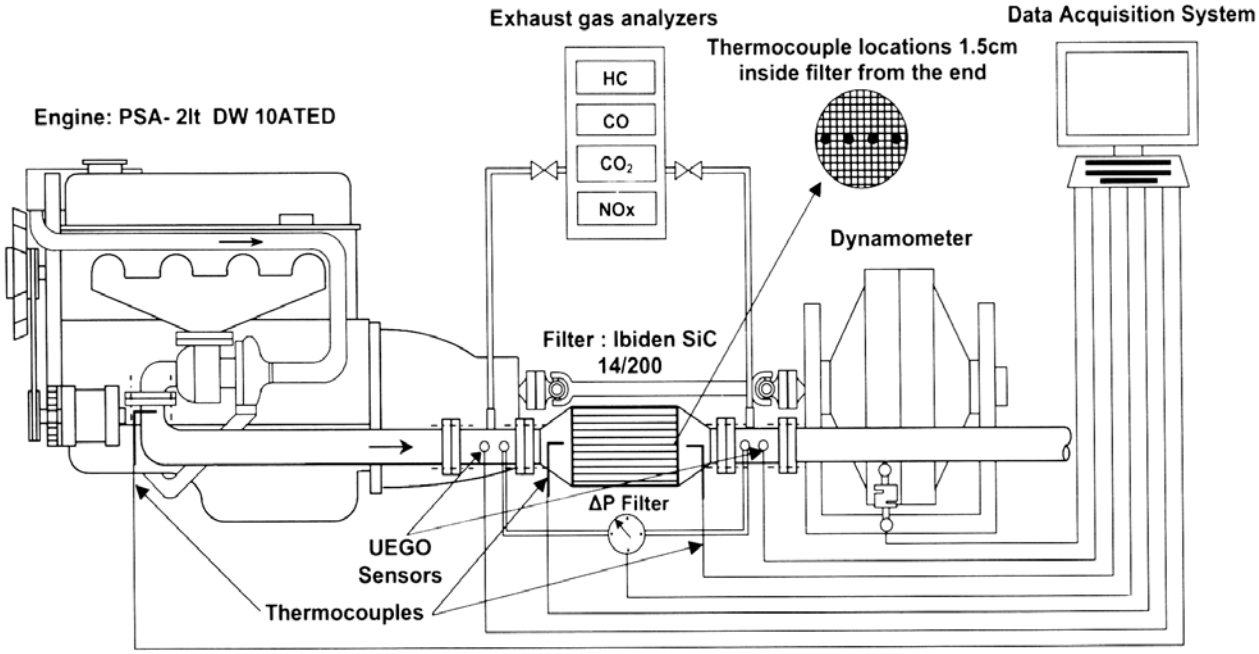

Figure 24. Experimental layout

The full-sized filter characteristics are listed in Table 9.

Table 9. Diesel particulate filter specifications

Manufacturer	Ibiden
Type	SiC 14/200
Diameter	143.8 mm
Length	150 mm
Cell concentration	200 cpi
Wall thickness	0.4mm

3.3 Operation principle of the experimental process for (ρk)p measurement

The operation principle of the experimental process is based on the following simple idea: A pressure vessel is employed, containing air, initially at 2 bar absolute pressure. If the pressurized air is forced to flow through two different single channels with different soot loading or soot layers with different soot permeability or density, then the pressure vessel will empty in less time when the air flows through the "lighter" in soot mass, or permeability, channel. The discharge time offers a first indication of the soot loading, but it would be better to record the pressure discharge process of the vessel. A pressure–time diagram would represent well the evolution of the phenomenon. The differences between the various discharge curves are clearly visible as it can be seen in the Figure 25 below.

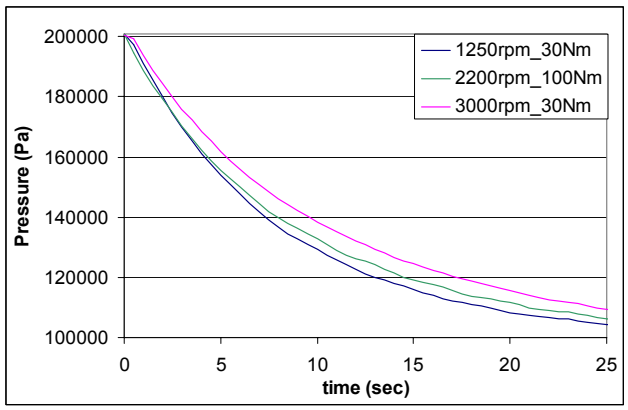

Figure 25 Curves obtained by a SiC single channel loaded in various engine operation points

The initial vessel pressure was set to about 2 bar, because when the air in the vessel was further pressurized the discharge flow could break and blow off soot pieces.

3.4 Experimental method and device used for $(\rho k)_p$ estimation

The following experimental methodology was employed: First, each single channel filter was weighed. Normally the mass at every measurement before loading must be the same and equal to that of the virgin filter but the weighing before is more secure in order to avoid problems such as those mentioned above. As a second step, the mini filters were connected to the exhaust gas duct as seen in Figure 22. Both the mini-scale and the full-scale filter were loaded at the same time in the same engine operation point. After the end of the trap loading process the mini scale filters were weighed again. The difference between the two mass measurements (before and after) gives the amount of soot trapped in the single channel filter and simultaneously it is used as input data in the calculations of $(\rho k)_p$.

Before the final weighing, the loaded filters were transferred and connected to the $(\rho k)_p$ measurement device. The device consists of the previous mentioned pressure vessel, which initially contains about 2 bar of pressurized air. Monitoring of the expansion process is carried out by means of recording the signal of a pressure sensor that is also mounted to the vessel. Recording by the data acquisition system starts when the solenoid valve opens. This solenoid valve opens on demand by the data acquisition software (Labview), and triggers the expansion of the compressed air from the vessel through the channel walls to the atmosphere. Two alternative types of discharge nozzles were designed and machined on the lathe, to allow the measuring device to be fitted to mini-scale filters and to specific channels of full scale traps, SiC and cordierite, as seen in Figure 26. The layout of the measuring device is presented in more detail in Figure 26 and Figure 27a.

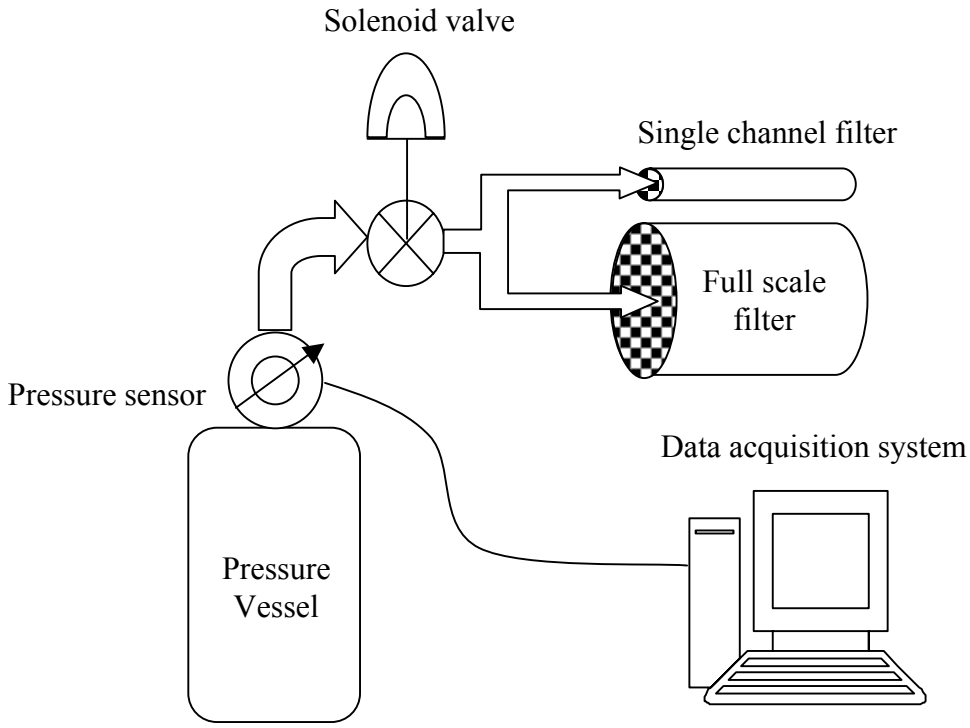

Figure 26 Schematic diagram of $(\rho k)_p$ measuring device.

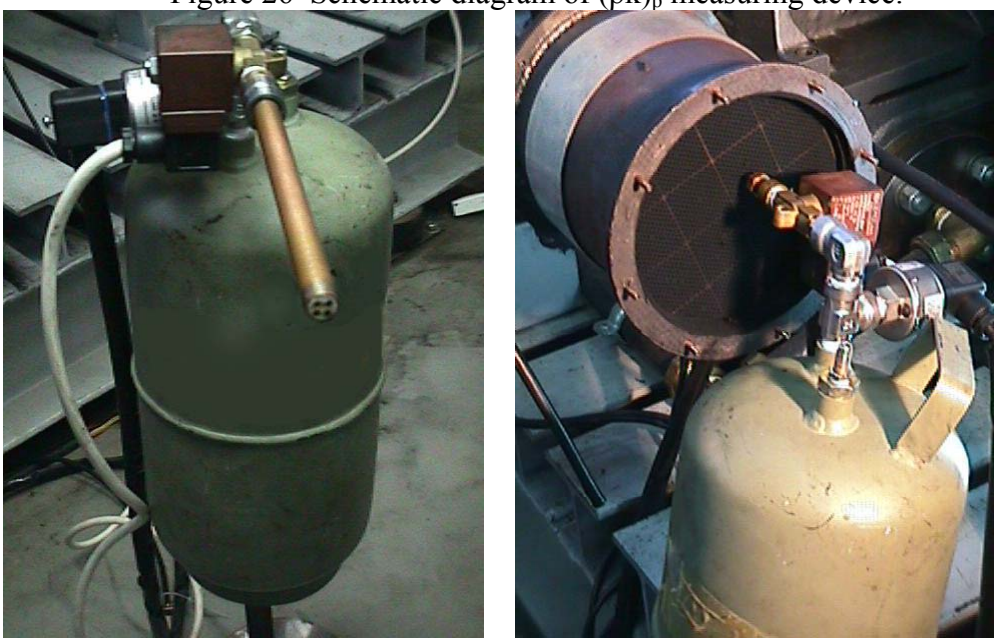

(a) (b)

Figure 27 Use of measuring device for (a) single channel filter loading measurement, (b) full scale filter channel loading distribution measurement.

The experimental curves of pressure drop against time such as those presented in Figure 25, are obtained from the experimental layout presented in Figure 26. A further set of soot loading experiments exists for specific engine operational points.

They are presented in Chapter5. The experiments are fully repeatable, the experimental curves of second and third repetition were identical.

A more detailed presentation of $(\rho k)_p$ measurement device which describes the parts of the apparatus can be seen in Figure 29. The nozzle in the figure is the one mountable to the full- scale filter/

3.4.1 Full-sized filter experiments

It has already been mentioned that a step–by–step procedure is followed in the experiments. The final target is the filter backpressure estimation using the following pressure drop calculation equation:

$$\Delta P = \frac{(mfr)}{\rho A_f} \cdot \frac{1}{\sum_{i=1}^{N}\left(\frac{1}{M + K(m_p)_i}\right)}$$

Where, i refers to one channel and N is the total number of channels and mfr is the mass flow rate.

$$M = \frac{\mu E_s}{k_s}$$

$$K = \frac{\mu}{A_f(\rho k)_p}$$

As a first assumption it could be considered that the product $(\rho k)_p$ is the same for all channels of the full- scale filter, to support a simplified 1D calculation. However, as can be seen from the above equation, only the accurate estimation of $(\rho k)_p$ in the various channels could support a realistic 3D calculation.

The full-scale filter measurements involve the specific examination of selected channels. A SiC filter consists of a number of blocks, namely unit filters with rectangular cross section mounted with other blocks. These unit filters are connected to each other with special adhesive cement. The selected channels for measurement, are located at the center of each unit section and they are named after the matrix elements as seen in Figure 28.

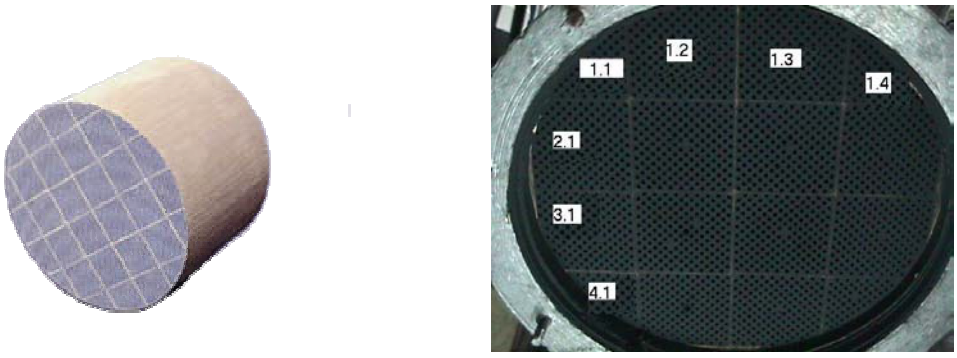

Figure 28 DPF inlet surface and channels selected for measurement

A basic experiment on the full-sized filter, aims to indirectly assess the differences in soot loading process and its distribution from filter center to the periphery channels. For that reason a special nozzle was designed by PhD candidate G. Stratakis and mounted into the device so that can be tightly connected to the selected inlet channels of the full-scale engine filter. The exhaust pipe of the vessel was carefully connected to the inlet of various trap channels. Then the pressure drop characteristic was recorded by the already mentioned way (see Figure 27b or Figure 29).

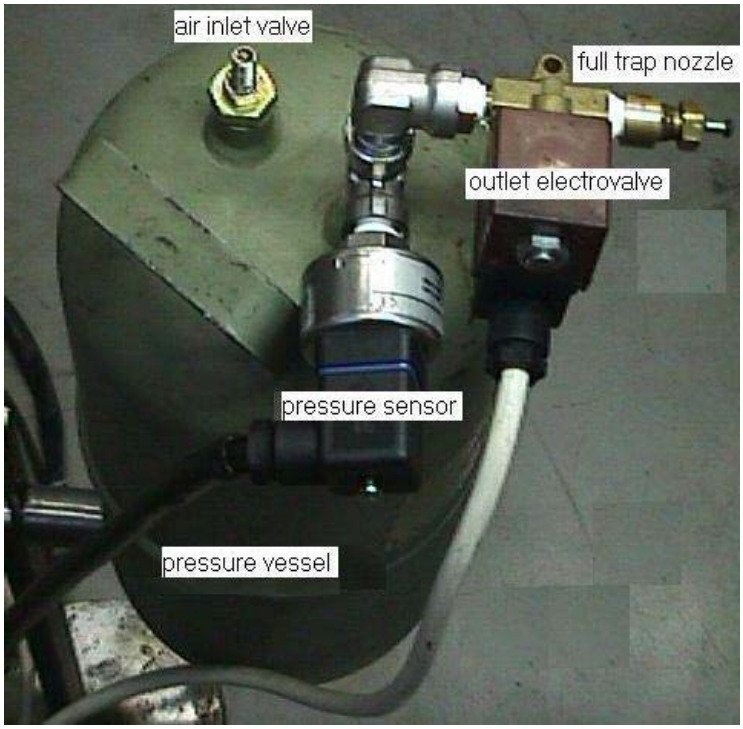

Figure 29 $(\rho k)_p$ measurement device and consisting parts

The measurement of the selected filter channels pressure drop helps in the investigation of regeneration effects in three dimensions. Sections insufficiently regenerated can be traced and the results of this type of measurement support further improvement of the 3D Catwall Code and thermal stresses calculations [30].

3.5 Measurements' protocol

The following strategy is applied in the determination of the exact protocol for filter loading tests:

A mapping process is performed to assess the engine exhaust gas mass flow rate and filter wall temperature in the low- and medium- load engine operating range, as more representative of city driving conditions (

Figure 30, Figure 31). The final design of the test protocol, based on the results of engine mapping, is presented in Table 10.

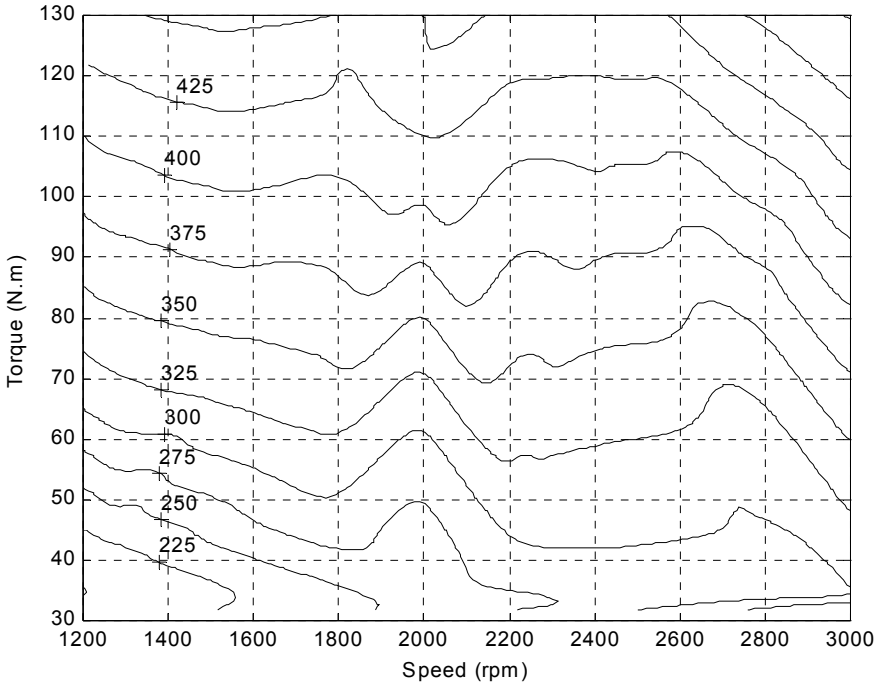

Figure 30. Map of filter wall temperature at the centerline, 15mm from filter exit.

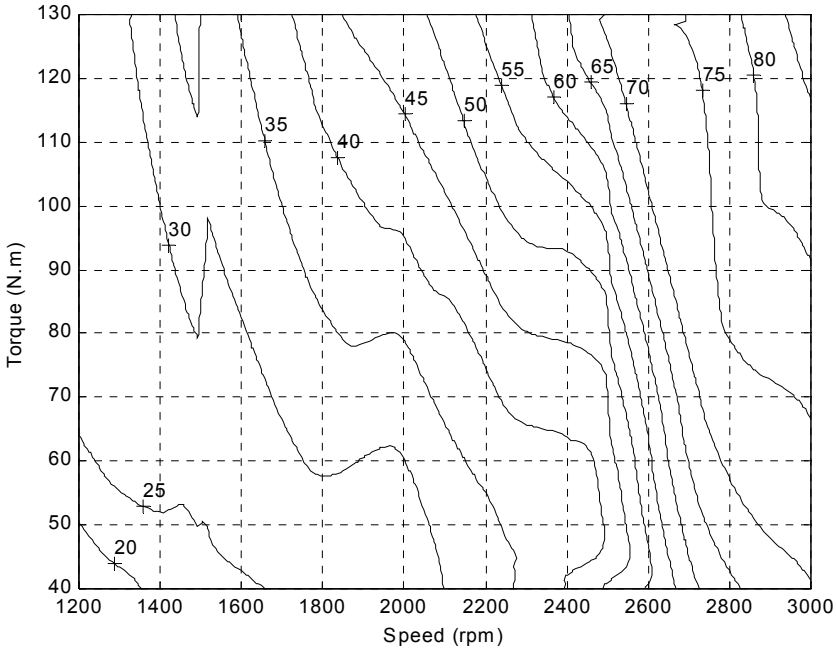

Figure 31.Map of engine exhaust gas mass flow rate.

It comprises medium and low load versus medium and low speed operation points. At each operation point, both single-channel and full-sized filters are loaded in parallel. Soot loading mass cannot be fixed in advance, due to the lack of knowledge of the function of mass versus Δp. After the completion of an approximate loading (order of 100 mbar independent of engine operation point), the expansion device can be fitted to both types of filter, in order to perform measurements for the assessment of soot loading. Especially for the case of the full-sized filter, the device is fitted to a number of characteristic channels' inlets (Figure 27b).

After the end of the recording of the single channel filter's expansion process, the single-channel filter is weighed in order to get the amount of accumulated soot mass. Afterwards the filter is regenerated in order to be useable for the next experiment. Unfortunately, the weighing process is not practical with the full-sized filter, due to the large experimental error caused by the order-of-magnitude difference between filter mass (1 kg and more) and collected soot mass (10-30 g) or the presence of moisture inside the trap. Thus, in the case of full filters we do not have this possibility of cross checking the soot mass.

Table 10.Experimental protocol

N (rpm)	Torque (Nm)	Mfr (gr/sec)	T exhaust (^{o}C)	TF inlet (^{o}C)	TF wall center (^{o}C)	TF wall side (^{o}C)
1250	30	18	225	198	193	178
	60	21	300	270	261	240
	80	25	355	317	310	285
	100	28	419	385	380	364
1800	30	30	254	236	234	216
	60	35	340	317	314	291
	80	38	400	370	370	344
	100	42	433	400	400	372
2200	30	34	276	257	255	238
	60	38	360	340	340	315
	80	43	415	388	388	365
	100	50	423	392	392	371
3000	30	69	305	300	297	287
	60	74	373	364	364	342
	80	79	395	384	384	377
	100	83	427	415	415	407

Chapter4. COMPUTATION OF FLOW THROUGH EXPERIMENTAL DEVICE

4.1 Computational Concepts

A simplified model of the discharge flow process through the device and filter channel was developed to support the experiment. As explained above, aim of the single – channel filter experiments is the estimation of the product $(\rho k)_p$ of soot collected in the filter channel. For that reason a computational assistance to the experiments is necessary.

The calculation method, illustrated in this section, was employed in the processing of experimental results. This method which estimates the (ρk)p product by a tuning process, requires the accurate knowledge of two significant factors as it can be seen from the analysis placed below.

The factors that are necessary to accurately estimate the product $(\rho k)_p$ are the discharge coefficient of the vessel nozzle and the mass collected in the filter channel. To this end, the single-channel filter was weighed before and after each loading experiment, and the soot mass determined in this way was employed as input factor in the computer calculation that was written to support the pressure drop characteristics calculations.

The calculation method, which simulates the flow process through the vessel and the filter channel, is realized by a computer program, which is written in Fortran 77. The output of this calculation offers a graph of vessel pressure as a function of time, during the discharge process. The calculation can be done for three cases. First of all can be applied for the simulation of a flow passing through a single channel (made of Cordierite or SiC), clean or loaded with soot, second for one channel that belongs to a full – scale Diesel Particulate Filter clean or loaded, or just for the discharge nozzle, without any filter channel connected, for validation purposes.

As long as the first significant factor, namely the soot mass collected in the filter channel, has been determined, two other factors remain unknown and must be tuned in this calculation process: The first is the discharge coefficient C_D and the second is the above-mentioned $(\rho k)_p$ product, which represents the final output of the tuning process. These two factors in combination with the amount of the accumulated soot, govern the pressure drop characteristics of the experimental apparatus. The tuning process is based on the comparison of the experimentally recorded and the calculated discharge characteristic of vessel pressure versus time.

In order to validate the computer calculation program, a virgin single channel filter is placed to the measuring device. Thus the experimental characteristic of the vessel discharge process, (pressure drop as function of time) is obtained. Then the tuning process is activated using the computer code output. This preprocessing work is repeated for the measurement case of a single channel that belongs to a full trap. So the final output of the first step of this tuning process offers the discharge coefficient for the above – mentioned cases.

Afterwards the single-filter specimens or the full-scale trap are ready to be mounted to the specified places on real engine exhaust line as previously described and as it can be seen in Figure 22. This is the starting point for the (ρk)p product estimation for various operational points as the loading process can go ahead.

Subsequently, and when the trap loading has already finished they can be connected again to the measuring device and another experimental curve of the discharge process can be recorded. In the case of a full scale filter the measuring device will be modified in order to be able to measure a single filter of the whole DPF. The pressure drop characteristics are recording again and a new tuning process is on time to start, using as input parameter the discharge coefficient determined as explained above.

The soot mass estimation belongs to the next step, which is the weighing of the filter specimen. Thus the value obtained from the measuring of the soot mass collected in the mini filter completes the input data list.

The tuning process for the estimation of the $(\rho k)_p$ is based on the fitting of the experimental discharge curve of the loaded mini or full scale channel filters with the calculated curve from the computer calculation process.

The main input factors to the computer calculation except from the soot mass in the channel or the discharge coefficient, which have been mentioned above and the

$(\rho k)_p$ product (this last is tunable as already explained), are the initial vessel pressure, the vessel air temperature, the dimensions of the single channel, the substrate thickness (E_s) and permeability (k_s).

4.2 Filter pressure drop approximations

During the measurement process, the air flows out of a pressure vessel and passes through a single channel of either a mini scale or a full-scale filter. The channel's wall consists of two different and successive layers. The first layer that the airflow meets as it passes through the wall is the soot layer, which has been formed from the accumulated soot particles during the trap loading process. The second is the substrate ceramic layer of the trap matter. Both of them are porous media.

The two different layers present different resistance to the flow. Thus the total pressure drop across the particulate filter wall can be expressed as the sum of the porous ceramic substrate pressure drop and the soot layer pressure drop [37]:

$$\Delta P = \Delta P_s + \Delta P_p \qquad \textbf{(4-1)}$$

As seen in Chapter2, it is generally accepted [38], that the pressure drop associated with flow through ceramic filters or porous media, can be approximated by Darcy's law. According to this law, the total pressure drop due to flow through the two layers of the ceramic wall and the soot layer can be approximated by the following simplified relation:

$$\Delta P = \frac{\mu U E_s}{k_s} + \frac{\mu U E_p}{k_p} \qquad \textbf{(4-2)}$$

Unfortunately the soot layer thickness presented in the above formula is not an easily manageable quantity magnitude. First of all the thickness is not the same in the whole length of channel and the filter must be destroyed in order to measure it. Then the soot particles may be trapped inside the porous wall, thus making difficult a physical definition of soot layer thickness.

As an alternative to actually measuring the thickness, the concept of effective particulate layer thickness [38] is used. The assumptions made are that the particles are evenly distributed over the entire face of the filter and that there is, in effect, a sharp boundary between the particles and the filter material. Since the filter material is

porous, this assumption may not be very accurate, especially in the first stages of particle collection. So the latter formula can be rewritten as follows:

$$\Delta P = \frac{\mu U E_s}{k_s} + \frac{\mu U m_p}{A_f (\rho k)_p} \qquad \textbf{(4-3)}$$

This formula allows, in principle, the backward approximate calculation of collected soot mass as function of measured filter backpressure at a certain engine and filter loading operation point, once an approximate value for the product (ρk_p), that is, (soot layer density) times (soot layer permeability) is known for the specific engine – filter – operation point combination. Now, both factors of the above product are variable thus, the product of ρk_p is widely varying, depending on engine type, injection pressure, filter type, operation point, possible use of fuel additives etc. The wide dispersion (several orders of magnitude) of this parameter has already been mentioned by various researchers [37]. Aim of this study is to further investigate these discrepancies and possibly narrow their range of variation by the previously mentioned experimental setup, which is presented below in more detail.

4.3 Physics of the process employed in the computation

The formulas listed in the above section are related to the porous media air-flow. But the pressurized air has to pass through another section first. During the discharging of the vessel air, air passes through a nozzle (or throat) that concurs with the inlet of the channel. The throat is the minimum surface that air meets when exits from the vessel and enters to the channel.

So it is possible to have choked conditions of flow, with sonic velocity (Ma=1) in the throat. For that reason the computer calculation checks whether there exist choked or subcritical flow conditions and makes use of the corresponding formulas, at each calculation time step. In choked flow, the following formula is employed for the mass flow rate estimation [39]:

$$\dot{m}_{real} = \frac{C_D A_T p_o}{\sqrt{R T_0}} \gamma^{1/2} \left\{ \frac{2}{\gamma + 1} \right\}^{(\gamma+1)/2(\gamma-1)} \qquad \textbf{(4-4)}$$

on the other hand in subcritical flow condition, the following formula is employed:

$$\dot{m}_{real} = \frac{C_D A_T p_o}{\sqrt{RT_0}} \left(\frac{p_T}{p_0}\right)^{1/\gamma} \left\{ \frac{2\gamma}{\gamma - 1} \left[1 - \left(\frac{p_T}{p_0}\right)^{(\gamma-1)/\gamma} \right] \right\}^{1/2} \quad \textbf{(4-5)}$$

Thus the mass leaving the vessel is known at each time step of calculations. The determination of the flow condition in the throat is designated by the pressure ratio between the pressure in the throat and the stagnation pressure, which is identical with the vessel pressure. Computer calculation continuously checks the pressure ratio and compares it to the critical pressure ratio $\frac{p_T}{p_0}$, which is taken equal to 0.528 (air at near-ambient pressure and temperature conditions can be assumed to behave like an ideal diatomic gas - γ=1.4).

Also the previously mentioned discharge coefficient C_D is a flow coefficient taking values between 0.2 and 0.8, which accounts for the effective flow restriction due to the specific orifice and flow conditions. Generally when a fluid flows through a restriction or reduction in flow area the real flow can be related with an equivalent ideal flow. The equivalent ideal flow is the steady adiabatic reversible (frictionless) flow of an ideal fluid through a duct of identical geometry and dimensions. For a real fluid flow, the departures from the ideal assumptions are taken into account the discharge coefficient. Furthermore the discharge coefficient is determined by the ratio of actual mass flow to the ideal mass flow and is mainly a function of the shape of the passage. It needs always to be experimentally determined.

As it was written above, the stagnation pressure is identical with the pressure in the vessel. Thus the vessel pressure at any time step must be given by the equation of state:

$$P_0 V = m_v R T_0 \quad \textbf{(4-6)}$$

where P_0 and T_0 are the pressure and temperature inside the vessel or, in other words, the stagnation pressure and temperature. For the throat region, the following expression is valid:

$$\dot{m}_{real} = \rho_T u_T A_T \quad \textbf{(4-7)}$$

The u_T velocity is the velocity of the air in the throat. However for the next step of calculations the filtration velocity U is necessary. The filtration velocity is the velocity or airflow through the porous walls of the channel because each channel has

one inlet area and four outlet sections. Thus the filtration velocity can be correlated to the throat velocity or the real mass flow $\dot{m}_{real}$ by means of the continuity equation:

$$\rho_T u_T A_T = \rho_{ch} U \ A_{ch} \quad \textbf{(4-8)}$$

so,

$$\dot{m}_{real} = \rho_{ch} U \ (4Lw) \quad \textbf{(4-9)}$$

or,

$$U = \frac{\dot{m}_{real}}{\rho_{ch}(4Lw)} \quad \textbf{(4-10)}$$

4.4 Computer calculation procedure

The computer calculation procedure consists of two discrete parts, as it can be seen from the flowchart in Figure 32 . In the first part, the real air mass outflow from the vessel is calculated by the use of equation (4-4) for choked flow or (4-5) for subcritical flow. In the second part, a pressure P_{TG} is guessed that results to a first estimation of pressure drop $(\Delta P)_c$ between the throat or the input section of the channel (the minimum area that the air flow passes through) and the exit of the channel in atmospheric pressure (see Figure 26).

The next step is the confirmation of the estimated pressure in the throat. The initial amount of air mass in the vessel is estimated by the use of state equation (4-6). During the discharging process, two conditions of flow may prevail, choked or subcritical flow. The mass flowrate at each time step is computed according to the critical pressure ratio using the appropriate formula. From the second time step and on, the throat pressure is unknown and so it is guessed (P_{TG}). The outgone mass for the (i)th time step is (the $\dot{m}_{real}$ has already been calculated):

$$dm_{(i)} = \dot{m}_{real(i)} \cdot dt \quad \textbf{(4-11)}$$

and the remaining mass in the vessel is:

$$m_{v(i)} = m_{v(i-1)} - dm_{(i-1)} \quad \textbf{(4-12)}$$

therefore the new vessel pressure is known from the equation of state (4-6).

Then the filtration velocity U is calculated by equation (4-10). The latter velocity is used in $(\Delta P)_c$ calculation with the aid of equation (4-3). Also, because the filter is discharging to the free atmosphere, ΔP can be assumed equal to the difference between pressure at throat and atmospheric pressure:

$$\Delta P = P_T - P_{atm} \quad \textbf{(4-13)}$$

from equation (4-13) we get:

$$P_{Tc} = (\Delta P)_c + P_{atm} \quad \textbf{(4-14)}$$

Thereby two pressure values have been estimated for the throat region. This is a checkpoint for the code. The above values must satisfy the condition of equality in the same region (throat). If the difference between the two calculated pressures is small enough, or $\frac{P_{TG} - P_{Tc}}{P_{TG}} < 0.001$ then, the calculations are continued for the next time step. Otherwise the previously mentioned process is repeated with another guessed pressure value in the throat until the solution for this time step has converged. Afterwards the computation code enters the next time step calculations and this procedure terminates when the vessel pressure has reached ambient pressure.

To synopsize, the assumptions made for the calculations are: (i) the air flowing through the channel is assumed to be ideal gas (ii) the flow resistance is mainly due to the porous media and thus the Darcy law governs the phenomenon; (iii) mean values of inlet and filtration velocities have been assumed, thus the filtration and inlet velocity is uniform; (iv) the procedure consists of successive equilibrium stages.

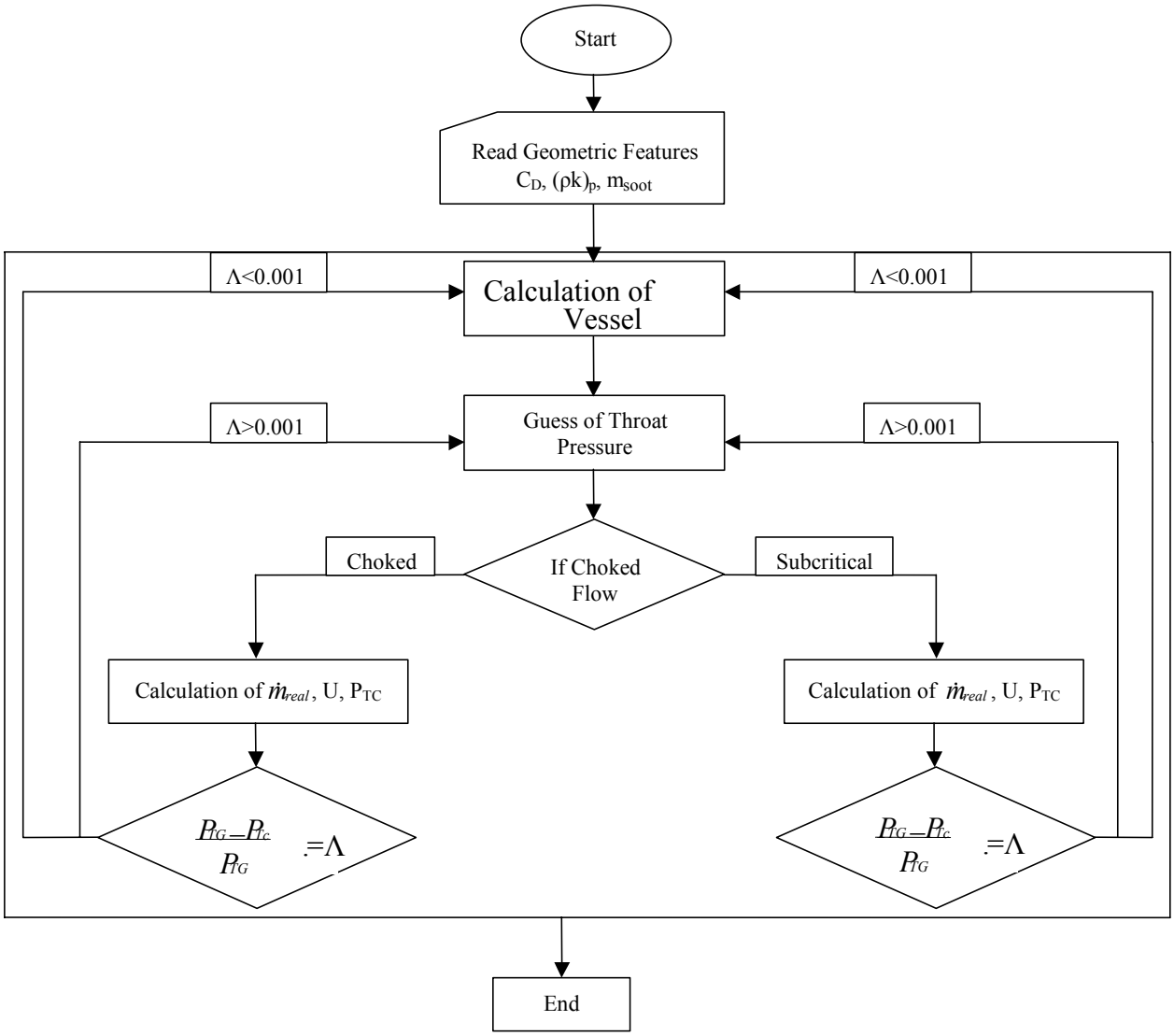

Figure 32. Computer calculation flowchart

Table 11 below represents the values of input data used for the calculation

Table 11 Parameters used for the calculation procedure

P (air)	1.2kg/m^3	Tvessel	305 K
Dt (time step)	0.001	R (air)	287kJ/(kg K)
Γ (air)	1.4	Cd (DPF)	0.49
Cd (SiC)	0.96	Cd (Cordierite)	0.73
Es (SiC)	0.0004m	Es (Cordierite)	0.0004318m
Ks (SiC)	1.225E-13m^2	Ks (Cordierite)	3.70E-13m^2

Air density is assumed constant and equal to the ambient density in normal indoor conditions (1 atm and 20^{o}C).

The appropriate time step was found to be equal to 0.001 sec, limited by the stability test.

Air was assumed to be ideal gas because of low pressures and temperatures in usual conditions and thus the (γ) coefficient was assumed equal to 1.4.

The vessel temperature changes during the discharge. However this change is low and so it can be assumed that the temperature is constant and equal to 305K.

The manufacturer of the filters gives the Es and Ks parameters, and the tuning process described in Chapter5 gives the Cd coefficients.

Chapter5. EXPERIMENTS AND COMPUTATIONS FOR (ρk)p MEASUREMENT. RESULTS AND DISCUSSION.

5.1 Mini scale filter

As already mentioned, the final objective of the combined experimental and computational method, is the determination of the $(\rho k)_p$ parameter by a tuning procedure. The main parameters to be estimated before the tuning process are the soot mass and the discharge coefficient. Soot mass is easy to be estimated by weighing the mini filter. On the other hand the C_D coefficient must be tuned by measuring a mini filter, and subsequently execute the program file. The C_D tuning process offers simultaneously the validation of the computer calculation program, something that is necessary in order to prove its acceptable performance. Thus, a set of validation tests was first performed.

The validation procedure involved the determination of the discharge coefficient C_D calculation for both single-channel filter specimens (made from Cordierite and SiC respectively). These two single-channel filters are taken from full-scale filters, as explained in Chapter3. Their main features are presented in Table 7. Each validation test consisted of a particular experiment, in which each mini filter was connected to the vessel and the compressed air was discharged through the filter channel. The validation curves are presented in Figure 33. It can be seen that the computer code behaves better with the SiC mini-filter, whereas in the cordierite case there is a small but observable deviation from the experimentally measured curve.

As a next step, loading experiments were performed with soot emitted by the engine operating on 25ppm DPX9- doped fuel at the previously described operation points (see Table 10).

After the loading procedure, the mini-filter was weighed, and subsequently connected to the measuring device, where the pressure –versus- time curve was obtained.

As it can be seen from the following figures, the pressure - versus time experimental curve is presented in the same graph with the corresponding curve

obtained from calculations not only for space and time economy but in order to demonstrate the tuning process of (ρk)p or C_D parameter.

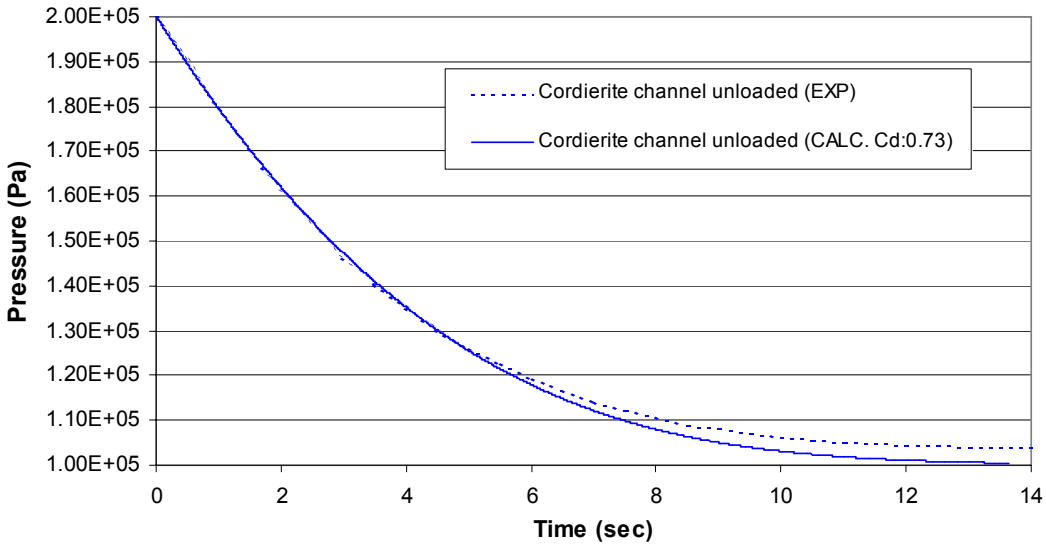

(a)

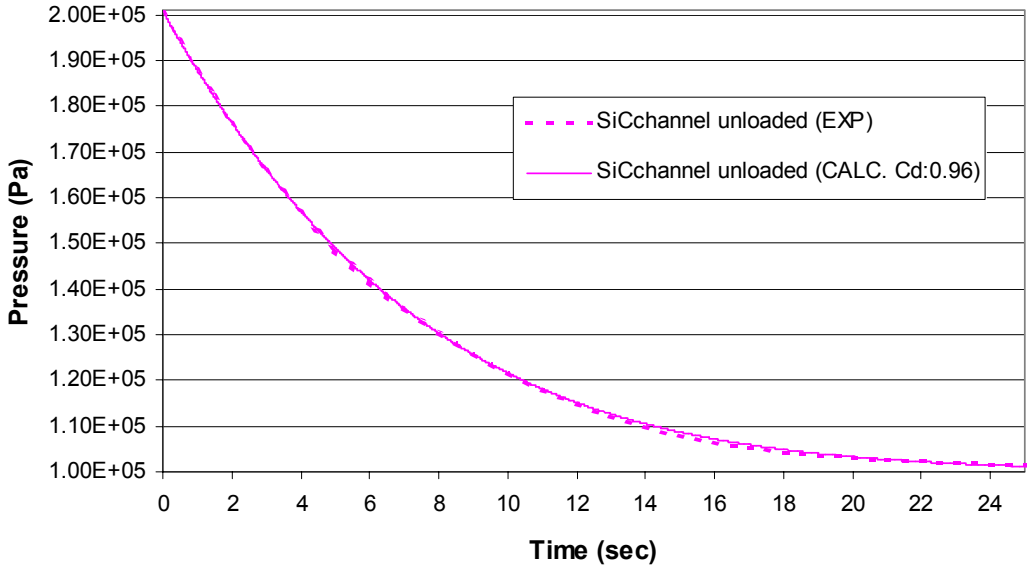

(b)

Figure 33.Code validation-Cd estimation curves for Cordierite (a) and SiC (b) single channel filters

The tuning process of the two previously mentioned parameters, was repeated so many times until the best fitting of these two (the experimental and the computational) curves had been succeeded.

Two representative curves of vessel pressure -versus- time characteristics with a loaded Cordierite mini-filter that were employed in the tuning process are presented in Figure 34(a). The tuning is implemented by comparison between the experimental and computational curves.

The computation is seen to behave well with the simulation of the two experiments, resulting in different $(\rho k)_p$ product values for the two different soot loading levels. For the Cordierite case it is observed that the greater soot mass retards the discharge process of the pressurized air, and the $(\rho k)_p$ decreases as the mass of the accumulated soot increases.

A series of loading experiments has been performed at various engine operation points. The object of these experiments was the investigation of (ρk)p parameter variation as function of the engine load and speed. After each experiment, the mini filters were disconnected from the engine exhaust line, measured using the measuring device, weighted, and afterwards the tuning process was performed.

The results for a representative sample of tuned values of $(\rho k)_p$ is presented in Figure 35(a). The total list with the tuned values of $(\rho k)_p$ as function of engine operation point are presented in a more compact form in Table 12 and the tuning graphs that correspond to Table 12 are presented in the Appendix (tuning procedure graphs).

According to these results, the variation of $(\rho k)_p$ with the engine operation point over the low and medium range of speed and load is measured in the range of 3.5E-12 to 1.15E-11 kg/m .

In order to investigate the same effect with a different filter material, a new set of measurements was performed with the SiC single-channel filter. Two more coupled curves of experimental and calculated pressure discharge curves are presented in Figure 34(b). Also in this case it is observed that for higher soot mass the air discharges slower, the $(\rho k)_p$ value decreases, and the values determined vary in the same range as with the cordierite samples, as would be expected. The values of the determined $(\rho k)_p$ product as function of engine operation point are presented in Figure 35(b). The results for both the two types of filter materials are summarized and presented in Table 12 and in the Appendix dedicated to tuning process graphs.

A more detailed analysis of the above-mentioned experimental results shows that $(\rho k)_p$ product does not depend only on the accumulated soot mass, but it is also a function of engine operation point. That is, the pressure discharge versus time curve,

which is employed in the indirect determination of the soot loading of each filter channel, is affected at least by the collected soot mass, the engine speed and torque, and the presence of a fuel additive component. Furthermore the role of adsorbed hydrocarbons on the soot particulate and the ceramic substrate must be considered [40]. Research in this subject is underway in LTTE/UTh.

As a general conclusion for both types of filter material, it can be observed that the higher soot mass is associated with a decrease of the $(\rho k)_p$ parameter value. This is apparent in Figure 36 at which the $(\rho k)_p$ parameter is determined for various filter loading experiments at the same engine operation point and for the Cordierite case. This could have the meaning that the decrease in soot permeability prevails over the increase in soot density during the assumed compression of the particle layer at higher soot loading levels.

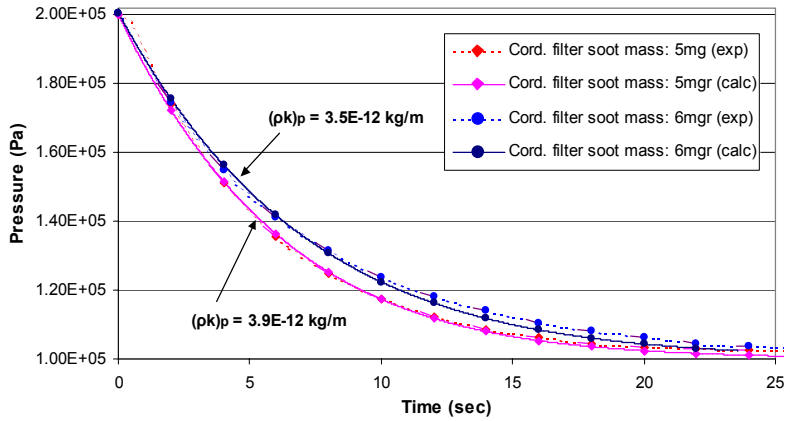

(a)

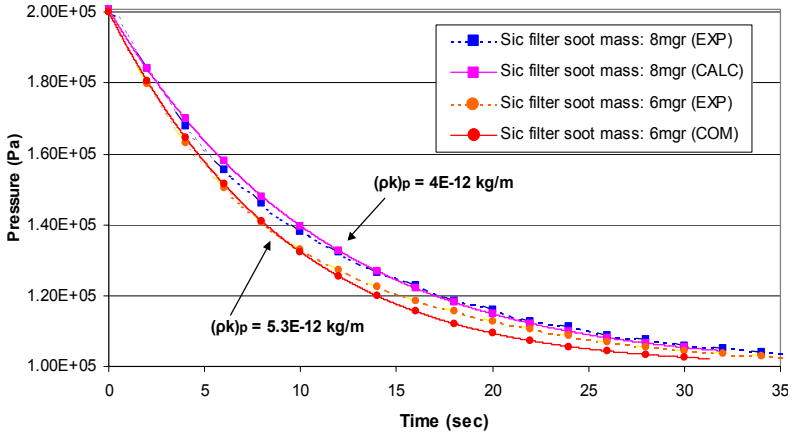

(b)

Figure 34. Representative curves of (ρk)p parameter tuning in various filter loads and engine operational points. (a) cordierite single channel filter, (b) SiC single channel filter

Table 12. Summarised results for $(\rho k)_p$ parameter for various single channel filter loads and engine operation points.

Operation Point		**Cordierite Single Channel**		**SiC Single Channel**	
Speed (rpm)	*Torque (Nm)*	*Soot mass collected (mgr)*	*(ρk)p (kg/m)*	*Soot mass collected (mgr)*	*(ρk)p (kg/m)*
1250	30	10	7.00E-12	4	5.50E-12
1250	60	12	1.00E-11	8	5.60E-12
1250	80	5	3.90E-12	6	5.30E-12
1250	100	7	6.40E-12	7	6.20E-12
1800	30	9	7.95E-12	8	1.10E-11
1800	60	5	4.10E-12	8	5.85E-12
1800	80	4	4.10E-12	6	3.80E-12
1800	100	4	4.80E-12	6	3.70E-12
2200	30	10	6.00E-12	8	4.00E-12
2200	60	9	7.60E-12	7	3.50E-12
2200	80	12	1.15E-11	8	8.30E-12
2200	100	3	3.90E-12	4	3.40E-12
3000	30	5	4.70E-12	7	3.50E-12
3000	60	6	3.50E-12	5	5.00E-12
3000	80	7	1.00E-11	6	9.10E-12
3000	100	8	1.10E-11	5	9.90E-12

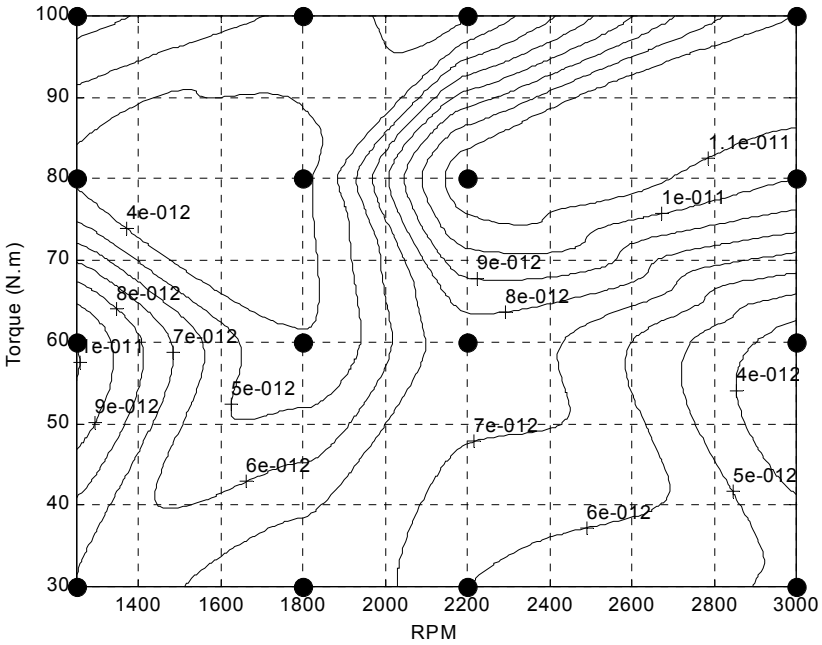

(a)

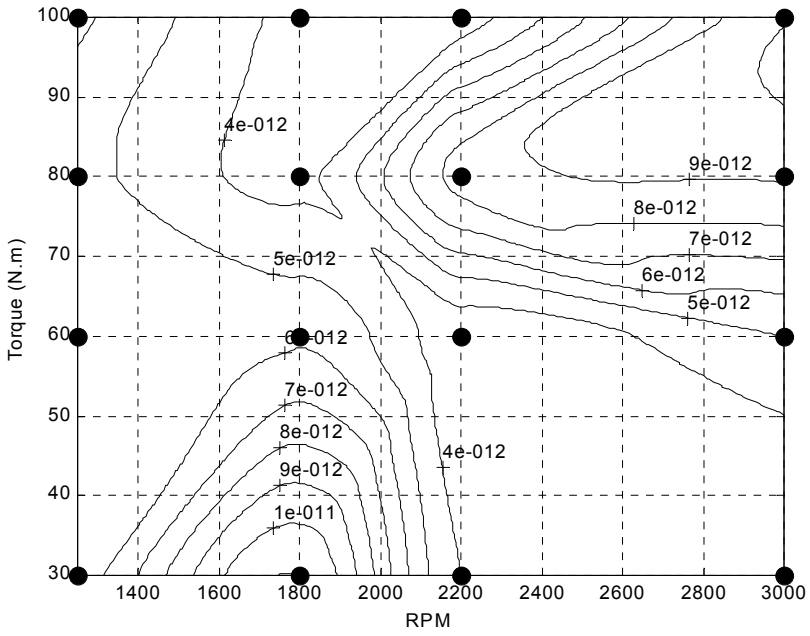

(b)

Figure 35. Map of (ρk)p parameter as function of engine operation point. (a) cordierite single channel filter, (b) SiC single channel filter

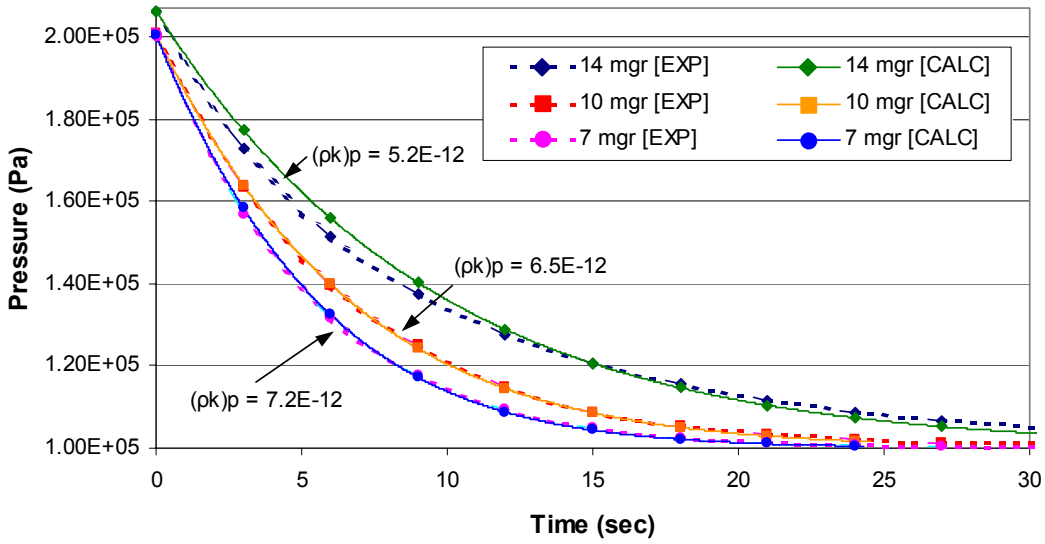

Figure 36.$(\rho k)_p$ value calculation for various Cordierite single channel filter loading levels with engine running on the same operation point (3000 rpm – 40 Nm). [41]

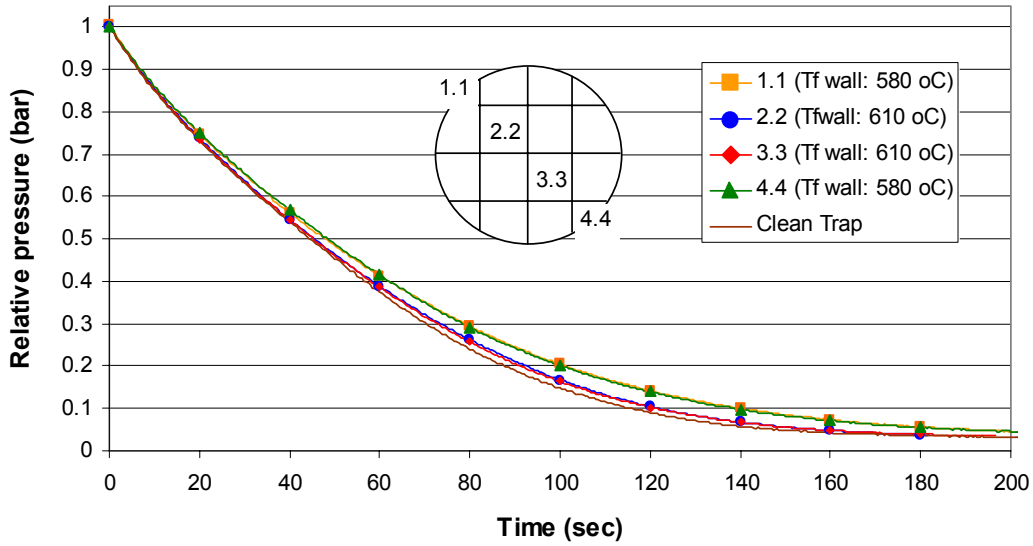

Figure 37. Pressure drop measurements along a diameter after the regeneration of a filter loaded until 150mbar at 2000 rpm 90Nm with 0 ppm fuel additive.

5.2 Mass and flow distribution in full scale DPF

As reported above, experiments with full-scale filters were also performed in order to investigate the exhaust flow characteristics and soot mass distribution along the filter channels during the loading and regeneration procedure. Figure 38 presents the vessel pressure discharge curves obtained at selected channels equi-distantly positioned along a filter diameter, after loading at the following two characteristics points:

- Speed: 2000rpm, Load: 90Nm, resulting filter backpressure ca. 150mbar, filter wall temperature varying in the range of 390^{o}C (center) to 370^{o}C (periphery)
- Speed: 2000rpm, Load: 90Nm, resulting filter backpressure ca. 450mbar, filter wall temperature varying in the range of 410^{o}C (center) to 390^{o}C (periphery)

The coincidence of the curves in the case of filter loading to 150mbar backpressure, indicates a uniform distribution of soot mass (and possibly exhaust gas flow). This is not observed in the case of 450 mbar filter backpressure. As it can be seen, at least two different zones are observed as the measuring device is removed from the central (hotter during operation) to the outer (colder during operation) channels, since the pressurized air is shown to discharge faster through the central channels than through the circumferential. This could be attributed to the effect of VOF present in the thick particulate layer, which should preferentially condense on the colder outer channels after engine stop, thus differentiating permeability characteristics between filter core and periphery channels, that would be expected to be comparable during hot operation.

The role of the wall temperature gradient during an incomplete regeneration to the soot mass distribution is further investigated with the experimental results of Figure 37. The resultant curves refer to the determination of the product $(\rho k)_p$ in central and peripheral channels, after filter regeneration at engine speed 2800 rpm, engine Load 180Nm, which results in filter wall temperature varying from 610^{o}C (filter center) to 580^{o}C (filter periphery). In order to exclude any secondary effects from fuel additive residuals, the filter was loaded without a fuel additive at a speed of 2000rpm, and a load of 90Nm up to the backpressure of 150 mbar.

The variation of the vessel discharge curves as we move from the center to the periphery indicates incomplete regeneration at the filter periphery, explainable due to the lower wall temperature measured (thermal regeneration!). This behavior during a partial regeneration, would result, during a subsequent loading phase, to a significant

differentiation of the exhaust flow distribution, with the exhaust flowing mainly through the central region of the filter. This mechanism could also explain the different loading behavior between a virgin and a previously incompletely regenerated filter.

Finally the role of fuel additive was investigated too. After prolonged filter operation with the engine having consumed about 1000 lt of diesel fuel doped with 25 ppm Ce additive running in loading and regeneration modes at various operation points, a new set of measurements along a filter diameter was performed. At this case the filter was completely regenerated.

The experimental curves obtained by the measurement of the full scale trap are presented in the below Figure 38. It is clearly seen that there are differences between the soot loading characteristics depending to the channel location

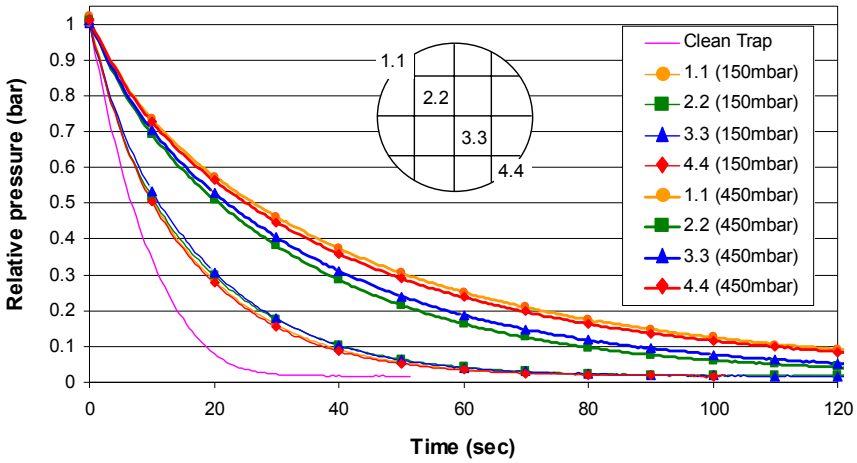

Figure 38Pressure drop measurements along a diameter for a full-sized filter loaded up to 150mbar and up to 450mbar pressure drop (measured at 2000 rpm – 90 Nm)

The results of Figure 39 indicates that the pressurized air discharges faster through the circumferential channels than through the central. This means that the fuel additive ash is concentrated mainly on the central region of the filter. Again, such an observation can be explained by the previously proposed mechanism, because the central filter region tends to regenerate more completely than the outer region, thus attracting a higher total exhaust flow during a large period of time.

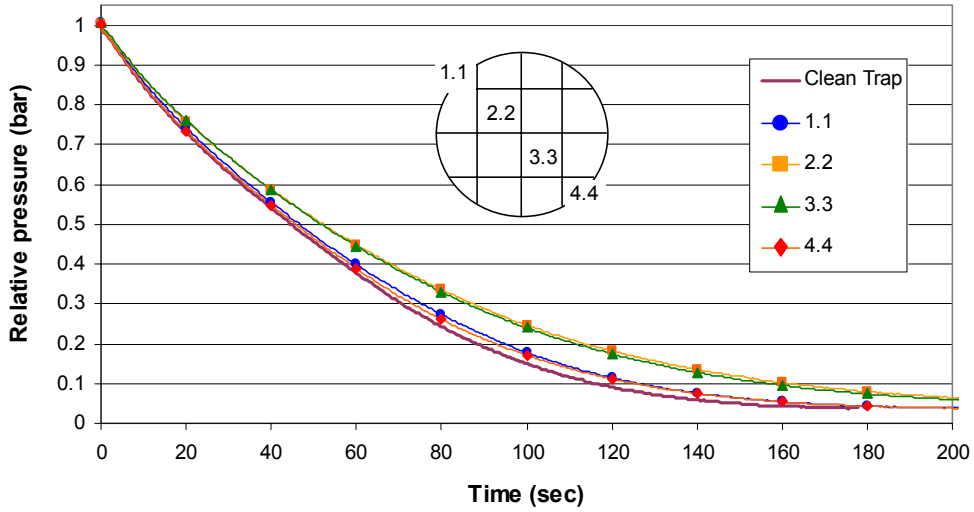

Figure 39.Pressure drop measurements for a complete regenerated filter after engine consumed about 1000lt diesel fuel doped with 25ppm additive (ash effect)

5.3 Correlation study between Single Channel and Full Scale DPF (ρk)p measurements.

The single channel measurement presents critical advantages as regard to the accurate estimation of soot mass trapped. The accurate knowledge of soot mass collected into the mini filter leads to the accurate estimation of (ρk)p parameter. On the other hand, this methodology is not applicable to the full - scale filter case. For that reason, the range of applicability of the (ρk)p values obtained from single channel experiments to a full scale filter will be examined next.

Two different engine operational points are examined. The first experiment involves soot loading of the DPF, at engine speed of 3000 RPM and engine load of 40 Nm before the regeneration. The second experiment involves measurement of the full scale – filter channels after loading of the DPF in engine speed at 2200RPM, engine load at 90Nm and after the regeneration.

After the loading procedure the DPF was disconnected from the exhaust line and the measurement device was modified especially for the measurement of the single channel that belongs to a full trap measurement. The single channels of the full scale trap that are measured have been chosen to be the centers of the corresponding unit filters (unit filter is a compact part of the DPF which contains about 320 single

channels and it is bounded from the neighbors by a special type of cement. For further details the reader can see also Chapter3 and Figure 28).

Afterwards the measuring device is connected to each of the before mentioned single channels inlet and the pressure drop versus time graph is recorded and presented in Figure 40 for the case of 3000RPM and 40Nm and in Figure 45 for the case of 2200RPM and 90Nm.

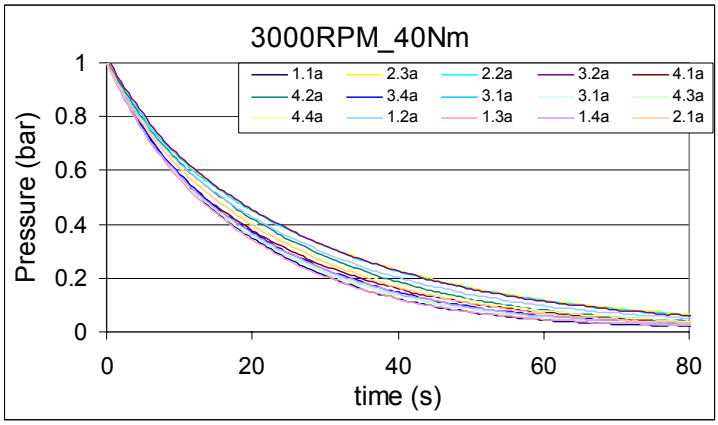

Figure 40 Pressure drop versus time graph. Case: 3000RPM_40Nm.

5.3.1 Case study: 3000RPM_40Nm

Afterwards, the tuning procedure is performed to each of the measured single channel filter of the full scale DPF. As it has already been written the main problem that the tuning procedure faces when it attempts to simulate the discharge through a full - scale filter channel is the unknown soot mass that each channel contains. Thus, in the next presented tuning sequences, the (ρk)p parameter was assumed constant and equal to the (ρk)p value determined by the single channel experiments, in the same engine operational point. The (ρk)p value obtained from single channel experiments in the same engine operation point was equal to 3.5E-12.

Then it follows that the new parameter to be tuned is the mass collected in each channel. This is simultaneously a checkpoint for the assumption of equality in values of (ρk)p obtained in mini- and full- scale filters.

The experimental curves recorded for each channel, were grouped in groups of two or three channels, which had almost the same pressure drop characteristic. Thus the simulation of a number of representative characteristics was performed.

Furthermore this was the first time that the computer program was used to simulate the discharge through a full-sized filter channel with the above-mentioned difficulties. Thus, first of all a sensitivity analysis was performed in order to have an idea of the effect of (ρk)p parameter to the calculation outputs. The Channel 32 was chosen for the sensitivity analysis.

The first best fitting between the two curves obtained from the experimental data and computational output, is presented in the next Figure 41.

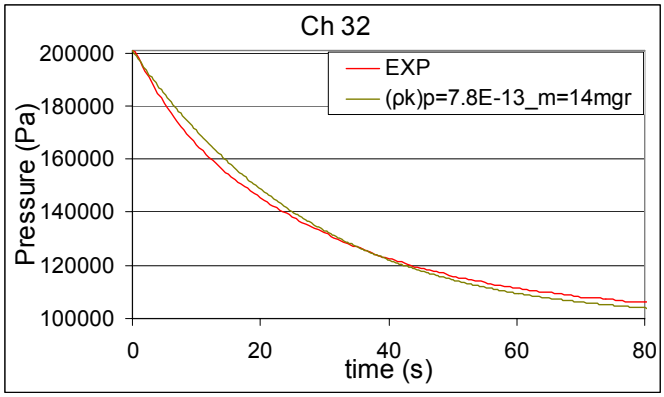

Figure 41 Sensitivity analysis – best fitted tuned values of (ρk)p and collected mass

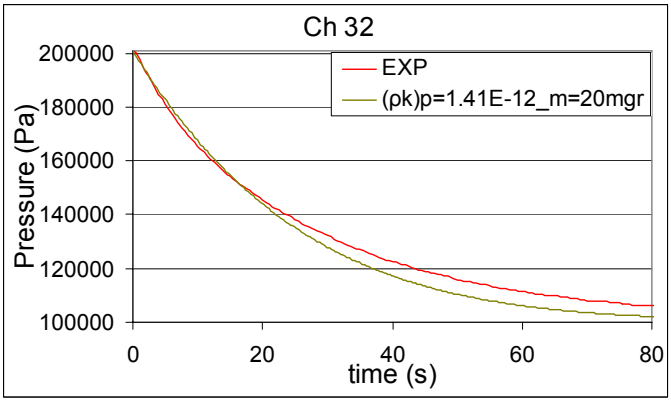

Figure 42 Sensitivity analysis.
Parameter (ρk)p assumed equal to the mini filter.

It is observed from the Figure 42 above that the curve obtained from the calculation procedure using as input the (ρk)p value determined by the single channel experiment does not fit well to the experimental.

The same tuning procedure was performed for the rest channels as it can be seen in Figure 43 below.

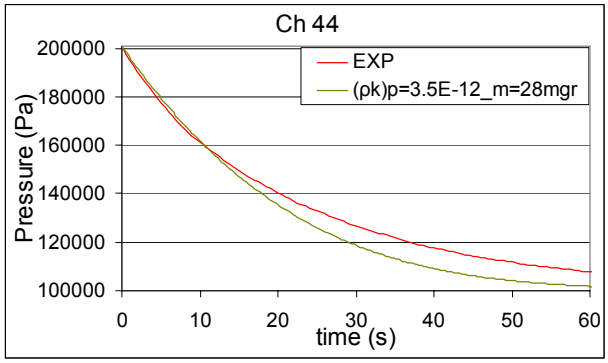

Figure 43 Mass estimation by calculation. (ρk)p equal to the mini filter experiments

The tuning procedure was performed to the other representative of the formed group channels. The tuning graphs are presented in the relative Annex III: Full – Scale Trap Tuning Graphs. The values of the mass estimated by the tuning procedure if the (ρk)p parameter assumed equal to that obtained by the mini filter experiments, for each channel are presented in a compact form in the Table 13 below. The number of cells corresponds to the number of cells that each unit filter contains. The total mass at each unit filter is assumed to be equal to the measured filter. This is an assumption that can be valid due to the central placing of the measured channels inside a unit filter.

At the last row of Table 13 it is presented the mass obtained from the Catwall regeneration simulation as a parameter for comparison. The specific value of (ρk)p employed, seems to overestimate the collected mass in the trap in the case of 3000RPM and 40 Nm.

Table 13 Channels of Full Trap and corresponding trapped mass.
Estimation by the Experiment-Calculation System. (ρk)p assumed constant and equal to mini filter estimation. 3000_40 loading case in 300mbar.

Channel ID	Radius (mm)	Mass (mgr)	Number of Channels	Mass in Section (mgr)
1.1	63	18	50	900
1.2	58	33	150	4950
1.3	57	18	150	2700
1.4	62	18	50	909
2.1	50	28	150	4200
2.2	30	50	162	8100
2.3	18	50	162	8100
2.4	57	24	150	3600
3.1	62	18	150	2700
3.2	29.5	50	162	8100
3.3	34	47	162	3888
3.4	57	18	150	2700
4.1	62	21	50	1050
4.2	48	33	150	4950
4.3	53	18	150	2700
4.4	69	28	50	1400
Catwall Total mass		27000	Total mass	64673

The values of the estimated mass for each channel of a DPF are presented in Figure 44, which shows the distribution of soot mass inside the DPF. According to this map the majority of collected mass is concentrated in the central channels, and the soot mass decreases as we move to the peripheral channels. This shows that during the loading procedure the majority of soot particles is collected to the central section of the trap. This is maybe due to the boundary layers formed in the exhaust line duct, at the inlet diffuser upstream the DPF.

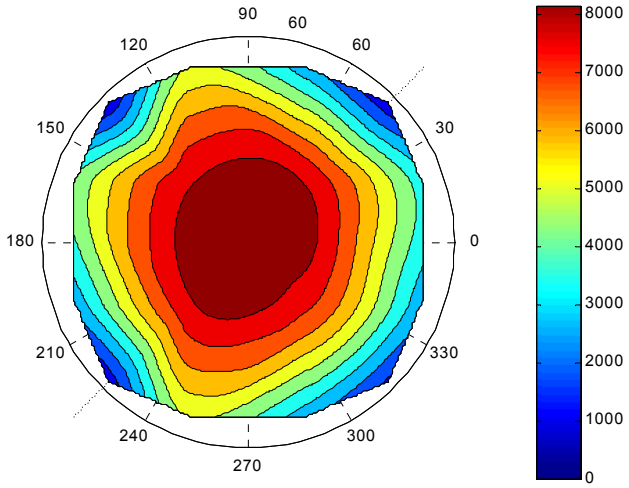

Figure 44 Mass distribution on a full - scale DPF. (ρk)p assumed constant for each channel and equal to the mini filter calculated value

5.3.2 Case study: 2200RPM_90Nm after regeneration.

The second case study was related to the measurement of a DPF after regeneration. The engine was operated at 2200RPM speed and 90Nm torque. The scope of the measurement was the investigation of the regenerated section inside the DPF. (Figure 44)

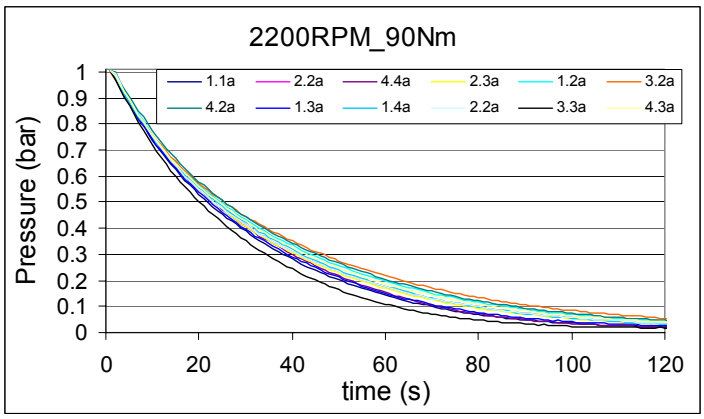

Figure 45 Pressure drop versus time graph. Case: 2200RPM_90Nm.

Also, the same difficulty for the estimation of soot mass collected was faced again. The other subject is the assumption of the value of (ρk)p used in discharge simulation. It is not clear whether the (ρk)p parameter remains constant during the regeneration process. To overcome these difficulties a constant value of (ρk)p parameter was assumed for each channel of the DPF. Furthermore this parameter was assumed to be equal to the parameter determined by the single channel experiments.

The (ρk)p obtained from single channel experiments in the same engine operation point was equal to 6.5E-12.

The same procedure with the previous mentioned case study was followed. A sensitivity analysis performed first, in order to have an idea of the effect of (ρk)p parameter to the mass estimation. Figure 46 and Figure 47 present the results of the sensitivity analysis.

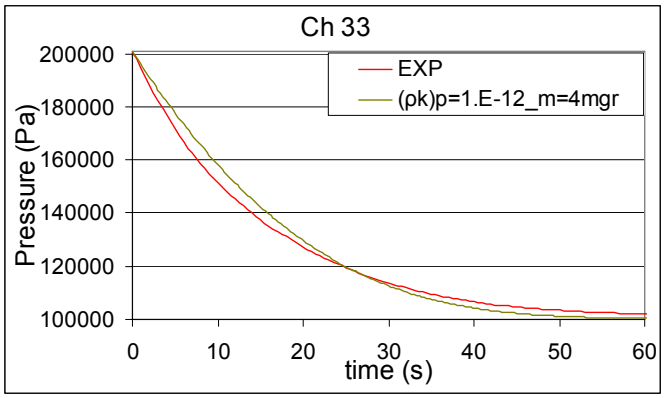

Figure 46 Sensitivity Analysis. Examined parameters (ρk)p and mass collected.

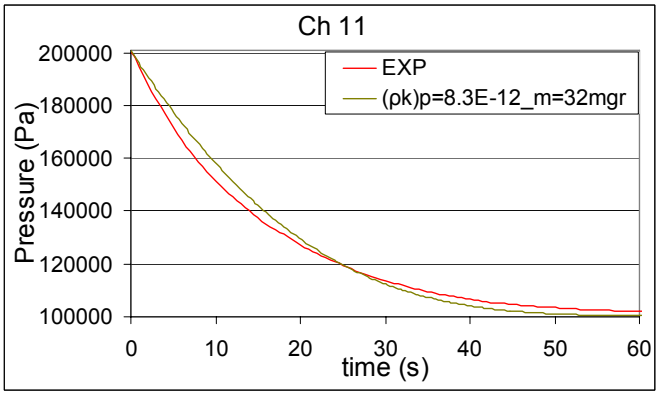

Figure 47 Sensitivity Analysis. Examined parameters (ρk)p and mass collected

It can be seen from the above figures that a small increase in (ρk)p may lead to a big increase in estimated soot mass.

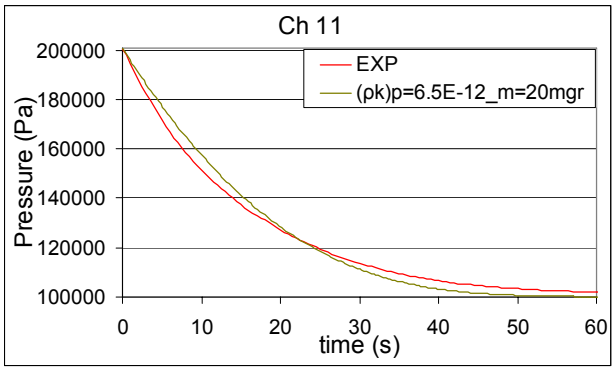

Figure 48 Mass estimation by calculation. (ρk)p calculated from the mini- filter experiments.

The estimated trapped mass by the tuning process (Figure 48 and Annex III: Full – Scale Trap Tuning Graphs) for each channel and for the whole of the DPF is presented in the Table 14 below.

Table 14 Channels of Full Trap and corresponding trapped mass.
Estimation by the Experiment-Calculation System. (ρk)p assumed constant and calculated from the mini filter experiments. 2200_90 Case.

Channel ID	Radius (mm)	Mass (mgr)	Number of Channels	Mass in Section (mgr)
1.1	63	20	50	1000
1.2	58	28	150	4200
1.3	57	20	150	3000
1.4	62	28	50	1400
2.1	50	28	150	4200
2.2	30	28	162	4536
2.3	18	28	162	4536
2.4	57	20	150	3000
3.1	62	22	150	3300
3.2	29.5	40	162	6480
3.3	34	18	162	2916
3.4	57	20	150	3000
4.1	62	18	50	900
4.2	48	28	150	4200
4.3	53	28	150	4200
4.4	69	20	50	1000
Catwall Total mass		15600	Total mass	51868

In the last row of Table 14, the soot mass obtained from the Catwall regeneration simulation is presented as a parameter for comparison. The specific value of (ρk)p employed seems to overestimate the collected mass in the trap in the case of 2200RPM and 90Nm as it was observed in the case of 3000RPM and 40Nm.

The above values are placed into a map – graph in order to have a view of the mass distribution in a DPF. This is presented in Figure 49.

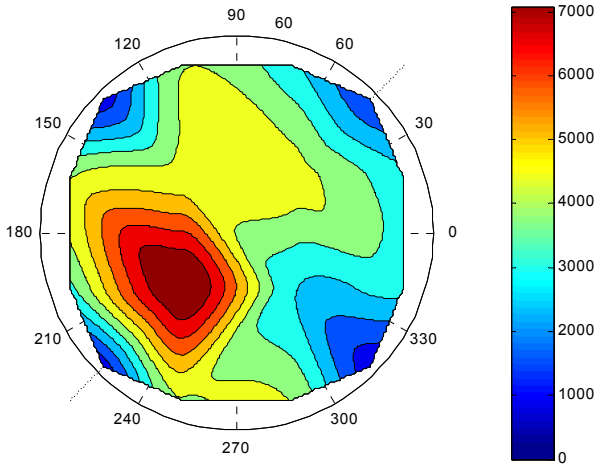

Figure 49 Mass distribution on a full scale trap. (ρk)p assumed constant for each channel and equal to the mini filter calculated value.

From the above Figure it is seen that there is a region in the heart of the DPF that is not cleaned. On first sight, this could mean that the specific region was not fully regenerated. However the other region placed on the right seems to be cleaner. A possible explanation could be that in the left side of the trap there exists a significant fuel additive ash accumulation.

As a synopsis of this chapter it can be written that we could not succeed in a direct correlation between the single channel and full - scale trap measurements. First of all the sensitivity analysis performed to both of the case studies shows that a little increase in (ρk)p product results in a big increase in the estimated value of collected mass in the filter. This indicates that at least one of the two main parameters of the simulation must be accurately known.

When the tuning process is applied to the full-scale trap measurement, we do not obtain the same degree of success as with the mini filter measurements (Figure 43,

and Annex II). The experimental and the computational curves do not fit exactly for the full- scale filter measurements and a possible reason for that is the existence of more than four adjacent channels next to the single channels. Thus the air can escape from the single channel and the four adjacent channels to the rest DPF.

By this way the discharge model does not catch exactly the physical phenomenon. However the experimental – computational method results to (ρk)p estimations close to the corresponding of the Catwall Code output as it will be seen in the next paragraph (6.2). Especially the (ρk)p value obtained for the 3000RPM_40Nm case study is tuned in the value of 7.8E-13 kg/m whether in the corresponding regeneration simulation is 8.1E-13. Thus the calculations model and the program are capable of a full filter channel tuning process.

The (ρk)p estimated by the Experiment – Calculation System for the mini scale filter is of the same order of magnitude with the full scale filter. However then the assumed trapped mass exceeds the corresponding mass computed by Catwall code. Its value is estimated two times to this of Catwall code computations. That is, the use of (ρk)p parameter determined from mini scale trap experiments leads to overestimated absolute values of trapped mass.

It can be seen from the tuning graphs presented above and from the data in Annex III that the experimental and the computational curves for a full scale trap does not match well. Furthermore the use of (ρk)p values obtained from single channel experiments leads to the overestimation of collected mass.

Thus the (ρk)p parameter is not directly applicable to full scale filter experiments and a possible reason for that is the presence of accumulated ash inside a full scale DPF channel. On the contrary a mini scale filter contains no ash which changes the (ρk)p.

The (ρk)p product determined from mini scale trap experiments when is used to the estimation of mass collected into a real DPF does not result to the accurate mass estimation. However it offers a good indication about the percentage of mass trapped in the various channels of the trap as it can be seen from Figure 44 and Figure 49.

It is clear that for different operation points and for different conditions the loading of each channel is different from another. Even if the estimation of (ρk)p is not so accurate, the use of the same value for each channel shows a mass maldistribution into the full scale filter (Figure 44 and Figure 49). Also the history of

the filter plays a significant role because during the regeneration the soot maybe burned but metallic ash may remain trapped to the porous channels. For that reason the simplifying assumption of homogeneous loading cannot realistically be applied to the DPF.

On the other hand, the homogeneous loading assumption could be tested using a CFD code only in the case of a clean or virgin trap. The developed boundary layers and the simulation of the interaction between fluid and particles could indicate the streamlines and the streaklines backwards of a new or clean filter inlet. However this could be useless because the homogeneous loading assumption could be performed only in the first stages of filter loading when the backpressure is not too high and the necessity for regeneration does not exist.

5.4 Conclusions.

- A measuring device and a computer calculation procedure have been developed in order to assist the experimental study of soot loading distribution and pressure drop characteristics of wall flow diesel particulate filters.
- The measuring device records pressure versus time, as the pressurized air from a vessel discharges through selected channels of a cellular particulate filter or through a single- channel mini filter (Cordierite or SiC).
- The interpretation of experimental results by the aid of the computer calculation procedure described in this thesis, allows the estimation of the product $(\rho k)_p$, as demonstrated in this chapter.
- After extensive validation, the results show that the product $(\rho k)_p$, (soot layer density times permeability), for the specific engine- and filter- combinations, lies in the range of 3.5E-12 to 1.15E-11 kg/m , both for a cordierite and a SiC filter.
- The use of (ρk)p parameter determined from mini-scale filter experiments in the calculation of soot mass distribution in the channels of a full scale filter is a workable methodology. However it fails to give an accurate assessment of the absolute value of the collected soot mass.
- Thus the (ρk)p parameter determined from single channel experiment is not directly applicable to full scale filter experiment.
- The traditional assumption of homogeneous loading in the filter channels is not a realistic one, as concluded by the above series of experiments.

Chapter6. CATWALL PRESSURE DROP MODEL VALIDATION TO STUDY: (ρk)p.

A series of regeneration experiments was simulated by the use of Catwall code. The aim of the simulation of experiments was the validation of Catwall code when the given input parameter was the (ρk)p obtained from the single channel experiments. The comparative runs refer to the (ρk)p parameter and the first goal is the observation of the simulation process behavior by changing the previous mentioned parameter.

6.1 Catwall code

"Catwall" is a computer code able to simulate the regeneration process that take place in any Diesel Particulate Filter. The basic output parameters are the temperature of specific points of the simulated DPF, the backpressure ΔP, soot load and other characteristics of the exhaust gas flow through the filter. On the other hand the given input parameters are the initial and boundary conditions of the filter and the exhaust gases that pass through the filter. Annex IV contains more details about the Catwall code operation.

6.2 List of simulated experiments

In order to validate the Catwall code, a list of representative experiments was simulated. The features of each experiment as well the (ρk)p parameter obtained by single channel experiments and Catwall simulation are presented in Table 15

Table 15 List of simulated regeneration experiments

Test ID	Parameter							
	Cell structure	Filter length	PM load	Fuel-borne catalyst Concentration	PM accumulation Condition	Regeneration condition	(ρk)p Catwall	(ρk)p Single Channel measurement
C1	14/200	254mm	**4g/L**	25ppm	3000rpm x 50Nm	1250rpm x 60Nm	9E-13	4E-12
C2			**8g/L**				9E-13	4E-12
C3			**12g/L**				7.83-13	4E-12
E1	14/200	254mm	8g/L	25ppm	**1250rpm x 100Nm**	1250rpm x 60Nm	1.98E-12	6.2E-12
C2					**3000rpm x 50Nm**		9.E-13	4E-12
E3					**4000rpm x 150Nm**		2.2E-12	-
3000_40	14/200	152mm	-	25ppm	**3000rpm x 40Nm**	1900rpm x 200Nm	8.1E-13	3.7E-12
1250_60	14/200	152mm	-	25ppm	**1250rpm x 60Nm**	2600rpm x 180Nm	1.12E-12	5.6E-12
2200_90	14/200	152mm	-	25ppm	**2200rpm x 90Nm**	2600rpm x 180Nm	9.E-13	5.E-12

6.3 Results and Discusion

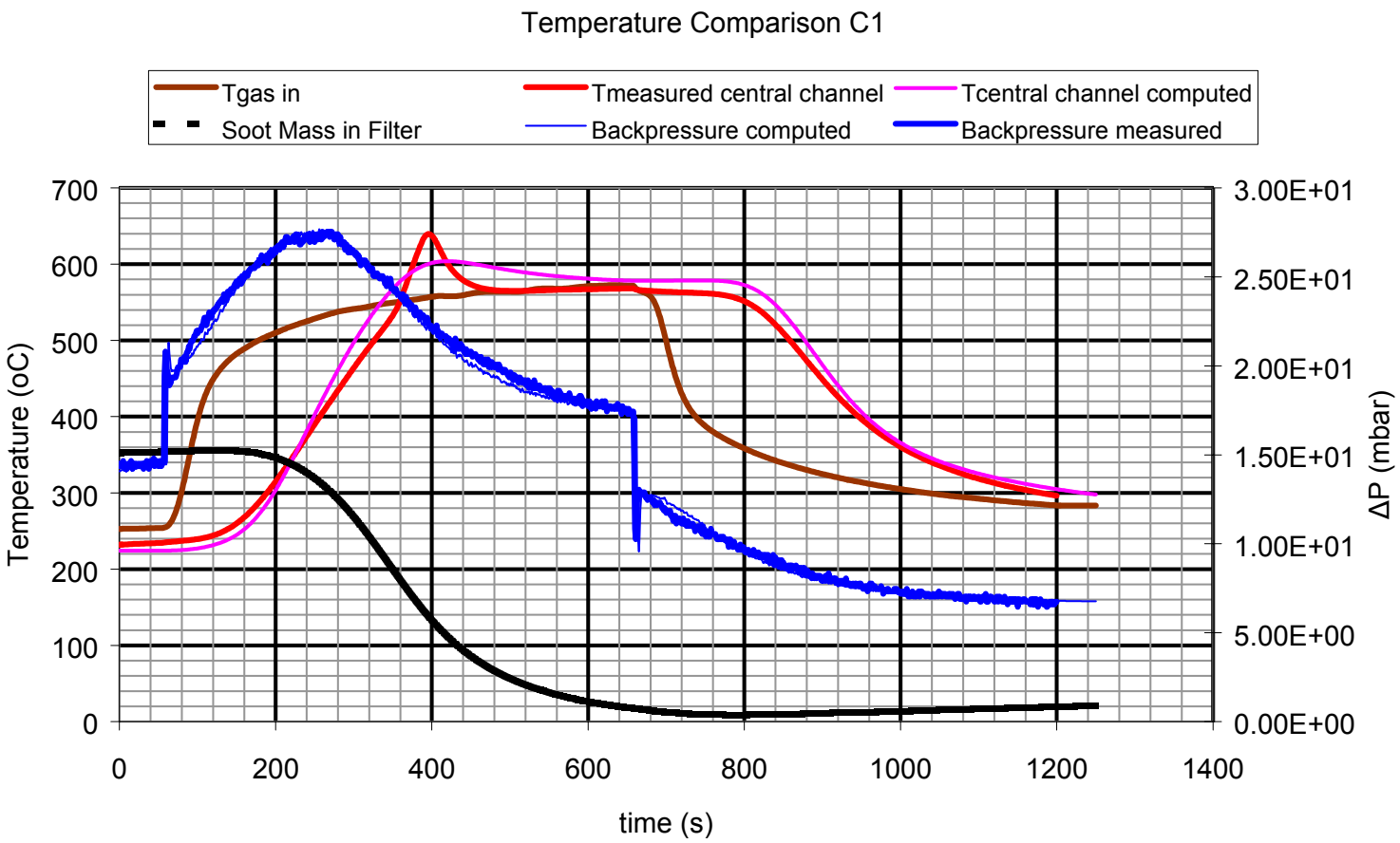

Figure 50 C1 test case Temperature Comparison and Pressure

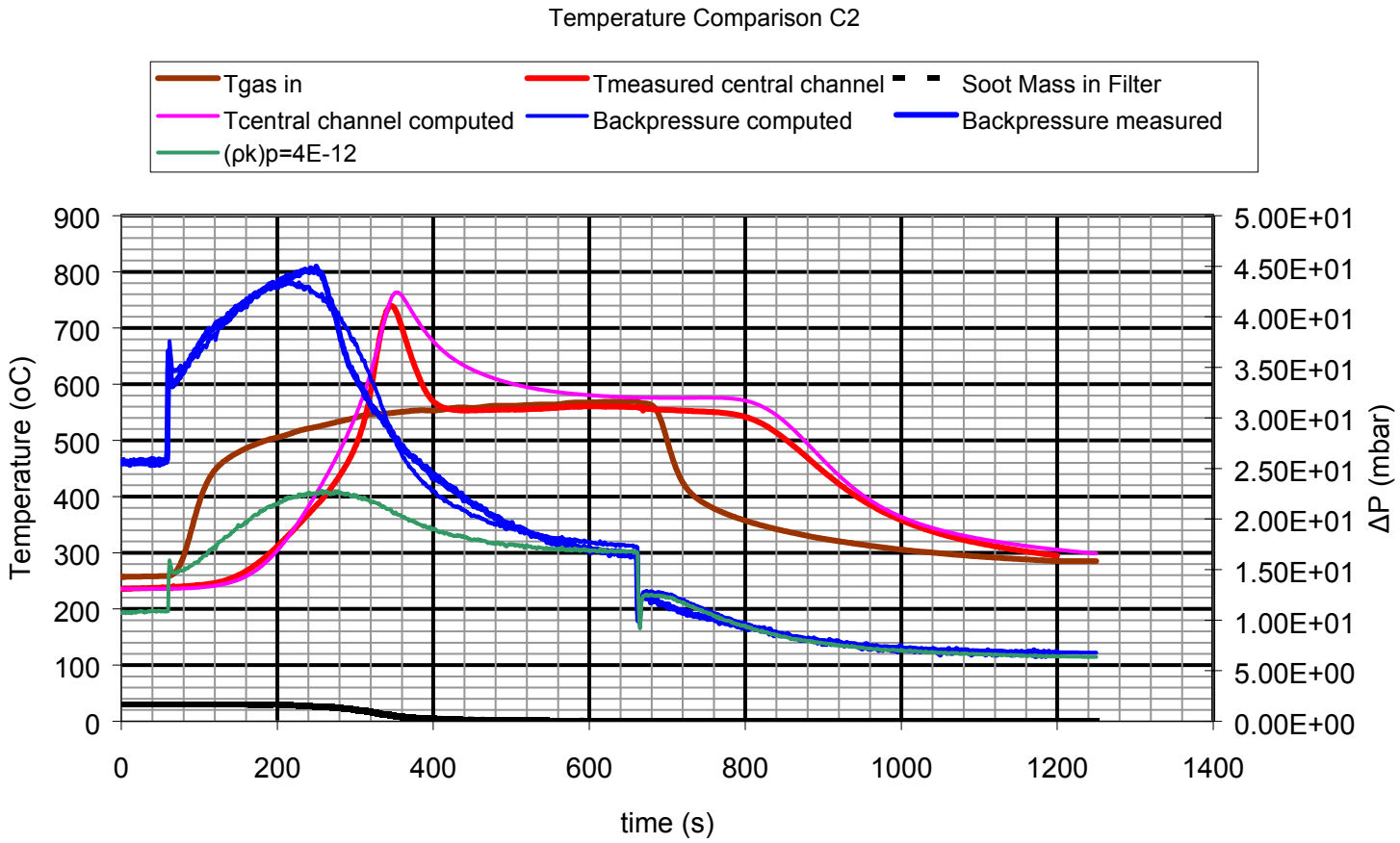

Figure 51 C2 test case. Comparison between:

Backpressure computed using (ρk)p= 8.1E-13 (thin blue line) and (ρk)p= 4E-12 (green line) obtained by single channel measurements

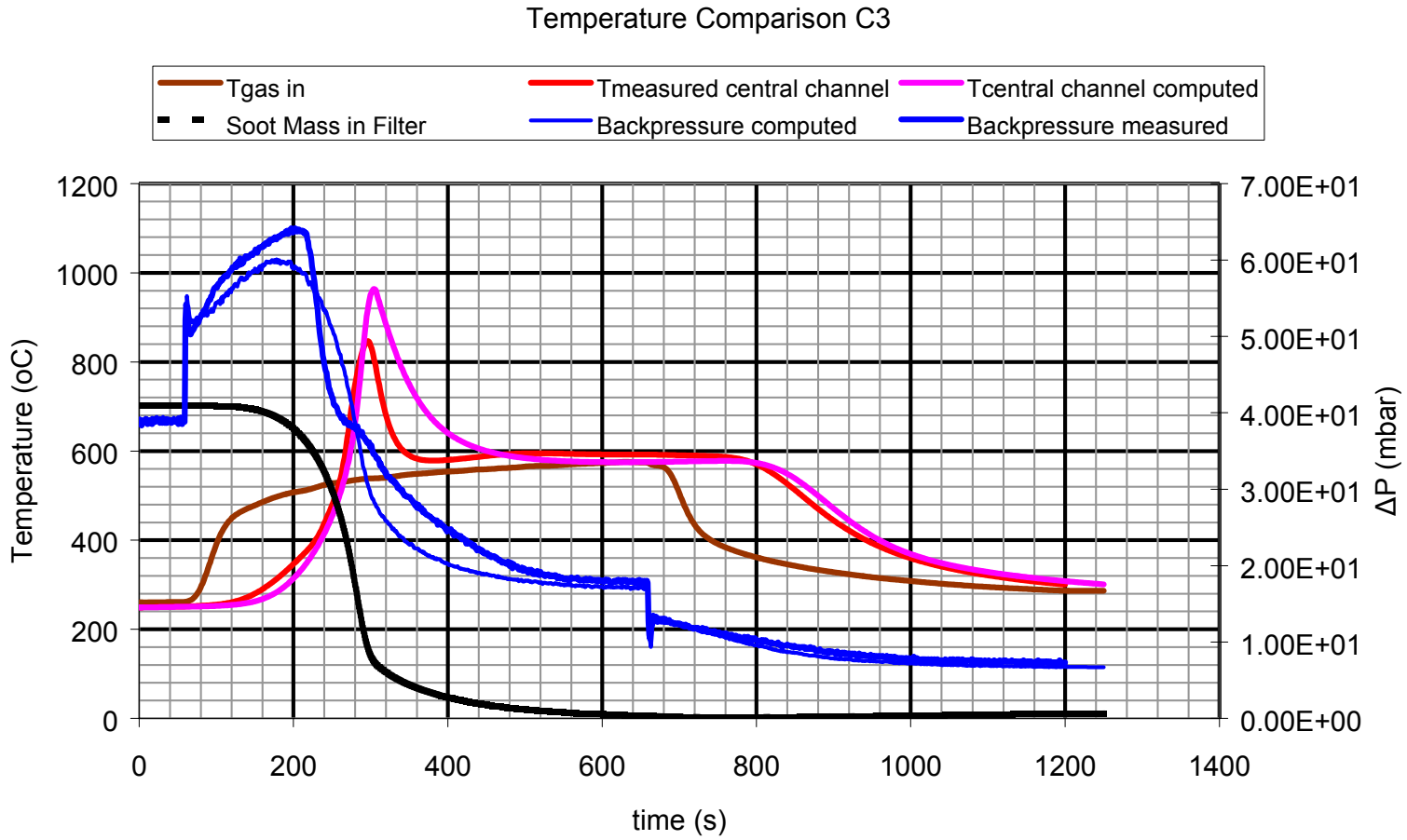

Figure 52 C3 test case Temperature Comparison and Pressure Drop

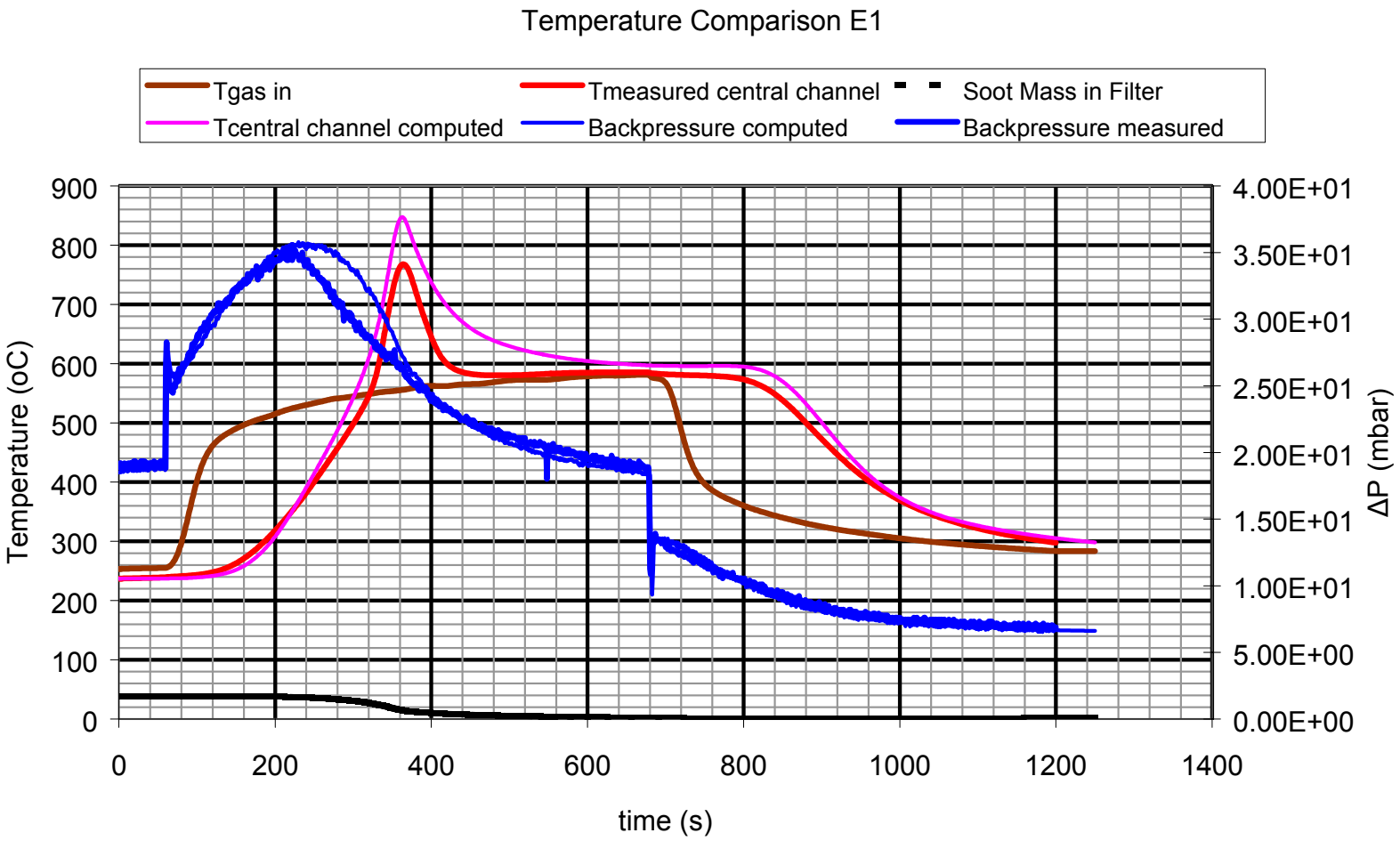

Figure 53 E1 Temperature Comparison and pressure drop

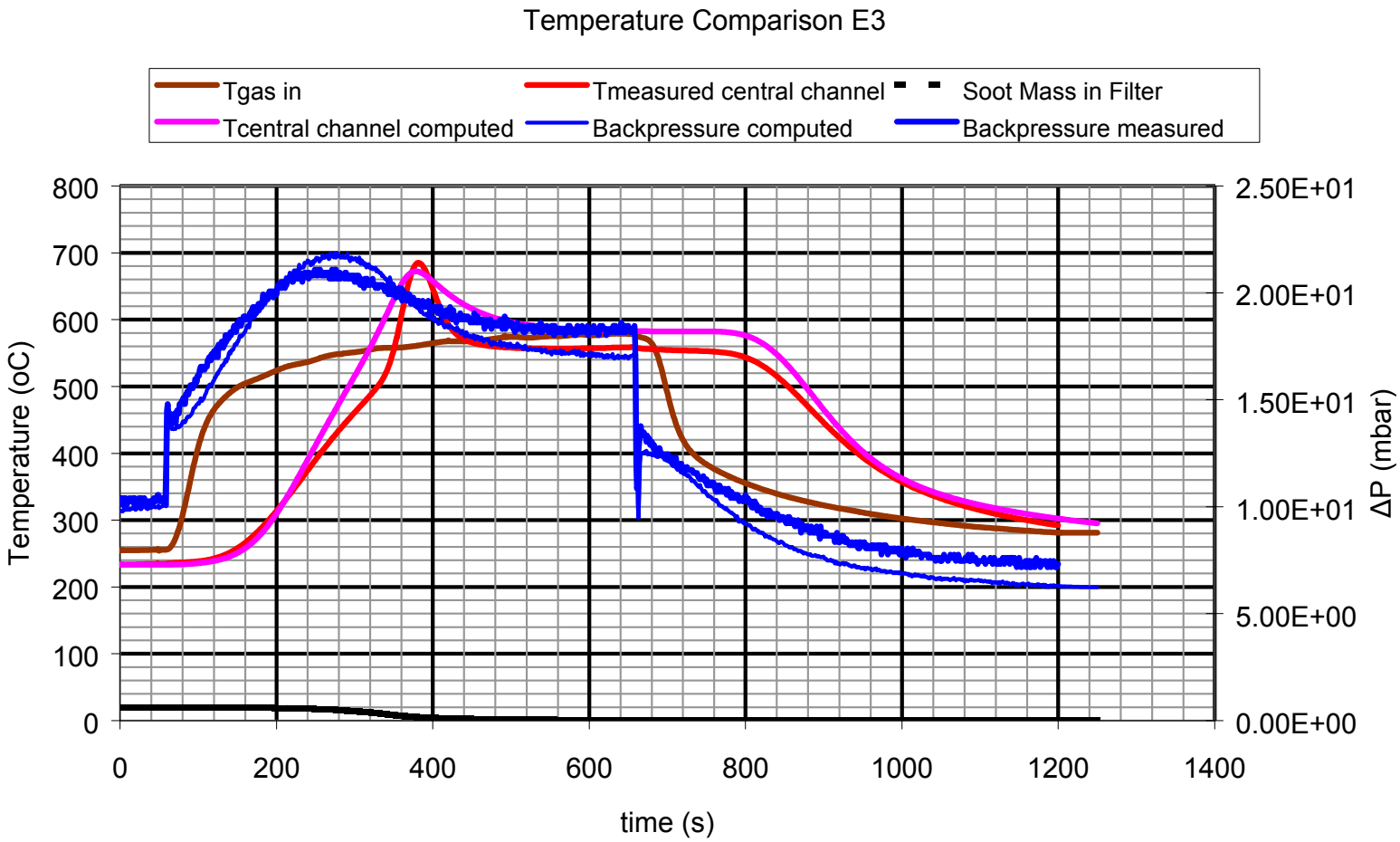

Figure 54 E3 test case. Temperature Comparison and pressure drop

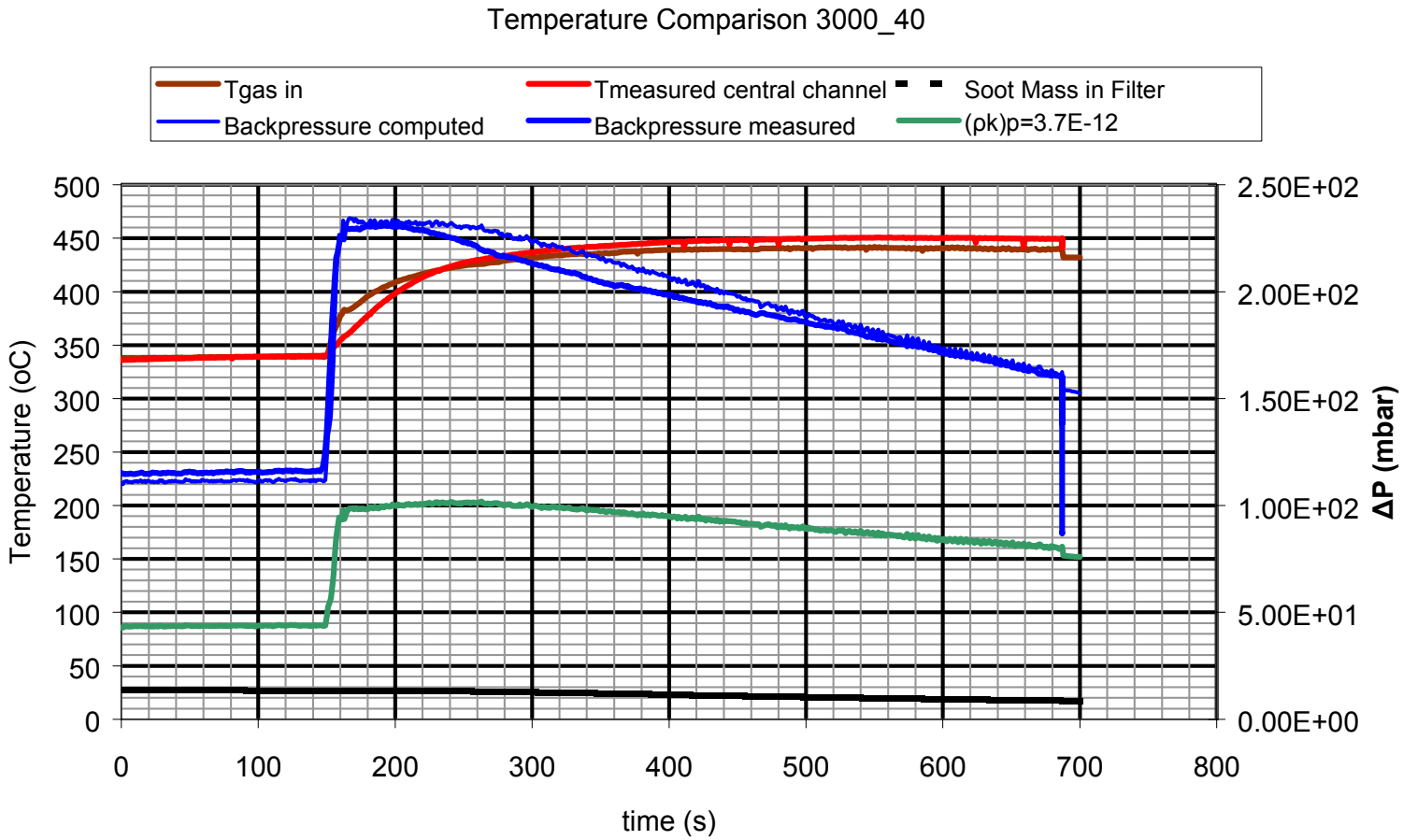

Figure 55 3000RPM_40Nm test case. Comparison between:

Backpressure computed using (ρk)p= 8.1E-13 (thin blue line) and (ρk)p= 3.7E-12 (green line) obtained by single channel measurements

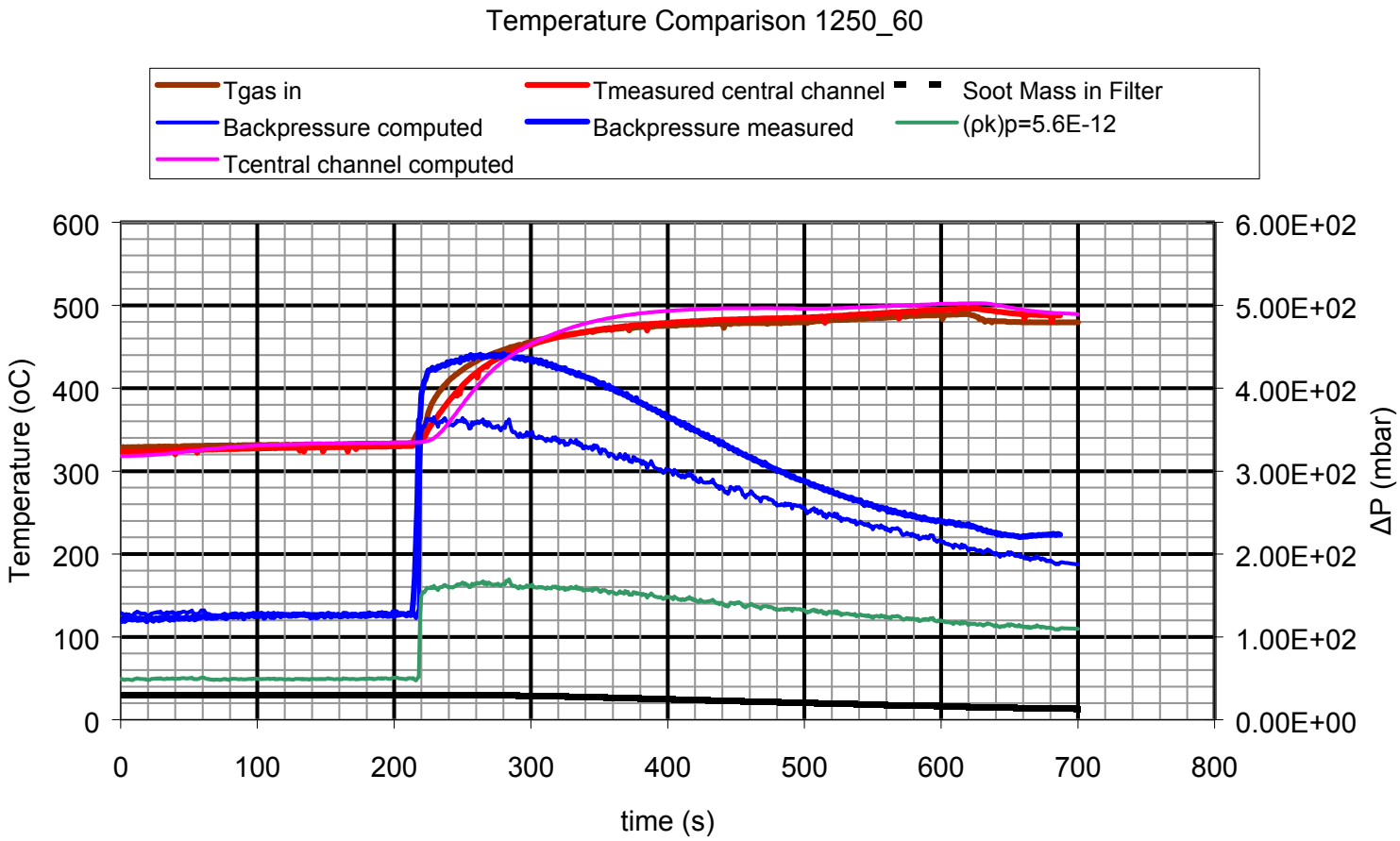

Figure 56 1250RPM_60Nm test case. Comparison between:

Backpressure computed using (ρk)p= 1.12E-12 (thin blue line) and (ρk)p= 5.6E-12 (green line) obtained by single channel measurements

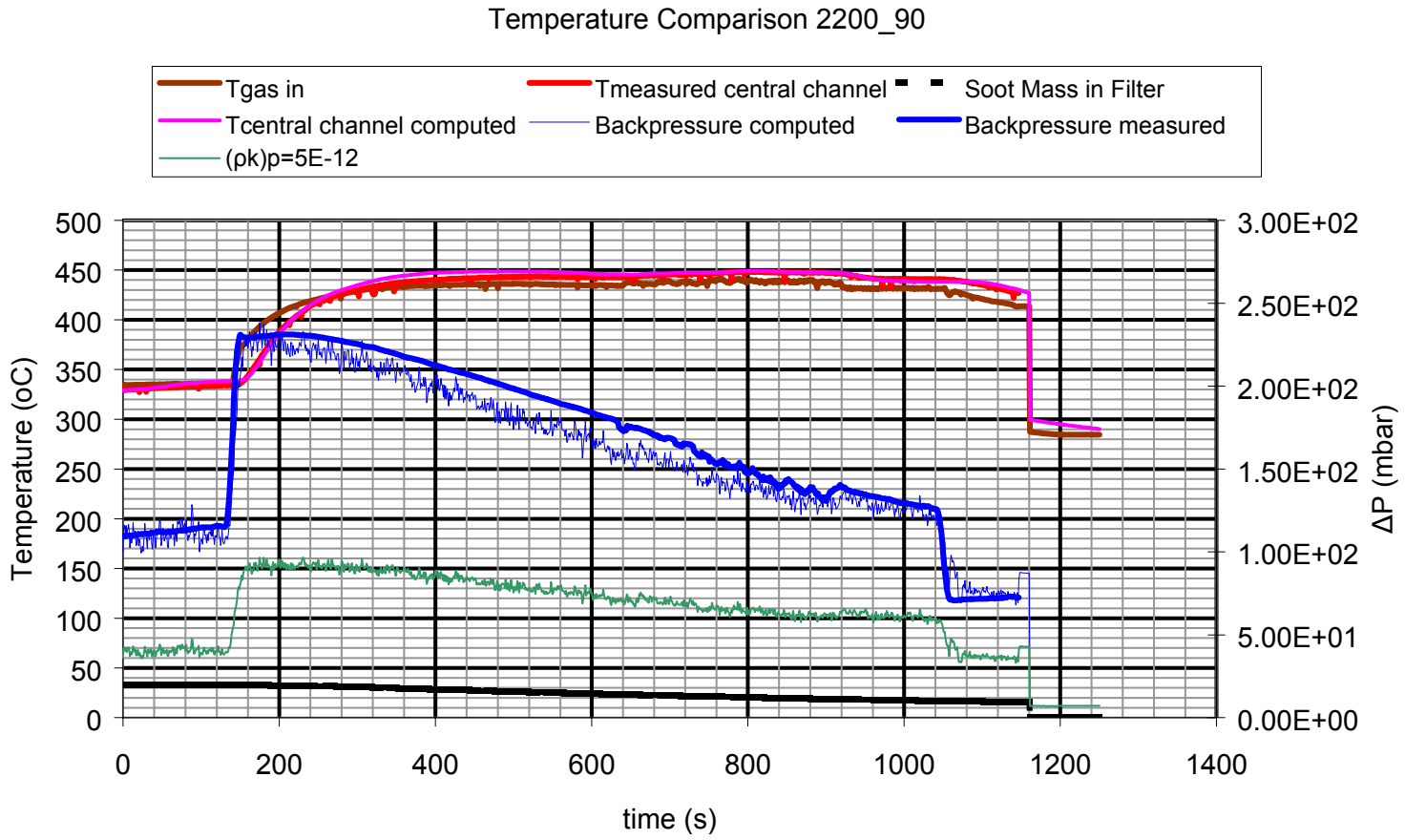

Figure 57 2200RPM_90Nm test case. Comparison between:

Backpressure computed using (ρk)p= 9.E-13 (thin blue line) and (ρk)p= 5E-12 (green line) obtained by single channel measurements

In Figure 50, Figure 51, Figure 52, the simulation of C1, C2, C3 experiments is presented. All these experiments have the same operation point but different particulate matter loading. The values of (ρk)p obtained by the use of Catwall computer code seems to be descending as soot mass increases. This could be attributed to the fact that a much higher decrease in soot permeability suppresses the expected increase in soot density.

In Figure 53 and in Figure 54 the simulation of E1, E3 test cases is presented. E1 and E2 experiments have the same Particulate Matter load but different PM accumulation condition. It is observed that the (ρk)p has not a stable behaviour probably due to the HC which, are not adsorbed.

The (ρk)p values obtained from the Catwall and the single channel measurements are presented in Table 15. The values are consistent with the values obtained from other researchers [38, 42, 43] as it can be seen in Figure 58.

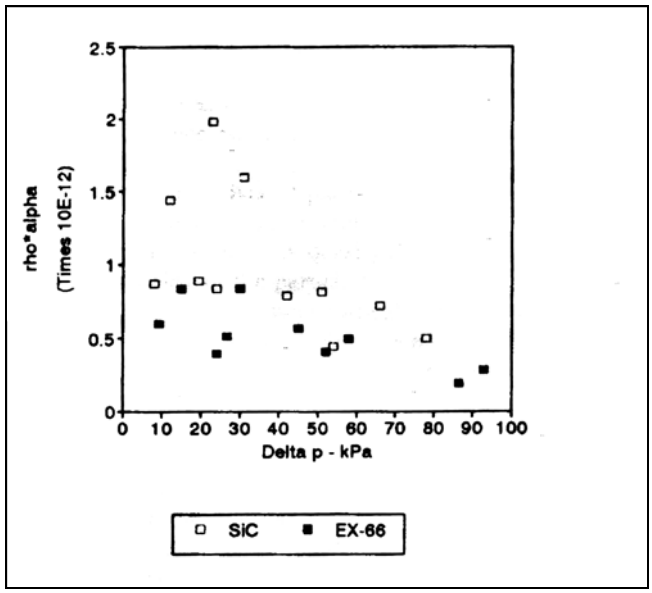

Figure 58 (ρk)p parameter as a function of trap backpressure during collection of particles [38].

The (ρk)p parameter determined from the single channel experiments was used as input data in four of the above simulations.

So, as it can be seen from Table 15 the single channel measured values of (ρk)p are not consistent with the values obtained by the Catwall code. The single

channel experiments and computations seem to offer a slightly higher (ρk)p value from the full scale trap simulation using Catwall.

When the higher (ρk)p values determined from single channel experiments are used as input data into the Catwall code then the computed backpressure decreases compared to the experimental curve. A small increase in (ρk)p leads to a decrease in computed backpressure almost two times compared to the experimental as it can be seen in Figure 51, Figure 55, Figure 56 and Figure 57 which present the results of the regeneration simulation using Catwall and the corresponding experimental curves.

However the values of (ρk)p parameter determined from single channel experiments and the corresponding values of (ρk)p tuned by the Catwall code vary in a range of the same order of magnitude.

Furthermore from the sensitivity analysis described in Figure 41 and Figure 46 and Table 15 it is seen that the values of (ρk)p measured in a full scale DPF are very closely placed to the corresponding values obtained by the simulation using Catwall Code. Thus the measurements could be applied directly into the full scale filter. However this does not exclude the major disadvantage of the unknown amount of soot mass collected in each channel of the real DPF.

The observed difference could be related to the following factors:

- During the loading process the single channel filter is placed perpendicular to the DPF. Thus the flow field for the two traps (full and mini scale) is not the same.
- There are pressure losses on the mini filter inlet section because the flow follows a 90^{o} turn. Thus the pressure gradient between the inlet and the outlet section of the filter may be less than the corresponding pressure difference along the full DPF. Thus the accumulated soot during the loading in a real DPF is more compressed than in the single channel. So, its permeability could be lower.
- The loading history of the two filter types is nonidentical. The full - scale trap contains ash, which is not present in the mini filter and thus the first becomes less permeable.

6.4 Conclusions.

The Catwall code validation procedure led to the following conclusions:

- The (ρk)p values for each loading or regeneration experiment were obtained using two alternative ways. The first was the tuning of (ρk)p parameter using the single channel measurements and the second was performed by simulation using the Catwall Code.
- Both of these two alternative methods result in values of (ρk)p parameter that lie in the same order of magnitude. Furthermore the previously mentioned values of parameters vary in the same range of magnitude with the corresponding values of (ρk)p obtained from other researchers (Figure 58).
- The (ρk)p values estimated by the Experiment – Calculation System for the full scale filter lie very close to the (ρk)p values obtained from Catwall code.
- The single channel experiments and computations seem to offer a slightly higher (ρk)p value from the full scale trap simulation using Catwall.
- The regeneration process is very sensitive to the (ρk)p variation. A small increase in (ρk)p leads to a computed decrease in filter backpressure, almost twice the experimentally determined value.
- Thus the (ρk)p parameter determined from single channel experiments is not directly applicable to full scale DPF simulations.

Chapter7. SOOT MASS ESTIMATION METHOD

7.1 Necessity of trap loading estimation

Filter loading or the soot mass trapped into the filter is a major factor affecting the regeneration process in real conditions and also the simulation of particulate trap regeneration using a relevant computer code. A realistic estimation of the filter loading is essential, since the regeneration process is very sensitive to this quantity as regards both predicted temperature evolution as well as regeneration duration. Computer codes, such as "Catwall" which is used and evolved by the LTTE of UTh, that simulate the regeneration process, require a good estimation of the filter loading for the tuning of the model kinetic parameters to match real – world soot oxidation characteristics. For that reason trap loading estimation methodologies have been developed; some of them are listed below.

One obvious measurement method is the weighing of clean and loaded trap. The difference between the initial before loading and the final after the loading mass, will be equal to the trapped soot mass. However this method is impractical; for example the presence of moisture during the assembly may lead to significant errors in the estimation of soot mass. Moreover the amount of moisture in the ceramic filter must be the same before and after the loading process.

Thus other methods of trapped mass estimation have been developed [44]:

- Measurement of particulate emissions before and after the trap loading phase.
- Correlation of trap loading with backpressure data.
- Absorbance of electromagnetic energy from the loaded filter.
- Energy balance calculations.

The first method is simple and direct as it is materialized by a mass balance, but requires demanding instrumentation for the accurate measurement of particulate emissions.

The second method is widely in use for trap system control and safety purposes on vehicle as it indicates a critical permissible trap loading. However trap backpressure is a complex function of trap loading, exhaust gas flow rate, temperature, nature and composition of the accumulated particulate.

The third method is a specially designed technique that is based on the measurement of the amount of electromagnetic energy absorbed by a material.

The last, trapped soot mass estimation, method is used in the present thesis and is discussed in this paragraph. It is applied to a control volume that encloses the trap and cuts the system in two points, the inlet and outlet section as it can be seen in Figure 59.

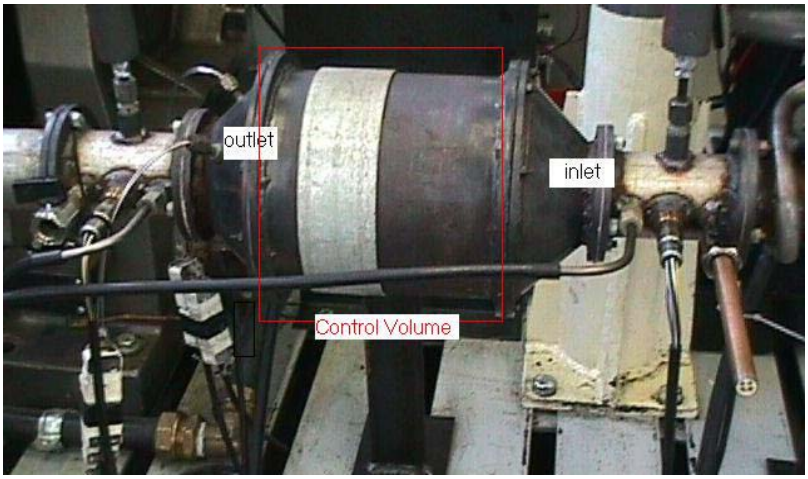

Figure 59 figure Trap and Control Volume for energy balance

The application of this method requires continuous flow rate, temperature recordings in the inlet and outlet of the trap during the regeneration and the estimation of coefficient α indicating the percentage of soot oxidized to CO.

7.2 Theoretical background of the method

Equation (2) can be integrated over a full regeneration with the engine operating at steady state point or during unsteady operation provided that the trap is thermally stabilized before and after the integration time at known temperatures. The assumptions are

- The experiment duration is adequate for the trap temperature to be stabilized at a constant value (equally to the exhaust gas temperature) in order to calculate the internal energy U.
- Any soluble organic part previously accumulated has already been desorbed due to the high regeneration temperatures. Thus it does not contribute in the regeneration producing extra thermal energy.

It is assumed that the reactions that take place during the regeneration process can be modeled as follows:

$C + \alpha O_2 \rightarrow 2(\alpha - 0.5)\, CO_{2\alpha} + 2(1-\alpha)\, CO$ (w)

which is a one – step kinetic scheme taking into account the incomplete oxidation.

Where α is an index of the completeness of the reaction taking values from 0.5 to 1 but usually α = 0.8. For further details about the estimation of 'α' the reader can see the paper [44].

Reaction (w) is exothermal with a combined reaction enthalpy resulting from the complete and incomplete oxidation of carbon:

$$\Delta H = 2(\alpha - 0.5)\, \Delta H_{CO2} + 2(1 - \alpha)\, \Delta H_{CO} \tag{7-1}$$

The energy balance applied in the trap control volume takes the following form:

$$\dot{H}_1(t) - \dot{H}_2(t) = \frac{dU_{trap}}{dt} - \Delta H \frac{dm_{soot}}{dt} \tag{7-2}$$

when the trap has no thermal losses to the surroundings. With 1 is called the inlet region and 2 the outlet.

The enthalpy of inlet and outlet flow is defined as

$$H_1(t) = m_{gas1} C_{pgas1} \left(T_{gas1} - T_{o1}\right) \tag{7-3}$$

and

$$H_2(t) = m_{gas2} C_{pgas2} \left(T_{gas2} - T_{o2}\right) \tag{7-4}$$

respectively. The enthalpy's rate of change with regard to the time is defined for both of the flows inlet and outlet:

$$\dot{H}(t) = \frac{dH}{dt} = \frac{dm_{gas}}{dt} C_{pgas} \left(T - T_o\right) \tag{7-5}$$

Also the internal energy of the trap is determined using the next formula:

$$U_{trap} = m_{trap} C_{ptrap} T_{trap} \tag{7-6}$$

and the rate of change is:

$$\frac{dU_{trap}}{dt} = m_{trap} C_{ptrap} \frac{dT_{trap}}{dt} \tag{7-7}$$

In case that the trap is not insulated then there are heat losses to the surroundings described by the next formula:

$$Q_{los} = hA(T_s - T_a) \tag{7-8}$$

which must be count in (7-2) as follows:

$$\dot{H}_1(t) - \dot{H}_2(t) = \frac{dU_{trap}}{dt} - \Delta H \frac{dm_{soot}}{dt} + \dot{Q}_{los}(t) \tag{7-9}$$

As it is obvious the above formulae contain derivatives of the magnitudes with respect to time. Thus the total amount of trapped soot in the filter can be then calculated by integration of Eq (9), which will give:

$$\Delta m_{soot} = \frac{1}{\Delta H} \int_0^{t\max} \left\{ \dot{H}_2(t) - \dot{H}_1(t) + \frac{dU_{trap}}{dt} + \dot{Q}_{los}(t) \right\} dt \tag{7-10}$$

Because the trap internal energy is a state magnitude there is no care for the intermediate path but for the initial and final state:

$$\int_0^{t\max} \frac{dU_{trap}}{dt} dt = \Delta U_{trap} = m_{trap} c_{ptrap} \left(T_{final} - T_{initial} \right) \tag{7-11}$$

Also as long as the temperatures are not constant, the variance of specific heat capacity must be introduced in the above equations. Thus the specific heat for gas and the trap is respectively:

$$C_{pgas}(T) = 537 T^{0.097} \tag{7-12}$$

$$C_{ptrap}(T) = 0.0000002 T^3 - 0.001 T^2 + 1.61186 T + 320.117 \tag{7-13}$$

7.3 Application of energy balance – Results and Discussion.

The trap loading estimation method by energy balance discussed before has been applied to a set of available test cases. The basic objective was the cross validation of both experiments (quality assurance) and energy balance calculations.

As it has been already written, a good estimation of the trapped soot mass is a major factor for the understanding of the regeneration. Thus the energy balance method was applied to each experiment. A part of those experiments will be presented in conjunction with the measured values of burned soot mass, in this thesis, in order to demonstrate the alternative soot mass estimation method of energy balance. Figure 60 presents a graph that shows the evolution of exhaust gas temperature before and after the trap. By integration, the lefthand side terms of equation (7-9) are taken. The specific figure refers to F1 test case of experiments. The method is materialized using

MS Excel. The basic Excel input columns contain time, fuel flow rate, inlet and outlet temperatures, representative temperatures of the trap and the temperatures of the surface of trap. The other columns contain the derivative magnitudes according to the theory discussed above.

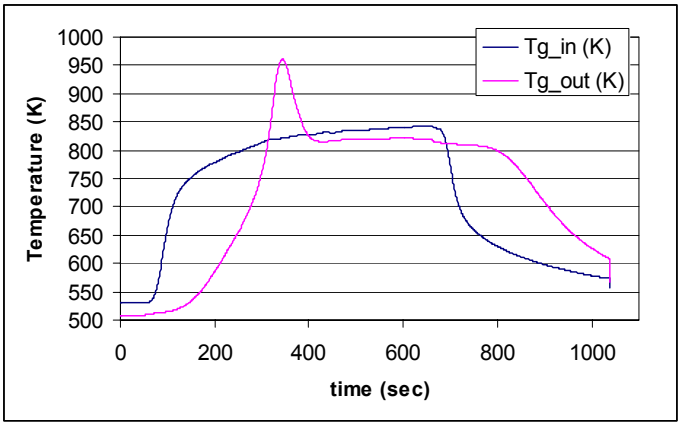

Figure 60 Evolution of inlet and outlet exhaust temperatures. F1 test case.

Table 16 Soot mass accumulation. Comparison between weighed soot mass and energy balance method estimation.

Test ID	soot mass burned (gr)		Test ID	soot mass burned (gr)	
	Weighed	En. Balance		Weighed	En. Balance
A1	15.7	9.8759822	D2	29.1	29.28316
A2	18.3	20.828316	D3	27.7	16.23061
A3	29.1	29.283165	E1	35.1	34.73522
A4	31	34.566472	E2	29.1	29.28316
A5	45.5	66.957522	E3	15.7	13.34541
A6	44.6	59.418272	F1	29.1	29.28316
B1	15.7	9.8759822	G1	29.1	29.28316
B2	29.1	29.283165	G2	31.7	35.54885
B3	45.5	66.957522	H1	36.1	72.42149
C2	29.1	29.283165	H2	38.6	68.25646
C3	39.9	41.726435			

The next table presents the test cases and the experimental parameters of each test case.

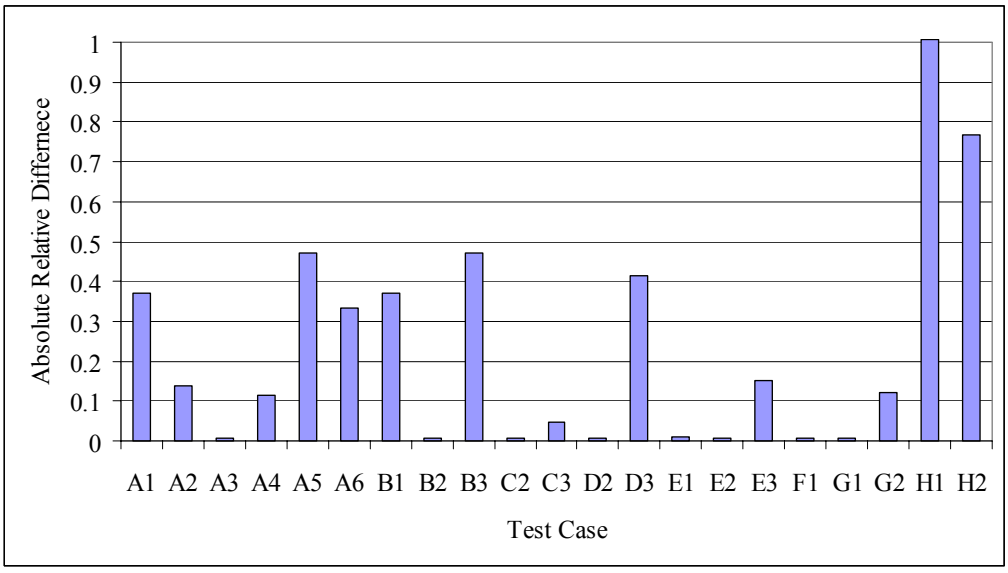

Figure 61 Test case and relative difference between the weighed soot mass and the mass obtained by the energy balance method

Figure 61 presents the differences for the soot loading estimations for each experiment between the weighed mass and the mass obtained by the energy balance method. The relative difference mentioned in this figure is determined from the equation:

Relative difference = $\left|\frac{m_{Weighed} - m_{Balanced}}{m_{Weighed}}\right|$. Also it should be noticed that the experimental procedure was not under Uth's control.

Table 17 Regeneration test cases and Experimental parameters

Test name	Test ID	Parameter					
		Cell structure	Filter length	PM load	Fuel-borne catalyst Concentration	PM accumulation Condition	Regeneration condition
Cell structure	A1	**14/200**	150mm	8g/L	25ppm	3000rpm x 50Nm	1250rpm x 60Nm
	A2	**12/300**					
	A3	**14/200**	254mm				
	A4	**12/300**					
	A5	**14/200**	381mm				
	A6	**12/300**					
Filter Length	B1	14/200	**150mm**	8g/L	25ppm	3000rpm x 50Nm	1250rpm x 60Nm
	B2		**254mm**				
	B3		**381mm**				
PM Load	C2	14/200	254mm	**8g/L**	25ppm	3000rpm x 50Nm	1250rpm x 60Nm
	C3			**12g/L**			
Fuel-borne Catalyst Concentration	D2	14/200	254mm	8g/L	**25ppm**	3000rpm x 50Nm	1250rpm x 60Nm
	D3				**50ppm**		
PM Accumulation Condition (VOF content)	E1	14/200	254mm	8g/L	25ppm	**1250rpm x 100Nm**	1250rpm x 60Nm
	E2					**3000rpm x 50Nm**	
	E3					**4000rpm x 150Nm**	
Regeneration Condition	F1	14/200	254mm	8g/L	25ppm	3000rpm x 50Nm	**1250rpm x 60Nm**
Heat Conduction Rateof Adhesive	G1	14/200	254mm	8g/L	25ppm	3000rpm x 50Nm	1250rpm x 60Nm
	G2						
Destructive Regeneration	H1	**14/200**	254mm	10g/L	25ppm	3000rpm x 50Nm	4000rpm x full to Idle
	H2	**12/300**					4000rpm x full to Idle

7.4 Conclusions

- An alternative method of trap loading estimation method developed elsewhere, has been applied also in this case study. The method's main advantage is that it requires simply the continuous recording of the temperature data before and after the trap.
- Although in the cases A2, A3, A4, B2, C2, C3, D2, E1, E2, E3, F1, G1, G2 the values of the relative difference are small, there are observed deviations during the same type of experiments.
- The method failed when it was applied to the test cases H1 and H2. These are destructive regeneration tests and probably the experiments are not reliable.
- The relative higher differences between the weighed soot mass and the soot mass estimated by the energy balance, which are observed in the rest test cases are probably because of the HC effects. These effects are not taken in account during the mass balance estimations.
- The adsorption and the subsequent burning of HC releases thermal energy and increases the measured temperatures. The energy balance demonstrated in this section overestimates the soot mass in order to balance the released thermal energy form HC burning.
- Furthermore the ambient conditions are not exactly known. Thus the total heat transfer coefficient is not constant for each experiment, and only an assumption can be done. In the above energy balance application the heat transfer coefficient was assumed constant.

Chapter8. DIRECTIONS OF FUTURE WORK

8.1 Synopsis

This thesis produced the following results:

1. The development of a (ρk)p estimation methodology. The methodology consists of two linked parts. The first part is the experimental procedure and the second contains the accompanying calculations. The calculation part simulates the experimental procedure and gives as output the (ρk)p value for each test case. It was applied in both mini scale and full scale DPF..
2. A cross checking of Catwall code with respect to backpressure. This part of the work contains simulations of representative regeneration experiments using the Catwall computer code of LTTE. The scope was the investigation of the effects that specific parameters such as soot mass load and (ρk)p have on the regeneration simulation. The parameters were tested in conjunction with the experimental results by the previously mentioned processes.
3. The results of the above investigations show that although the values of (ρk)p parameter obtained by the simulation of the regeneration in a full scale trap vary in the same range of magnitude with the (ρk)p determined from the single channel experiments, however the single channel measurement is not directly applicable to full- scale filter assessments. The different conditions that occur during the loading process of a mini scale filter and of a real filter on the other hand, could represent a possible reason for this slight but critical deviation
4. The last part of this thesis contains the development and application of an alternative trap loading estimation method, based on the energy balance performed to the trap. The method was applied to a series of available experimental data.

It could be useful to remind that the accurate knowledge of the basic parameters (ρk)p and soot mass trapped, is necessary as long as these parameters represent a basic part of the input data for Catwall regeneration simulation code. The specific conclusions for each of these discrete parts of the present thesis are presented in the respective Chapters.

8.2 Suggestions for future work

Future work on this subject could be directed in the following paths:

- Performing new experiments at higher engine speeds.
- The experiments could cover a wide range not only of engine operation points, but should take in account the accumulated mass of particulate matter.
- The single channel filter experiment and simulation could be further improved probably by the direct mounting of the single channel filter into the central region of a real DPF.
- The correlation between the mass loading and the (ρk)p in the various sections of DPF could be further investigated.
- The correlation of trap backpressure to the (ρk)p parameter, the accumulated mass in the DPF and the engine operation point could be further investigated.
- A correlation between the fully regenerated sections of DPF and the trap temperatures and backpressure could be sought.
- The measurements and calculations with the aid of the pressure vessel could be applied directly to the real DPF in order to assist the development of the 3-D version of Catwall Code. However in this case only assumptions for the accumulated soot could be done.
- Performing CFD simulations in order to have a better insight to the loading and regeneration phenomena based on first principles. The simulations could be performed in conjunction with specially designed experiments.
- Energy balance calculations for soot mass estimation should take in account HC adsorption – desorption effects.

ANNEX I: SIMPLIFIED COMPUTATION OF FLOW THROUGH MEASUREMENT DEVICE (FORTRAN)

```
PROGRAM DOXEIO 8
      PARAMETER(N=400000)
      REALMREAL(N), MREAL1(N), MREALCH(N), MREAL2(N), MREAL3(N), MDOX(N)
      REAL PT(N),P0(N),PCRI,PAT,PDOX(N),DM(N),TIM(N),VF(N),DPF(N)
      REAL DT,G,RD,AT,T0,VOL,K,M0,R,CRIN,CRINP(N),PTC(N),DPTRAP(N)
      REAL DVIS,ES,KS,EP,KP,RHO,L,W,ZMAX,RAT,MP,AF,RHOKP,OBO
      OPEN(12,FILE='DOXEIO8.DAT')
      NDOK=10000000
      DT=0.001
      G=1.4
      CD=0.73
      RD=0.002
      AT=RD*RD
      R=287.0
      T0=305.0
      VOL=0.005
      ZMAX1=0.001
      ZMAXI=0.001
      PAT=100000.0
      PEKS=100000.0
      P0(1)=201251.4
      PDOX(1)=P0(1)
      MDOX(1)=(P0(1)*VOL)/(R*T0)
      DVIS=0.0000185
      ES=0.0004318
      KS=3.70E-13
      RHO=1.2
      L=0.152
      W=0.002
      AF=4*L*W
      OBO=MP/(AF*RHOKP)
      RAT=0.99
      PT(1)=RAT*P0(1)
CCOMPUTATIONS FOR  I = 1
C INNER LOOP  TRY + ERROR
      DO 9 K=1,NDOK
      CRINP(1)=PT(1)/0.5283
C ELEGXOS STRAGGALISMENHS H MH ROHS
      IF(P0(1) .GE. CRINP(1)) GOTO 101
      IF(P0(1) .LT. CRINP(1)) GOTO 100
C SUBCRITICAL REAL FLOW COMPUTATIONS
 100  MREAL1(1)=((CD*AT*P0(1))/SQRT(R*T0))*(PT(1)/P0(1))**(1/G)
     MREAL2(1)=(((2*G)/(G-1))*(1-(PT(1)/P0(1))**((G-1)/G)))**(1./2.)
      MREAL(1)=(MREAL1(1))*(MREAL2(1))
      DM(1)=MREAL(1)*DT
      VF(1)=MREAL(1)/(RHO*AF)
      goto 115
C CHOKED FLOW COMPUTATIONS
 101  MREALCH(1)=((CD*AT*P0(1))/SQRT(R*T0))*(G**(1./2.))*(2/(G+1))
    +**((G+1)/2*(G-1))
      DM(1)=MREALCH(1)*DT
      VF(1)=MREALCH(1)/(RHO*AF)
```

```
C INNER LOOP (PT(1) - PTC(1) TEST)
 115  PTC(1)=PAT+DVIS*VF(1)*((ES/KS)+OBO)
           DPF(1)=ABS((PT(1)-PTC(1))/PT(1))
           ZMAX=ZMAX1
           IF(DPF(1) .LE. ZMAX) GOTO 116
           PT(1)=PT(1)-10.
   9  CONTINUE
 116  TIM(1)=0.0
C COMPUTATIONS  FOR   I > 1
           DO 1  I=2,N
           MDOX(I)=MDOX(I-1)-DM(I-1)
     PDOX(I)=(MDOX(I)*R*T0)/VOL
           P0(I)=PDOX(I)
           PT(I)=PT(I-1)
C INNER LOOP  TRY + ERROR
           DO 21  K = 1,NDOK
           CRINP(I)=PT(I)/0.5283
C  ELEGXOS STRAGGALISMENHS H MH ROHS
           IF(P0(I) .GE. CRINP(I)) GOTO 111
           IF(P0(I) .LT. CRINP(I)) GOTO 110
C SUBCRITICAL  REAL FLOW COMPUTATIONS
 110       MREAL1(I)=((CD*AT*P0(I))/SQRT(R*T0))*((PT(I)/P0(I))**(1/G))
     MREAL2(I)=((2.*G)/(G-1.))*(1.-(PT(I)/P0(I))**((G-1.)/G))
     MREAL3(I)=MREAL2(I)**0.5000001
           MREAL(I)=(MREAL1(I))*(MREAL3(I))
           DM(I)=MREAL(I)*DT
           VF(I)=MREAL(I)/(RHO*AF)
           GOTO 125
C CHOKED FLOW COMPUTATIONS
 111       MREALCH(I)=(CD*AT*P0(I))/SQRT(R*T0)*(G**(1./2.))*(2/(G+1))
    +**((G+1)/2*(G-1))
           DM(I)=MREALCH(I)*DT
           VF(I)=MREALCH(I)/(RHO*AF)
C INNER LOOP (PT(I) - PTC(I) TEST)
 125  PTC(I)=PAT+DVIS*VF(I)*((ES/KS)+OBO)
           DPF(I)=ABS((PT(I)-PTC(I))/PT(I))
           ZMAX=ZMAXI
           IF(DPF(I) .LE. ZMAX) GOTO 126
     PT(I)=PT(I)-2.
           PRINT*, PDOX(I),PT(I),PTC(I),K,I
           IF(PT(I) .LT. PEKS) GOTO 22
 21   CONTINUE
 22   GOTO 23
 126       TIM(I)=(I-1)*DT
           A=I
           IF(PDOX(I) .LE. PEKS) GOTO 105
  1   CONTINUE
 23        GOTO 105
 105       DO 4 I=1,A,300
           DPTRAP(I)=PT(I)-PEKS
11         WRITE(12,3) TIM(I),PDOX(I),PT(I),PTC(I),I
  4  CONTINUE
  3   FORMAT(F23.6,F23.6,F19.9,F19.9,I5)
 14        CLOSE(12)
           STOP
           END
```

ANNEX II. MINI FILTER TUNING GRAPHS

In this section the mini filter tuning graphs are presented. The graphs contain the experimental and the computational pressure drop characteristics performed on SiC and Cordierite mini scale filters.

Four numbers characterize each figure. The first number denotes engine speed in RPM, the second denotes engine torque in Nm, the third is the mass trapped in the filter and the fourth is the estimated (ρk)p product value. The first part of the figures below refers to Cordierite mini scale filter and the second part refers to the SiC mini scale filter tuning curves.

Cordierite mini scale filter tuning curves.

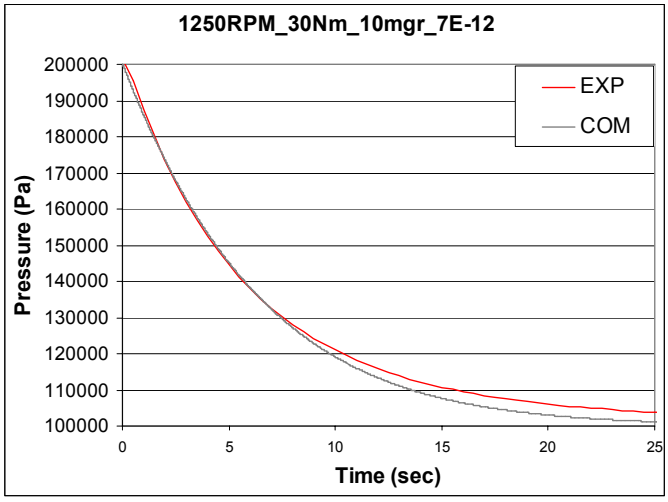

Figure 62 1250RPM_30Nm_10mgr7E-12

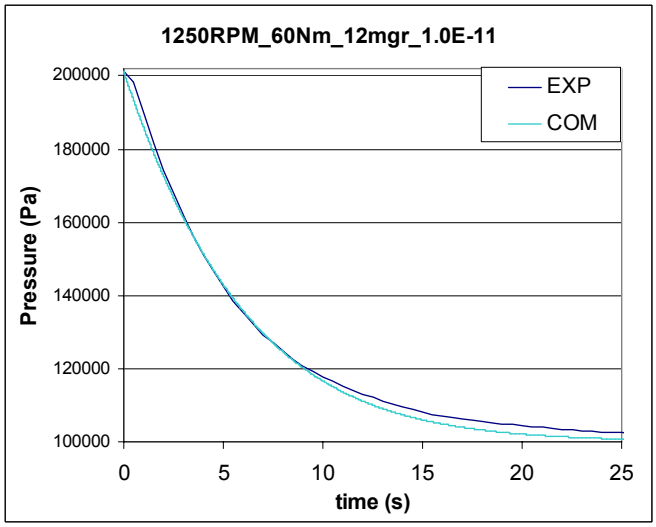

Figure 63 1250RPM_30Nm_12mgr1E-11

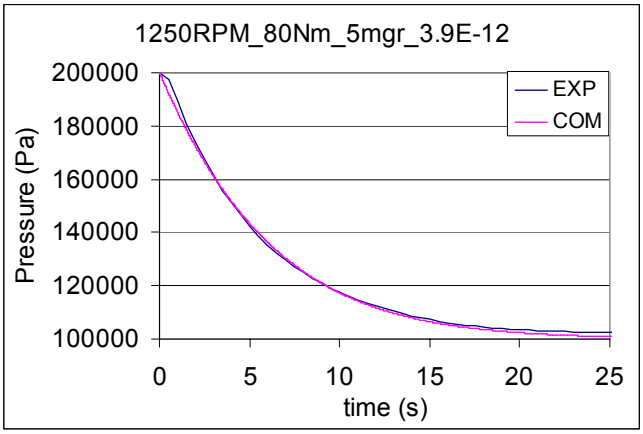

Figure 64 1250RPM_80Nm_5mgr_3.9E-12

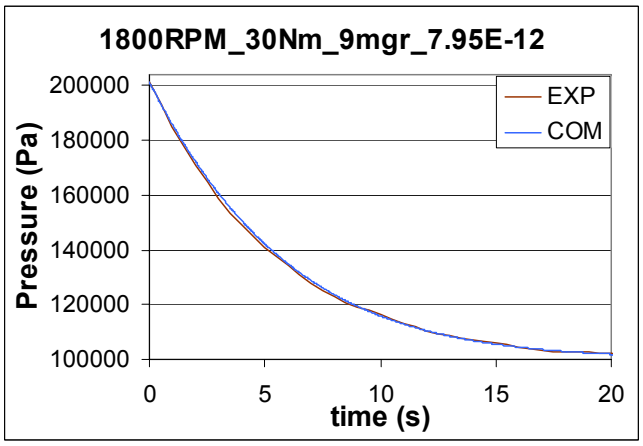

Figure 65 1800RPM_30Nm_9mgr_7.95E-12

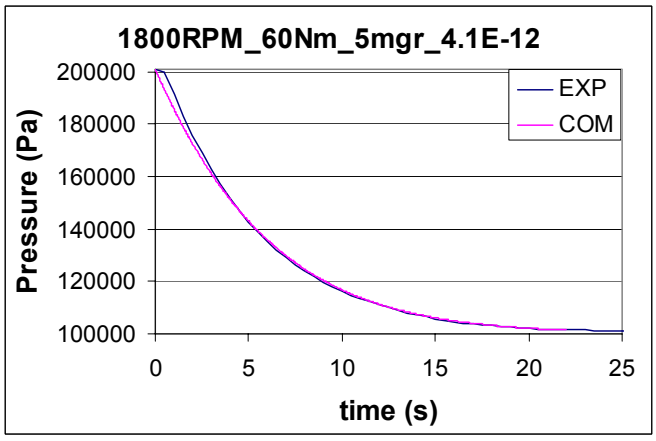

Figure 66 1800RPM_60Nm_5mgr_4.1E-12

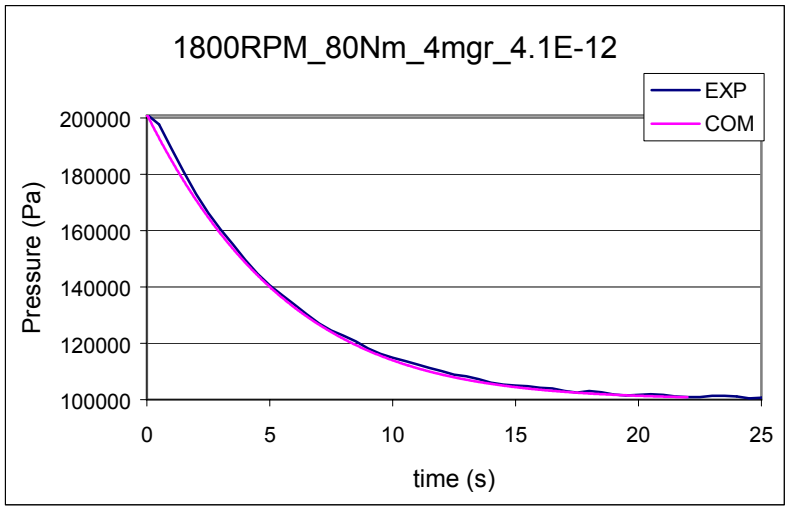

Figure 67 1800RPM_80Nm_4mgr_4.1E-12

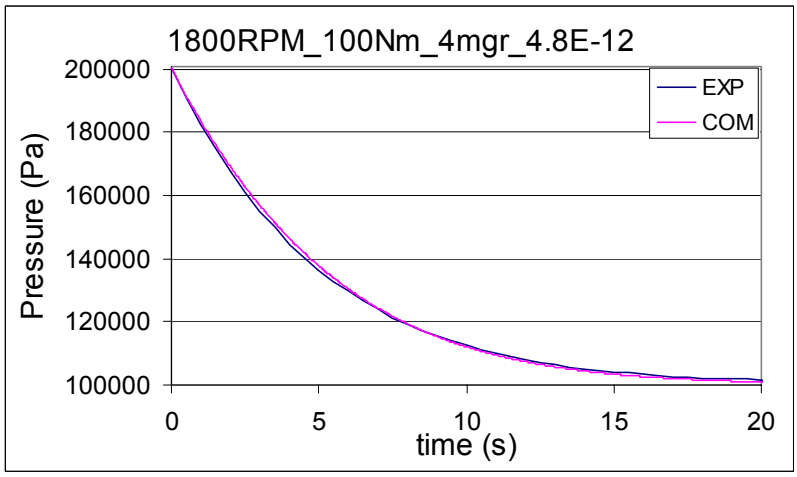

Figure 68 1800RPM_100Nm_4mgr_4.8E-12

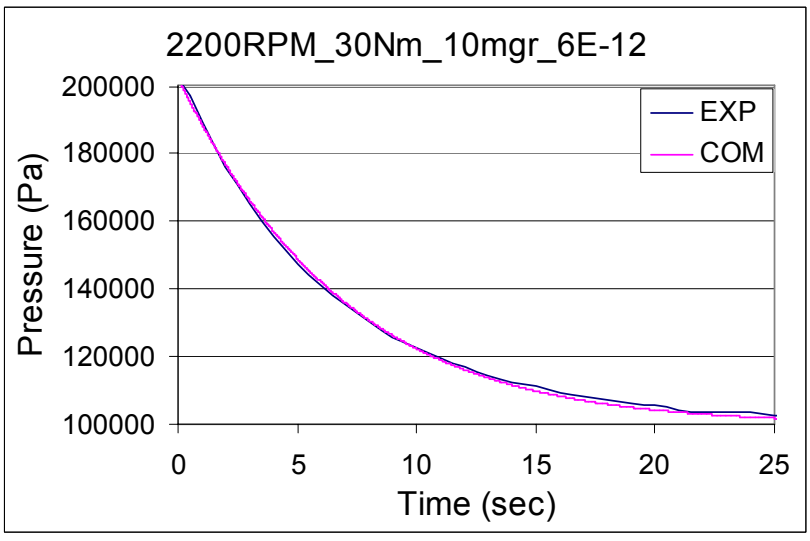

Figure 69 2200RPM_30Nm_4mgr_6E-12

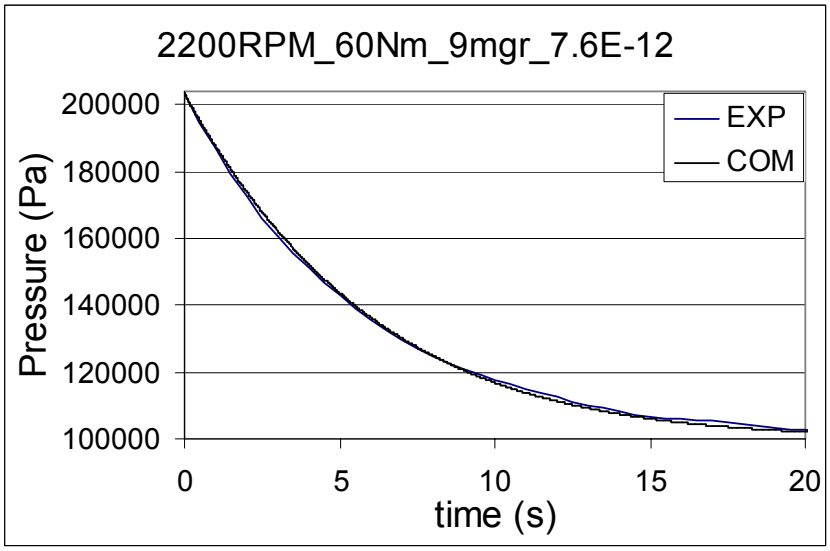

Figure 70 2200RPM_60Nm_9mgr_7.6E-12

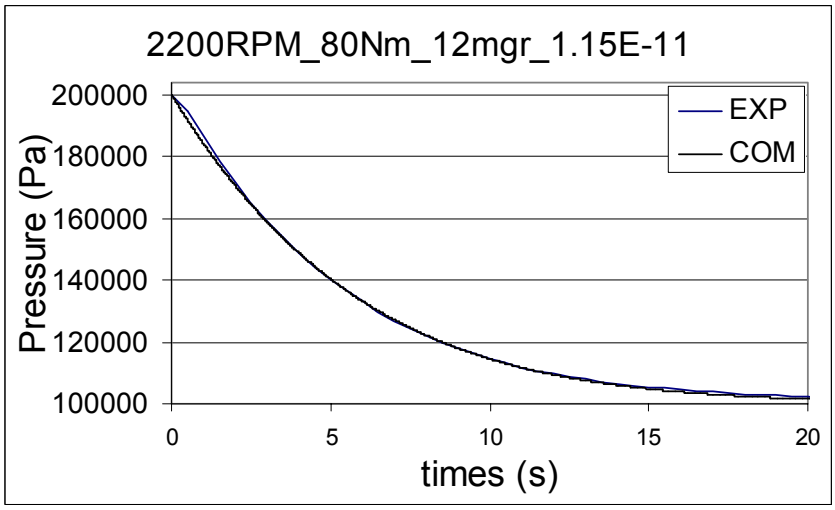

Figure 71 2200RPM_80Nm_12mgr_1.15E-11

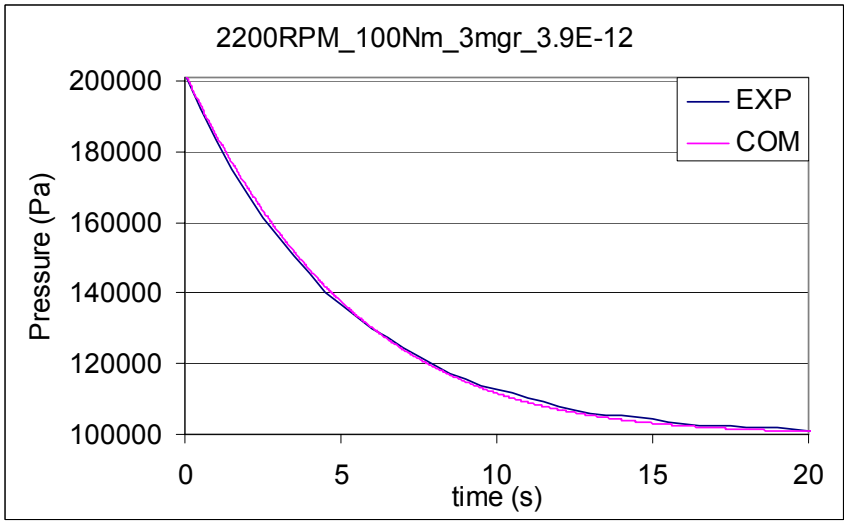

Figure 72 2200RPM_100Nm_3mgr_3.9E-12

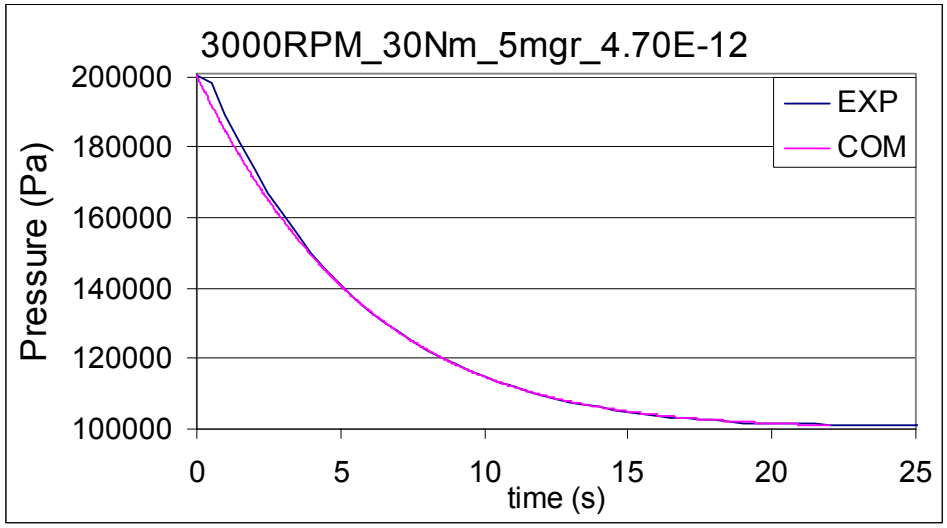

Figure 73 3000RPM_30Nm_5mgr_4.7E-12

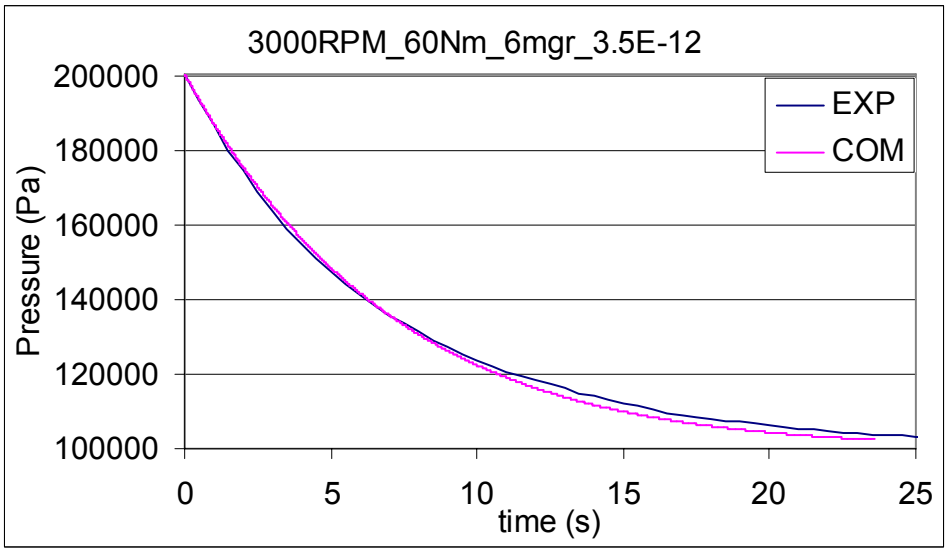

Figure 74 3000RPM_60Nm_6mgr_3.5E-12

SiC mini scale filter tuning curves

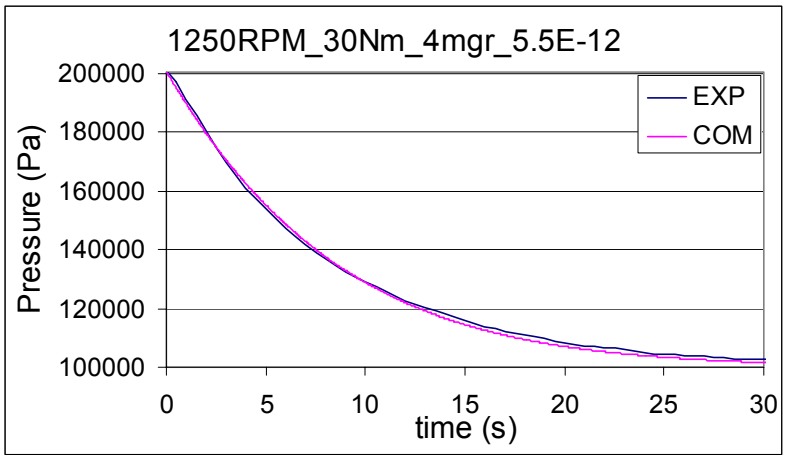

Figure 75 1250RPM_30Nm_4mgr_5.5E-12

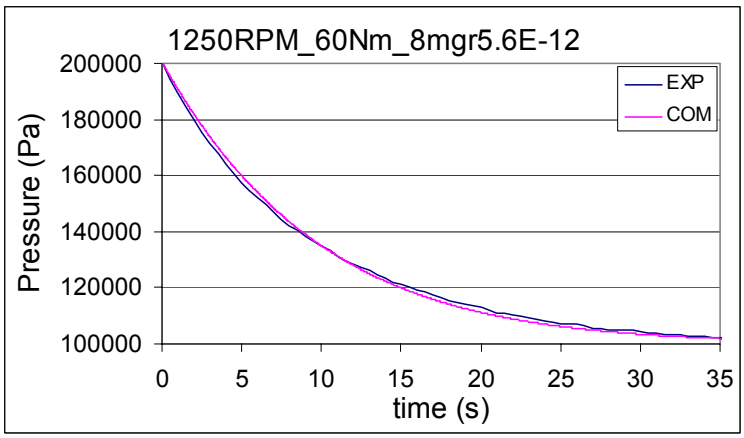

Figure 76 1250RPM_60Nm_8mgr_5.6E-12

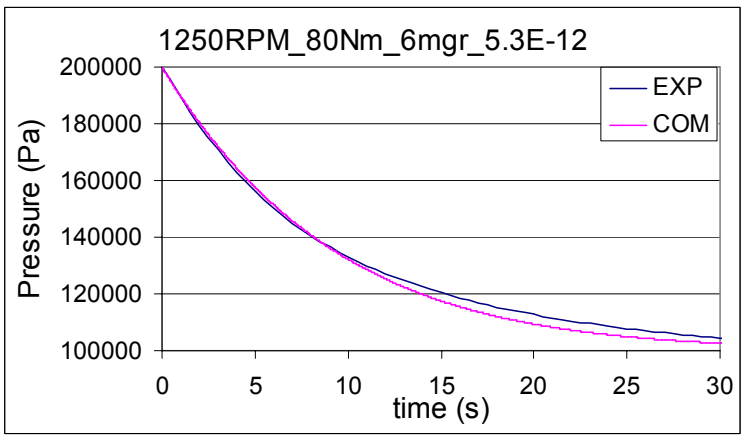

Figure 77 1250RPM_80Nm_6mgr_5.3E-12

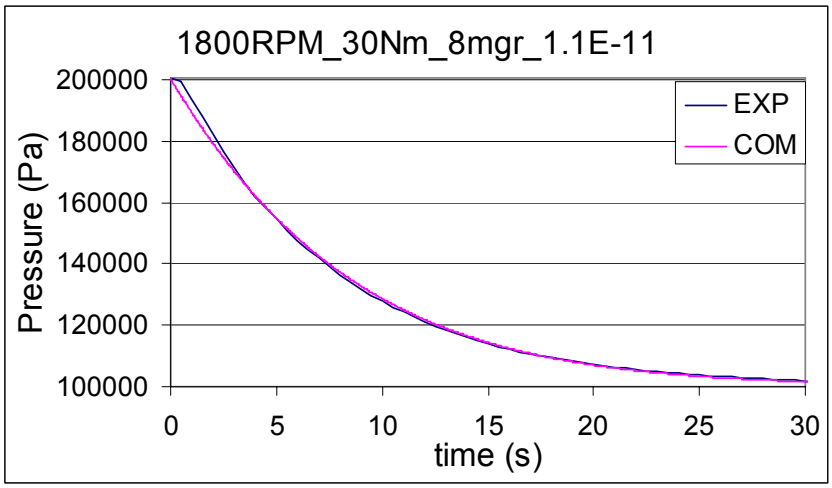

Figure 78 1800RPM_30Nm_8mgr_1.1E-11

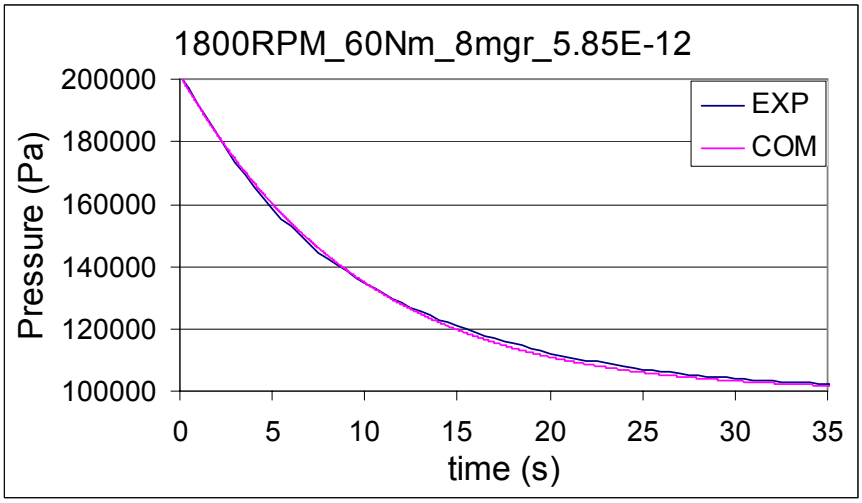

Figure 79 1800RPM_60Nm_8mgr_5.85E-12

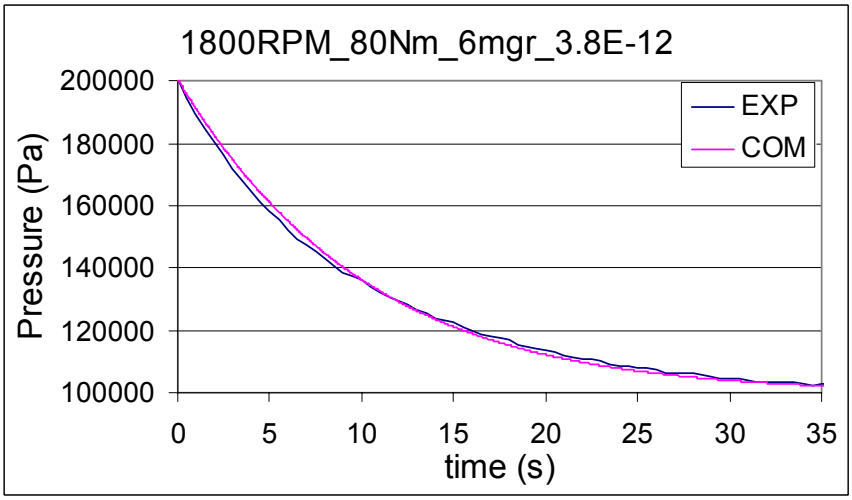

Figure 80 1800RPM_80Nm_6mgr_3.85E-12

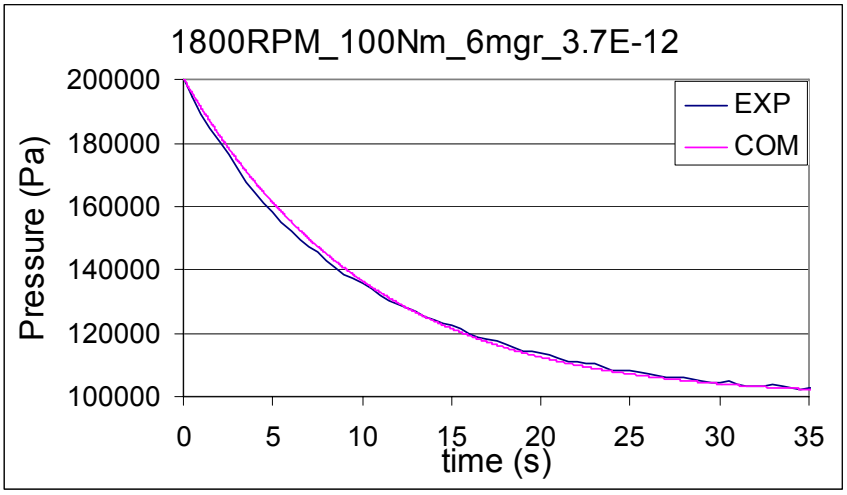

Figure 81 1800RPM_100Nm_6mgr_3.7E-12

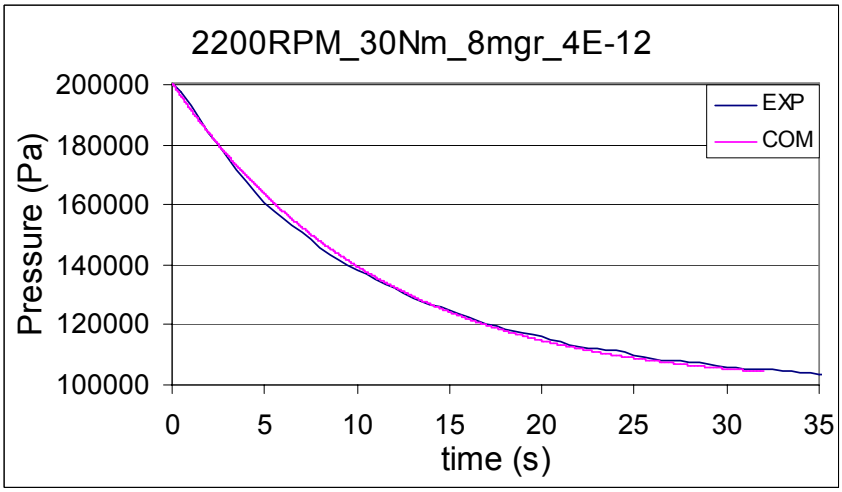

Figure 82 2200RPM_30Nm_8mgr_4E-12

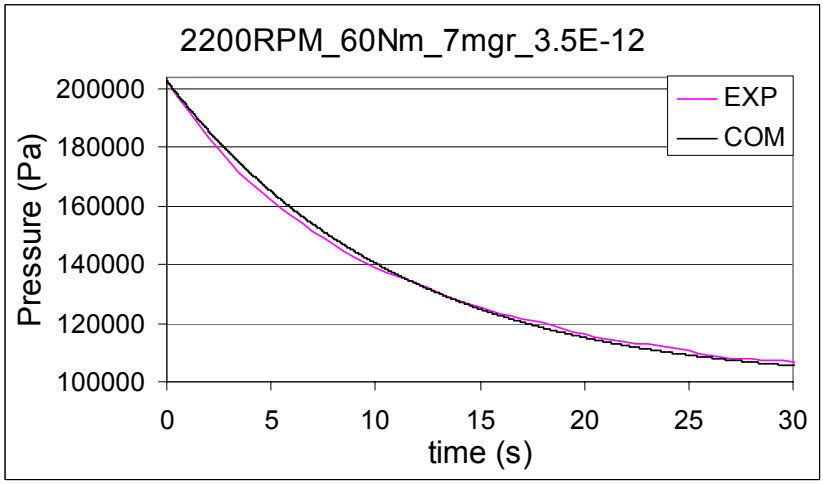

Figure 83 2200RPM_60Nm_7mgr_3.5E-12

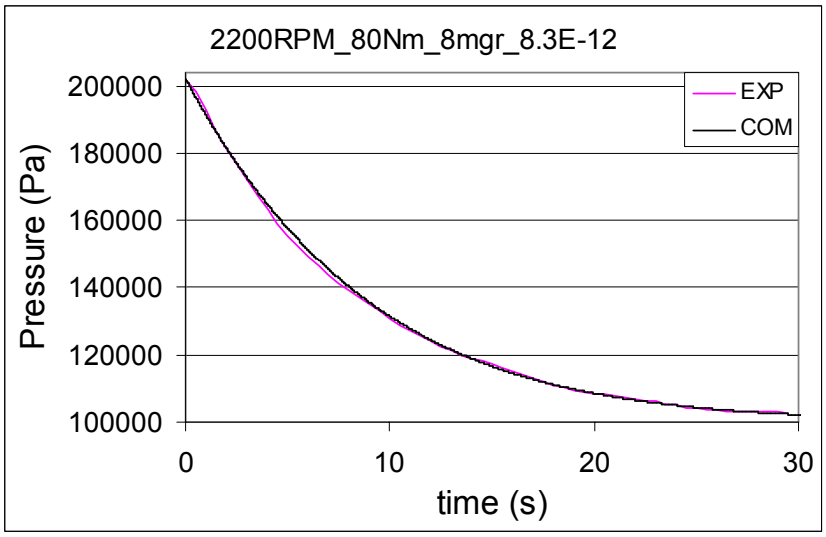

Figure 84 2200RPM_80Nm_8mgr_8.3E-12

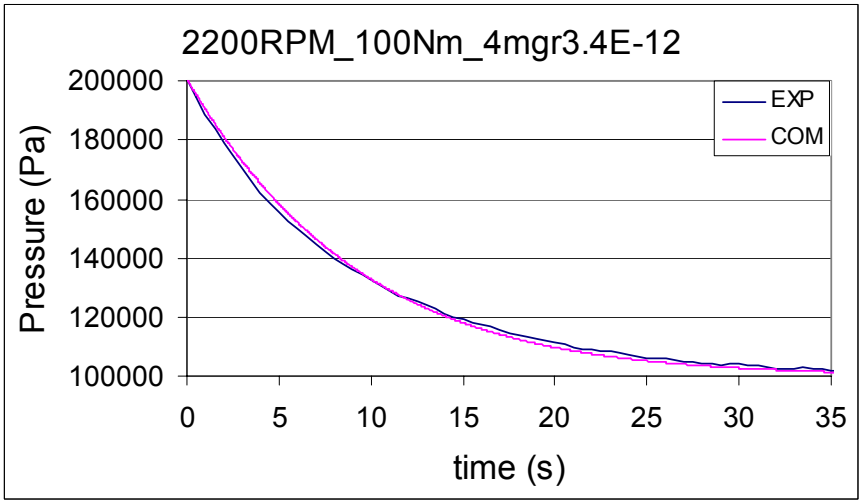

Figure 85 2200RPM_100Nm_4mgr_3.4E-12

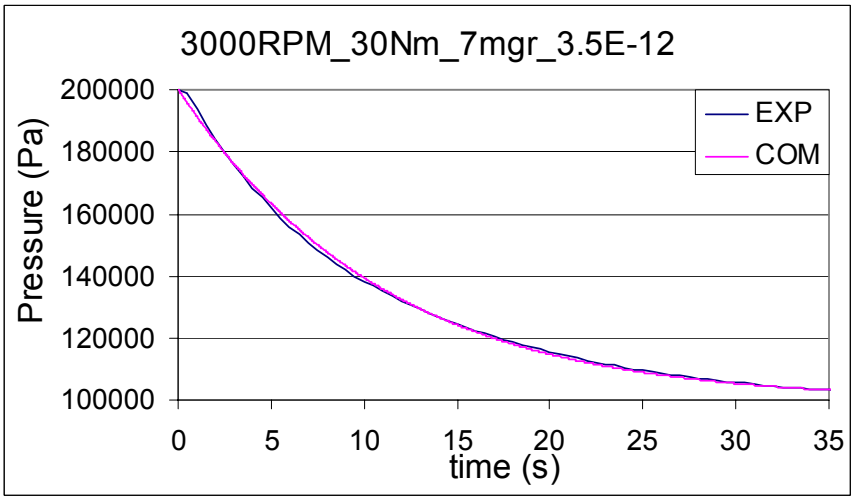

Figure 86 3000RPM_30Nm_7mgr_3.5E-12

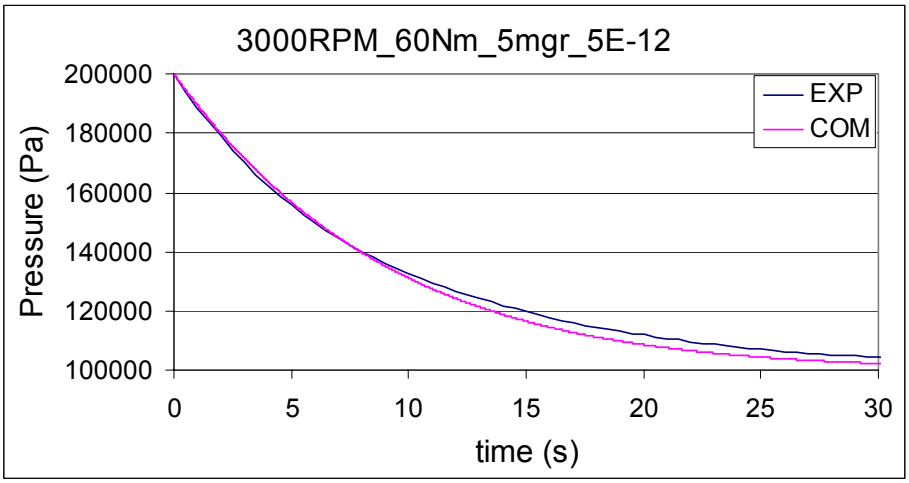

Figure 87 3000RPM_60Nm_5mgr_5E-12

ANNEX III: FULL – SCALE TRAP TUNING GRAPHS

The Full Scale DPF tuning graphs are presented in this section.

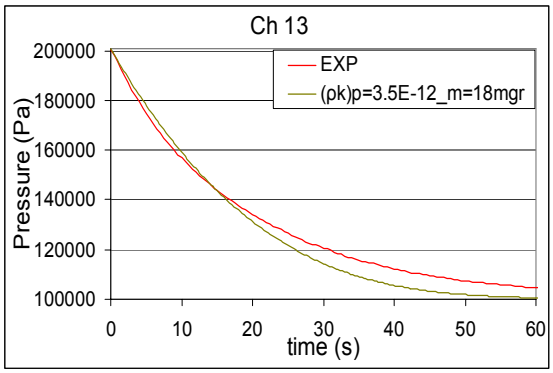

(a)

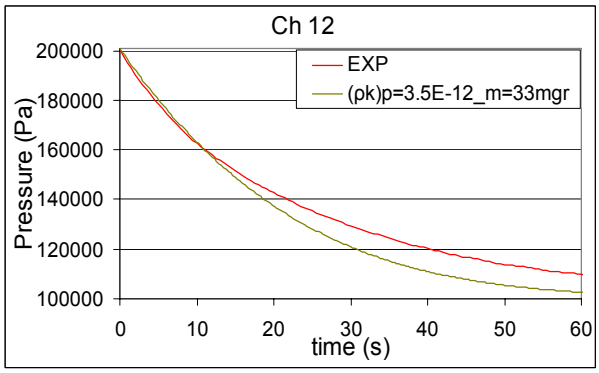

(b)

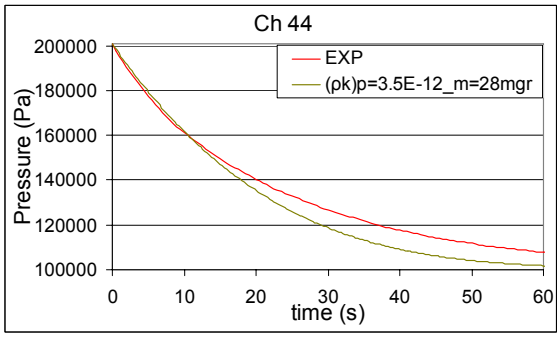

(c)

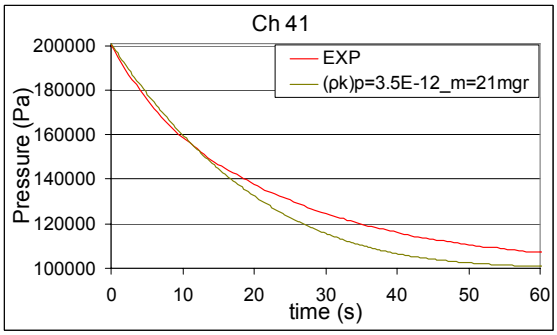

(d)

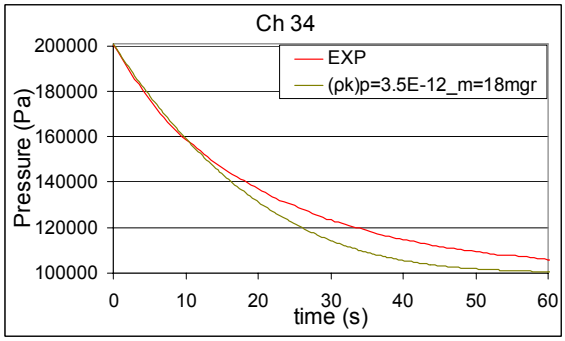

(e)

Figure 88Case study 3000RPM_40Nm. Tuning graphs of single channel groups measurement

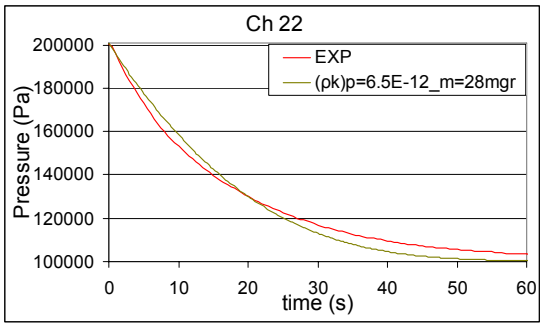

(a)

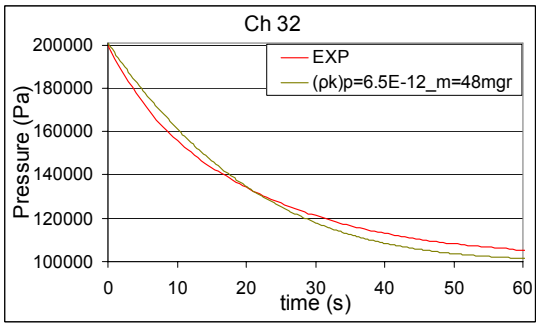

(b)

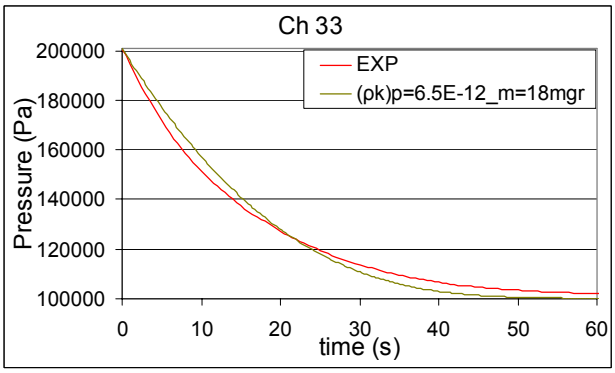

(c)

Figure 89 Case study 2200RPM_90Nm. Tuning graphs of single channel groups measurement.

ANNEX IV: CATWALL CODE OPERATION BACKGROUND

Thermal regeneration calculations

The flow through the filter is modeled as follows: the exhaust gas flow is considered to pass through two different layers. The first consists of the accumulated soot layer, which decreases as the regeneration proceeds, and the second is the ceramic porous media layer.

"Catwall" simulates the regeneration process with the assumption that the trap can be simulated by only one channel. Therefore the code uses two dimensions for the calculations. One axial (z - axis) along the channel and the other is the perpendicular to the z –axis (x - axis) as it is presented in figure 1.2. Also it is supposed that the soot accumulation is proportional to the local gas velocity in the channel, so that the sot particles follow continuously the streamlines.

Soot particles contain unburned hydrocarbons and sulfur combinations depending on the engine and the operational point of the engine. The major part of the unburned HC is gasified in lower temperatures than the soot oxidation temperatures. In order to simplify it is considered that the carbon oxidation is representative of the soot oxidation. The amount of CO in the reaction products is significant for the calculation of the thermal energy released during combustion because the reaction enthalpy of CO is high enough. Soot oxidation is considered that takes place with two reactions:

$C + 0.5O_2 \rightarrow CO$ and

$CO + 0.5O_2 \rightarrow CO_2$

The above reactions can be rewritten in the following familiar form:

$C + aO_2 \rightarrow 2(a-0.5)CO_2 + 2(1-a)CO$

The mass conservation equation in the exhaust gases is: $\rho v = \frac{F(t)}{A}$

where ρ is the density of exhaust gas, v the gas velocity, A the cross – section of the flow and F(t) the fuel flow rate.

The Oxygen balance is:

$$\frac{d(\rho vy)}{dx} = -s_j k_j \rho y \alpha \quad j=1,2 \qquad (1)$$

where 1 is the soot layer section and 2 is the porous media wall section and $k_2=0$. k_1 coefficient is determined from:

$$k_1 = k e^{-\frac{E}{RT}}$$

Another assumption is that the exhaust gas temperature is equal to that of the soot layer surface and that the heat transfer losses are negligible. Thus the energy balance has the following form:

$$\rho_j C_{pj} \frac{dT}{dt} = s_j (-\frac{\Delta H}{M_\alpha}) k_j \rho y + \frac{d}{dx}(\lambda_j \frac{dT}{dx}) - \rho v C_{pg} \frac{dT}{dx} \quad j=1,2 \qquad (2)$$

ΔH is the carbon oxidation enthalpy determined by the equation of paragraph (BAl)

The rate of decrease of the soot layer is proportional to the rate of consumption of O_2 and conversely proportional to the efficiency of oxidation α:

$$\rho_1 \frac{dw}{dt} = \frac{Mc}{Ma} \frac{F(t)}{A} [y(x=0)-y(x=-w)] \frac{1}{a} \qquad (3)$$

the initial conditions for the system of equations (1), (2), (3) are:

$T(x,t=0)=T_b$

$w(t=0)=w_b$

and the boundary conditions:

$y=y_i(t)$

$$\lambda_1 \frac{dT}{dx} = \rho v C_{pg}[T-T_i(t)]$$

while for $x=w_s$, $\frac{dT}{dx}=0$

Catalyst regeneration calculations

The soot without fuel additives oxidizes in high temperatures and the appropriate O_2 concentration. The fuel additives can reduce this temperature. Damkoehler is the critical dimensionless number for the type of regeneration:

$$\text{Da}=\frac{t_{flow}}{t_{reaction}}=\frac{W\rho_g y S_p k_1 T_w}{V_w \rho_p}$$

When Da number is less than a specific value then the soot cannot be oxidized the higher the Da number the more powerful the regeneration.

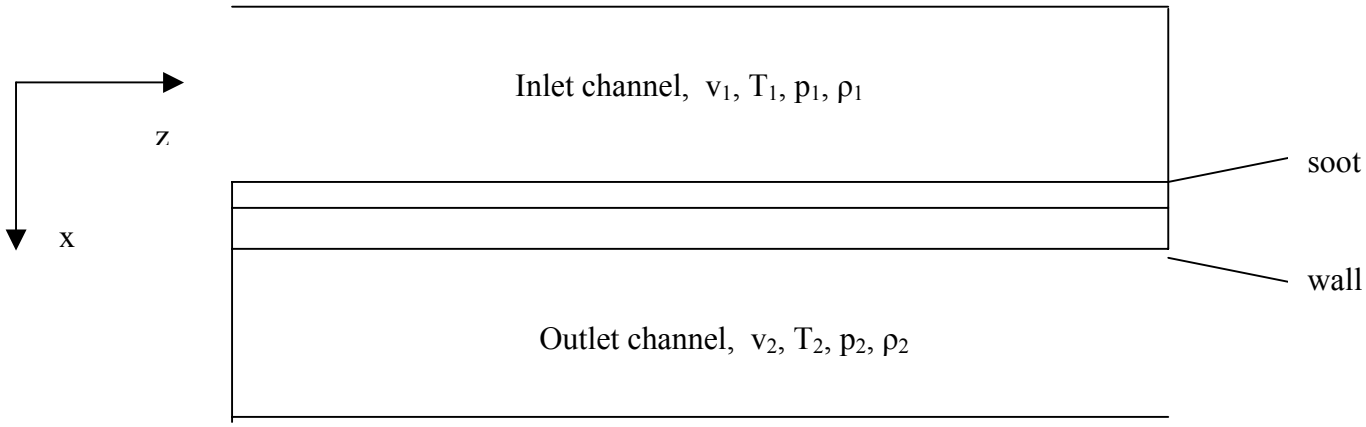

Figure 90 Input and outlet channels used in simulation

Two theories describe the influence of the additive in the soot oxidation. The first is the electron transfer theory. According to this theory there is an exchange of electrons between the atoms of fuel additive and carbon. As a result the bonds of carbon atoms on the surface are weaker and thus the carbon atoms can react with the oxygen. The second theory is called O_2 transfer theory and according to this theory the fuel additive stores and exchanges O_2 atoms with the carbon atoms. Catwall uses the second theory.

The exhaust gas temperature, density, velocity and pressure are equals to the mean value of each of them in x-axis. The released heat from soot combustion occurs only in the soot layer. However conduction in x-axis is dominant and so the wall temperature is independent of x. Heat transfer through the porous wall is quite high so

the exhaust gas temperatures can be considered equal except from a thin region on the wall surface to the inlet channel. The conservation of mass equation is:

$$\frac{d(\rho_i \upsilon_i^2)}{dz} = (-1)^i \frac{4}{D} \rho_w \upsilon_w \qquad (5)$$

the conservation of momentum along z- axis is:

$$\frac{d\rho_i}{dz}(\rho_i \upsilon_i^2) = -\frac{\alpha_1 \mu \upsilon_i}{D^2} \qquad (6)$$

the terms on the right side of the above equality represent the axial pressure drop due to the viscous forces. The mass flow rate through the wall is quite low from the mass that flows across the axial direction. Thus pressure drop can be determined by the equations that have been developed for rectangular closed ducts.

The heat transfer into the channel is driven by convection, so the energy balance into the channel can be written in the below form:

$$C_{pg}[D^2\rho_1\upsilon_1 T_{1(z+\Delta z)} - D^2\rho_1\upsilon_1 T_{1(z)} + 4D\Delta z\rho_w\upsilon_w T_{1(z)}] = h_1[4D\Delta z(T_w - T_1)] \qquad (7)$$

From combination of equations (5),(7):

$$C_{pg}(\rho_1\upsilon_1)_{(z+\Delta z)} \frac{dT}{dz} = h_1 \frac{4}{D}(T_w - T_1) \qquad (8)$$

The exhaust gas enters to the outlet channel with temperature T_w so:

$$C_{pg}[D^2\rho_2\upsilon_2 T_{2(z+\Delta z)} - D^2\rho_2\upsilon_2 T_{2(z)} + 4D\Delta z\rho_w\upsilon_w T_{2(z)}] = h_2[4D\Delta z(T_w - T_2)] \qquad (9)$$

Combination of the equations (5), (9) it can be written:

$$C_{pg}(\rho_2\upsilon_2)_{(z)} \frac{dT}{dz} = (h_2 + C_{pg}\rho_w\upsilon_w) \frac{4}{D}(T_w - T_2) \qquad (10)$$

As it has been already written the soot oxidation equation and the reaction enthalpy are determined from the equations below:

$C + aO_2 \rightarrow 2(a-0.5)CO_2 + 2(1-a)CO$

$\Delta H = 2(a-0.5)\Delta H_1 + 2(1-a)\Delta H_2$

The rate of reaction follows the Arrhenius law:

$k_1 = k e^{-\frac{E}{RT}}$

it is assumed that among the soot particles each atom of fuel additive is joint with other atoms of carbon or HC. When the soot layer temperature is sufficient the soot can react with the oxygen with the help of the fuel additive.

The catalyst concentration in the soot layer can be calculated from the below equation:

ξ=(moles of metal oxides present in the soot)/(moles of carbon in the soot)

ξ depends on the fuel additive concentration and the engine soot emissions.

The oxidation state of the metals oxides may be changed, by reacting with oxygen or with carbon. So the metal oxides can be found either in higher or lower oxidation state in the soot layer. The concentration of oxides can be determined as follows:

ψ=(oxides in soot layer in high oxidation state)/(total metal oxides in the soot)

Even more the following reaction can occur during catalyzed regeneration.

$C + 4\alpha_{cat}CeO \rightarrow 2\alpha_{cat}Ce_2O + 2(\alpha_{cat}-0.5)CO_2 + 2(1-\alpha_{cat})CO$ (11)

$Ce_2O + 0.5O_2 \rightarrow 2CeO$ (12)

Where α_{cat} is the catalyzed soot oxidation efficiency. The reaction rate of (11) is determined using the Arrhenius law:

$R_{reduction}=k_{reduction}\psi e^{-E_{reduction/RT}}$ (13)

Similarly the reaction rate of (12) is proportional to both the O_2 concentration in the exhaust gas and to the amount of oxidized metal oxide moles in lower oxidation state which is $1-\psi$. So the reaction rate of (12) is:

$R_{oxidation}=k_{oxidation}[O_2](1-\psi)e^{-E_{oxidation/RT}}$ (14)

And the rate of concentration change of ψ is:

$$\frac{d\psi}{dt} = R_{oxidation} - R_{reduction} \quad (15)$$

Considering the stoichiometry of the reaction the mass balance equation for the soot layer gives:

$$\rho_p \frac{dw}{dt} = -\frac{M_c}{M_{O2}} \rho_w \upsilon_w y \frac{1}{a}(1-\exp(-\frac{S_p k_1 T_w w}{\upsilon_w}\alpha)) - \frac{1}{2\alpha_{cat}} \rho_p w \xi R_{reduction} \quad (16)$$

the energy balance in the wall gives:

$$\frac{d}{dt}(\rho_p C_{p,p} T_w + \rho_s C_{p,s} T_w) = h_1(T_1 - T_w) + h_2(T_2 - T_w) + \rho_w \upsilon_w C_{p,g}(T_1 - T_w) + H_{reaction} + H_{conduction}$$

equation (16) can be used in the released heat calculation per unit of time and space:

$$H_{reaction} = (-\frac{\Delta H}{M_{O2}}) \rho_w \upsilon_w y \frac{1}{a}(1-\exp(-\frac{S_p k_1 T_w w}{\upsilon_w})) - \frac{1}{4\alpha_{cat} M_c} \rho_p w \Delta H \xi R_{reduction}$$

Also the heat transfer through conduction becomes:

$$H_{conduction} = -\lambda_p \frac{d}{dz}(w \frac{dT_w}{dz}) - \lambda_s w_s \frac{d^2 T_w}{dz^2}$$

The pressure drop across the two different layers of soot and the wall, can be calculated as it has been already mentioned in the chapter of porous media by the Darcy law:

$$p_1 - p_2 = \frac{\mu}{k_p} \upsilon_w w + \frac{\mu}{k_s} \upsilon_s w_s \quad (17)$$

The initial conditions that must be specified involve the temperature, loading and fuel additive concentration. The boundary conditions involve the fuel flow mass and the flow rate and concentration of O_2

The Diesel Filter simulation procedure uses the finite differences method and they are solved iteratively so that the axial velocity to the end of the inlet channel equals zero and the pressure in the exit of outlet channel is atmospheric.

The solution procedure consists of the following parts.

- Calculation of pressure, axial and wall velocity, temperature distribution in inlet and outlet channels, iteratively. A pressure value in the first node of exit channelis assumed, and arbitrary pressure in the first part of the channel. The wall velocity is calculated from (17). Then a numerical integration of equation (5) follows as long as the wall velocity is known, so the exhaust gas velocity is given. Equation

(8) gives the temperature in the next node. According to the flow rate change in z-axis and as long as the pressure drop equations are known the pressure of the next node can be calculated by integrating equation (6). This procedure continues along the channel and ends when the last node axial velocity has been calculated. If the latter is not low enough (less than 0.01 of the first node velocity) this procedure is repeated with a new pressure value in the inlet. A second criterion is that the last node pressure in outlet channel must be equal to the atmospheric. If this is not true then the solution procedure is repeated with another value in the first node of the outlet channel.

- Equations (15), (16) are solved for each node by the use of Runge-Kutta 4th order, since all of the flow magnitudes are known, in order to estimate the changes of w and ψ. Similarly the equation of reaction enthalpy $H_{reaction}$ gives the released heat from the soot oxidation. Thus the energy balance equation in the wall can be solved so the new temperature values can be calculated along the channel.

The factors that affect pressure drop are 4:

- ΔP_1 due to change of the flow area.

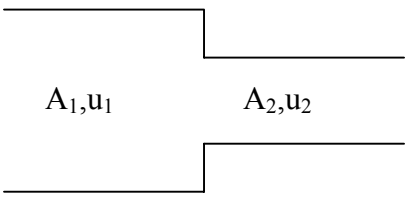

$$\Delta P_1=\rho g h_1=\rho(1-A_2/A_1)\frac{u_2^2}{2}$$

- ΔP_2 due to friction in the wall

Equation Darcy-Weibach gives:

$$\Delta P_2=\rho g h_2=\rho g(f\frac{Lu_c^2}{H2g})$$

Where f is the friction coefficient, L is the filter length, H the filter width, u_c the mean velocity in the channel.

- ΔP_3 due to the flow through the wall. Wall permeability depends on the pore size and number and it can be calculated from the below relationship.

$\Delta P_3 = \frac{1}{k_0} \mu u_s w$

Where $k_0 = \frac{\varepsilon^{5.5}}{5.6} D_f^2$ wall permeability, μ is the viscous, u_s is the velocity, ε solid porosity, D_f is the pore diameter

- ΔP_4 due to the flow through the sot layer. It can be assumed that the soot layer is uniform along the channel and that the soot is accumulated first in the end of the filter and then it is accumulated to the front of the filter. This changes the effective length and thickness of soot layer.

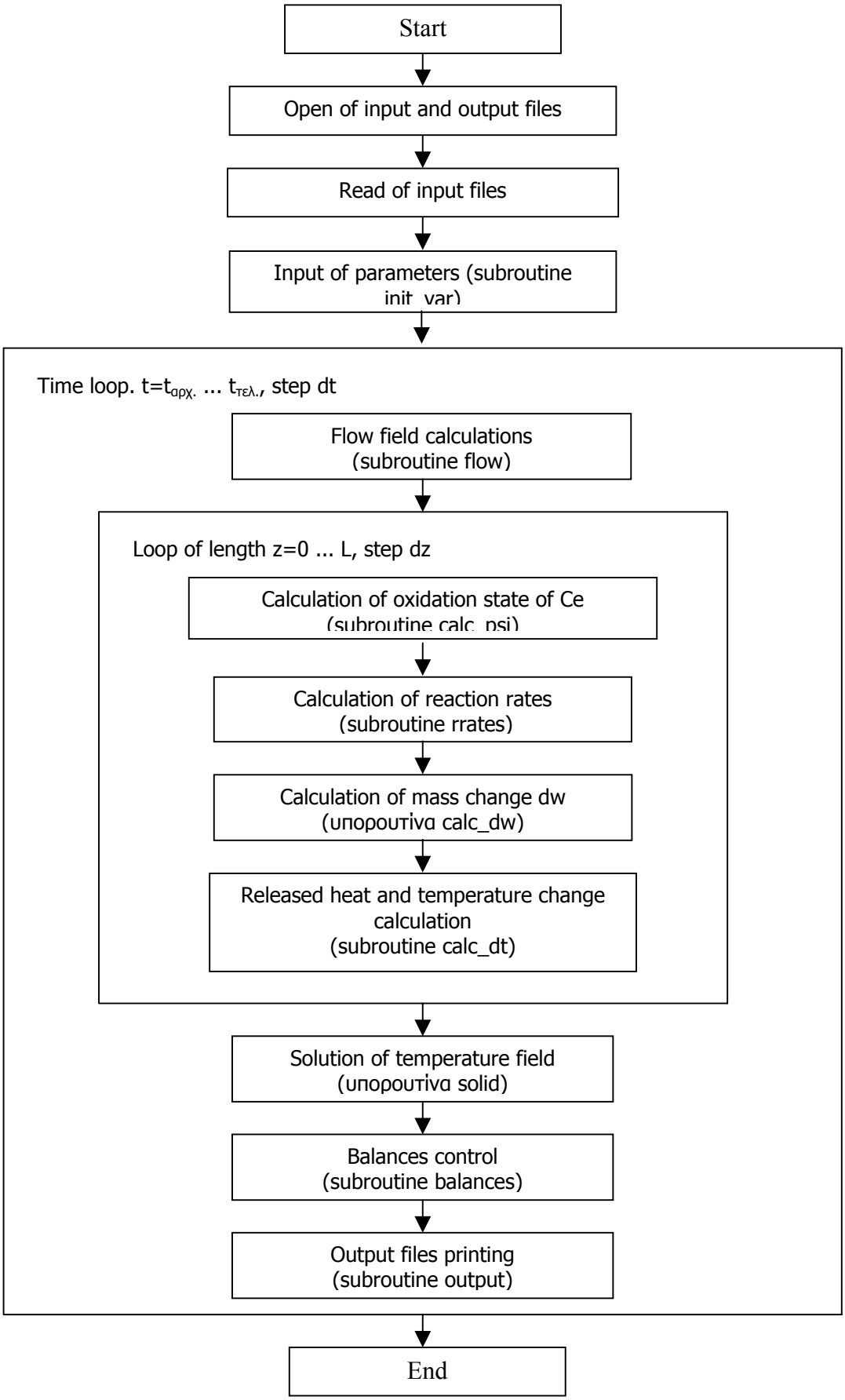

Figure 91 CATWALL Code Flowchart

REFERENCES

[1] Michael P. Walsh, '*Global Trends in Diesel Emissions Regulation-A 2001 Update*'. *SAE Paper* 2001-01-0183

[2] Ecopoint Inc. '*Technology Guide',* www.Dieselnet.com, 1999

[3] Δ. Κατσαούνης. '*Προϋπολογισμός Λειτουργίας Φιλτρων Αιθάλης',* Διπλωματική Εργασία Π.Θ.,2001

[4] A.M. Stamatelos '*A Review of the Effect of Particulate Traps on the Efficiency of Vehicle Diesel Engines, Energy Convers'*. Mgmt Vol. 38, pp. 83-9.

[5] H. Watanabe, T. Tahara, Mitsuo Tamanouchi, J.Iida, *'Study of the effects on exhaust emissions in direct injection diesel engines: Effects of fuel injection system, distillation properties and cetane number',* JSAE Review 19 (1998) 21-26

[6] S.Hori, NK. Narusawa, *'Fuel Composition Effects on SOF and PAH Exhaust Emissions from DI Diesel Engines',* SAE 980507, 1998

[7] Δ.Λ. Ψαριανός, '*Προσομοίωση Φαινομένων Ροής και Μεταφοράς με Ακτινοβολία-Εφαρμογή στην Υαλουργία',* Διπλωματική Εργασία Π.Θ. 2000

[8] Sytse J.Jelles, *' Development of catalytic systems for diesel particulate oxidation'*, PhD Thesis TU Delft 1999.

[9] Γ.Α.Στρατάκης, *'Σύγχρονες Εξελίξεις στην τεχνολογία του βενζινοκινητήρα'* , Άνωση 2000

[10] DieselNet '*Technical Report'* www.dieselnet.com

[11] Paul Degobert, *'Automobiles and pollution'*, Editions Technip 1995

[12] W. Addy Majewski. '*Diesel Particulate Matter'*, www.dieselnet.com, 2000

[13] D.B. Kittelson, '*Engines and Nanoparticles: a Review',* J. Aerosol ScienceVol29, No 5/6, 1998

[14] Ecopoint Inc '*www.dieselnet.com/standards/* 2001'

[15] Dieselnet Technology Guide, '*Emission Control Technologies'*, www. dieselnet. com/tech/ engine_ control

[16] J.C. Clerc: '*Catalytic Diesel exhaust aftertreatmen't*. Applied Catalysis B: Environmental 10 (1996) 99-115

[17] G.C. Koltsakis, A.M. Stamatelos, '*Modelling Catalytic Regeneration of Wall Flow Particulate Filter*s', Ind. Eng. ChemRes. 1996

[18] Ecopoint Inc. '*Diesel Filter Systems'*, www.Dieselnet.com, 2001

[19] Ecopoint Inc. '*Diesel Filter Materials'*, www.Dieselnet.com, 2001

[20] J.H. Johnson, S.T. Bagley, L.D. Graz, D.G. Leddy, *'A review of diesel particulate control technology and emissions effects'*. *SAE paper* 940233

[21] R.J. Farrauto, K.E. Voss, *'Monolithic diesel oxidation catalysts'*. Applied Catalysis B: Environmental 10 (1996) 29-51

[22] J.P.A. Neeft, M. Makkee and J.A. Moulijn, *'Catalysts for the oxidation of soot from diesel exhaust gases. I. An exploratory study'*. *Applied Catalysis B: Environmental* 8 (1996) 57-78

[23] J.P.A. Neeft, W. Schiper, M. Makkee and J.A. Moulijn, *'Feasibility Study towards a Cu/K/Mo/(Cl) soot oxidation catalyst for application in diesel exhaust gases'*. Applied Catalysis B: Environmental 11 (1997) 365-382

[24] Timothy V. Johnson*, 'Diesel Emission Control in Review'* SAE paper 2000-01-0184

[25] O. Salvat, P. Marez, G. Belot: *'Passenger Car Serial Application of a Particulate Filter System on a Common Rail Direct Injection Diesel Engine'*. SAE paper 2000-01-0473

[26] G. C. Koltsakis, A. M. Stamatelos, *'Catalytic Automotive Exhaust Aftertreatment'. Prog. Energy Combust. Sci.* Vol. 23, pp.1-39, 1997

[27] Bissett, E.; Shadman, F. *'Thermal Regeneration of Diesel-Particulate Monolithic Filters'*. AlChE J. 1985, 31 (5), May, 753.

[28] G. C. Koltsakis, A. M. Stamatelos, *'Modeling Catalytic Regeneration of Diesel Particulate Traps'* Industrial & Engineering Chemistry Research, 1996, (35), pp. 2-13.

[29] G. C. Koltsakis, A. M. Stamatelos, *'Modes of Catalytic Regeneration in Diesel Particulate Filters'* Ind. Eng. Chem. Res. 1997, 36, 4155-4165

[30] G. Pontikakis, A. Stamatelos, K. Bakasis and N. Aravas, *'3-D Catalytic Regeneration and Stress Modeling of Diesel Particulate Filters by ABAQUS FEM Software'*, SAE paper 2002-01-1017

[31] W.W. Pulkrabek, W.E. Ibele, *'The effect of temperature on the permeability of a porous material'*, J. Heat and Mass Transfer, Vol. 30, No 6, pp 1103 –1109, 1987

[32] R.M. Terrill, *'Laminar Flow in a Porous Tube',* Journal of Fluids Engineering Vol. 105 September 1983
[33] R.W. Johnson, '*The Handbook of Fluid Dynamics',* Springer 1998
[34] A.A.M. Oliveira, M. Kaviany, *'Nonequilibrium in the transport of heat and reactants in combustion in porous media',* Progress in Energy and Combustion Science, 27 (2001)
[35] Ecopoint Inc. *'Diesel Particulate Traps'*, www.Dieselnet.com, 2001
[36] G.N. Pontikakis, G.C. Koltsakis, A.M. Stamatelos, *'Dynamic Filtration Modeling in Foam Filters For Diesel Exhaust',* Chem. Eng. Comm. 2001
[37] P. Versaevel, H. Colas, C. Rigaudeau, R. Noirot, G. C. Koltsakis, A. M. Stamatelos, 'Some Empirical Observations on Diesel Particulate Filter Modeling and Comparison Between simulations and Experiments', SAE paper 2000-01-477
[38] S. C. Sorenson, Jacob W. Hoj, Per Stobbe, *'Flow Characteristics of SiC Diesel Particulate Filter Materials'*, SAE paper 940236
[39] J. B. Heywood, *'Internal Combustion Engine Fundamentals'*, McGraw Hill 1988
[40] G. A. Stratakis and A. M. Stamatelos, *'Thermogravimetric Analysis of Soot Emitted by a Modern Engine Run on Catalyst-Doped Fuel. Submitted*', Particulate Science & Technology, 2002.
[41] G. A. Stratakis, D.L. Psarianos, A.M. Stamatelos, *'Experimental Investigation of Pressure Drop in Porous Ceramic Diesel Particulate Filters',* submitted to ImechE proceedings 2002
[42] J.C. Tan, C.N. Opris, K.J. Baumgard, J.H. Johnson, *'A Study of the Regeneration Process in Diesel Particulate Traps Using a Copper Fuel Additive',* SAE 1996
[43] C.N. Opris, , J.H. Johnson, '*A 2-D Computational Model Describing the Flow and Filtration Characteristics of a Ceramic Diesel Particulate Trap'*, SAE paper 980545
[44] G.C. Koltsakis A.M. Stamatelos, '*Modeling Thermal Regeneration of Wall-Flow Diesel Particulate Traps',* AIChE Journal 1996 Vol42